

**RETROFIT OF EXISTING REINFORCED CONCRETE
BRIDGES WITH FIBER REINFORCED
POLYMER COMPOSITES**

by

**Bahram M. Shahrooz
Serpil Boy**

Report No. UC-CII 01/01

December 2001

A Report to Sponsor:
Federal Highway Administration
And
Ohio Department of Transportation

Contract # 14719(0)

Cincinnati Infrastructure Institute
University of Cincinnati
College of Engineering
Cincinnati, Ohio 45221-0071

**Prepared in cooperation with the Ohio Department of Transportation and the U.S.
Department Transportation, Federal Highway Administration**

Disclaimer

The contents of this report reflect the views of the authors who are responsible for the facts and the accuracy of the data presented herein. The contents do not necessarily reflect the official views or policies of the Ohio Department of Transportation or the Federal Highway Administration. This report does not constitute a standard, specification or regulation.

1. Report No. FHWA/OH-2001/17	2. Government Accession No.	3. Recipient's Catalog No.	
4. Title and subtitle. Retrofit of Existing Reinforced Concrete Bridges with Fiber Reinforced Polymer Composites		5. Report Date December, 2001	
		6. Performing Organization Code	
7. Author(s) Dr. Bahram M. Shahrooz		8. Performing Organization Report No. UC-CII 01/01	
		10. Work Unit No. (TRAVIS)	
9. Performing Organization Name and Address University of Cincinnati College of engineering Department of Civil and Environmental Engineering PO Box 210071 Cincinnati, OH 45221-0071		11. Contract or Grant No. State Job No. 14719(0)	
		13. Type of Report and Period Covered Final Report	
12. Sponsoring Agency Name and Address Ohio Department of Transportation 1980 W Broad Street Columbus, OH 43223		14. Sponsoring Agency Code	
15. Supplementary Notes			
16. Abstract <p>The first part of the reported research examined the performance of four 76-year, deteriorated reinforced concrete beams (which were removed from an existing bridge slated for reconstruction) retrofitted with external carbon FRP (CFRP) post-tensioning rods, bonded CFRP plates, bonded CFRP fabrics, and bonded CFRP plates with mechanical anchors, respectively. The various FRP systems studied in this research produced different failure modes and strength gains. Despite extensive deterioration and age of the beams, the retrofitted beams could develop and exceed the expected capacity computed based on available design guides. For cases where guidelines were not available, simple, yet effective, methods were developed to establish the capacity of the retrofitted beams.</p> <p>In the second part of the reported research, a 45-year old, three-span reinforced concrete slab bridge with insufficient capacity was retrofitted with 76.2 and 127-mm wide bonded carbon fiber reinforced polymer (FRP) plates, 102-mm wide bonded carbon FRP plates with mechanical anchors at the ends, and bonded carbon FRP fabrics. The use of four systems in one bridge provided an opportunity to evaluate field installation issues, and to examine the long-term performance of each system under identical traffic and environmental conditions. Using controlled truckload tests, the response of the bridge before retrofitting, shortly after retrofitting, and after one year of service was measured. The stiffness of the FRP systems was small in comparison to the stiffness of the bridge deck, and accordingly the measured deflections did not noticeably change after retrofitting. The measured strains suggest participation of the FRP systems, and more importantly the strength of the retrofitted bridge was increased. A detailed three-dimensional finite element model of the original and retrofitted bridge was developed and calibrated based on the measured deflections. The model was used to more accurately predict the demands needed for computing the rating factors. The addition of FRP plates and fabrics led to a 22% increase in the rating factor and corresponding load limits. During a one-year period, traffic loading and environmental exposure did not apparently affect the performance of the FRP systems. In view of the increased capacity and performance of the FRP systems, load limits were removed and normal traffic was resumed. Future tests are necessary to monitor the long-term behavior of the FRP systems.</p>			
17. Key Words Bridge, Field Testing, Fiber Reinforced Composite (FRP) Polymer Rating Factor, Reinforced Concrete Bridges, Repair, Retrofit, Strengthening, T Beams		18. Distribution Statement No Restrictions. This document is available to the public through the National Technical Information Service, Springfield, Virginia 22161	
19. Security Classif. (of this report) Unclassified	20. Security Classif. (of this page) Unclassified	21. No. of Pages 149	22. Price

RETROFIT OF EXISTING REINFORCED CONCRETE BRIDGES WITH FIBER REINFORCED POLYMER COMPOSITES

Executive Summary

A two-part research was focused on examining various issues related to the use of fiber reinforced polymer (FRP) composites for strengthening of existing reinforced concrete bridges. A summary of each phase is presented separately.

Part I: Flexural Strengthening of Four 76-Year Old T Beams with Various FRP Systems

Four 76-year old T reinforced concrete beams were retrofitted with four different systems employing carbon fiber polymer reinforced (CFRP) composites to examine the success of FRP systems to strengthen aged members with substantial deterioration. The beams were removed from FAI-37-2899 and FAI-37-2915. The systems used in this project were (a) external post-tensioning system with CFRP rods, (b) bonded CFRP plates, (c) bonded CFRP fabrics, and (d) bonded CFRP plates with mechanical anchors at the ends of the plates. The experimental data were augmented with analytical results to better understand the observed behavior, particularly when visual data or the measured data were insufficient. The analytical studies were also used for parametric studies, and developing the expected capacity of the as-is and retrofitted beams. Based on the presented data, the following observations and conclusions are drawn.

1. Despite significant deterioration in the beams, the retrofitted beams could develop and exceed the expected capacities computed from current guidelines for externally bonded FRP systems. The poor quality of concrete, however, apparently lowered the bond strength between CFRP plates and substrate. As a result, the plates in Beam 2 were debonded after developing only 22% of their ultimate strength.
2. The external CFRP post-tensioning rods in Beam 1, and anchored CFRP plates resulted in the largest strength gain, and did not exhibit an appreciable loss of strength at large deflections. The anchor system in Beam 1 and anchors at the end of CFRP plates in Beam 4 were adequate to allow formation of sufficient forces in the rods or anchored plates. If the anchor system in either beam had failed prematurely, the mode of failure would have been catastrophic, as large amounts of energy stored in the rods or plates would have been released suddenly. If adequate measures are taken to prevent anchorage failure, the systems used in Beams 1 and 4 apparently offer the best retrofitting option, particularly for members with extensive deterioration since these systems do not rely on the quality of bond between FRP plates and substrate.
3. Beam 3, with bonded longitudinal and transverse CFRP fabrics, displayed the highest level of redundancy. Fracturing of the fabrics, after widening of cracks, spread gradually to regions away from the midspan; hence, loss of strength was rather gradual. At large deflections (exceeding 1/100 of the span length), the fabrics could still enhance the capacity despite local fracturing at several locations. Although this system did not increase the capacity as much as external post-tensioning or bonded CFRP plates with mechanical anchorages, the use of bonded fabrics appears to be a viable choice for deteriorated members as bond to deteriorated substrate appears to be less critical.

4. The measured global responses of the retrofitted beams and/or their capacity could be correlated reasonably well through the use of relatively simple analytical models. These models can be used as effective design tools when current design guidelines do not provide specific recommendations about a particular retrofitting system.

Part II: Retrofit of a Three-Span Slab Bridge with FRP Systems – Testing and Rating

In an effort to strengthen a three-span reinforced concrete slab bridge (CLI-380-0032), which had been posted because of inadequate rating factors, and remove the load postings, four FRP systems were installed. The FRP systems included 76.2 and 127-mm wide carbon bonded plates, 102-mm wide carbon bonded plates with anchors at the ends, and bonded carbon fabrics. This project also provided a unique opportunity to examine the long-term performance of four FRP systems under identical environmental conditions and loading. For this purpose, detailed truckload tests were conducted to obtain benchmark responses of the original bridge, shortly after installation of the FRP systems, and after one year of service. The measured data proved useful for calibration of a relatively detailed three-dimensional finite element model of the bridge. The calibrated model was used to calculate the rating factors and associated load limits for the as-is and retrofitted bridge. Based on the experimental and analytical studies, the following general conclusions and observations are made.

1. The overall stiffness of the bridge was increased after the FRP systems were installed. The level of increase approximately corresponds to that indicated by transformed section analysis. After retrofitting, concrete strain in the slab dropped as the FRP systems participated toward resisting the applied live loads. The participation of the FRP retrofitting scheme was most pronounced at the location with the highest moment demands.
2. After one year of service, the effectiveness of the FRP systems, as gauged by the measured deflections and strains in the FRP systems, did not essentially change from that obtained shortly after installation of the FRP systems. Additional testing of the bridge in the future along with inspection of the FRP-concrete bond quality and condition of the FRP plates and fabrics would provide invaluable data regarding the long-term performance of four FRP systems under identical environmental exposures and loading.
3. The retrofitted bridge achieved larger rating factors and load limits than the corresponding values for the original bridge. Retrofitting with the FRP systems led to a 22% increase in the load carrying capacity of the bridge. The FRP systems proved to be a simple, yet effective, method to strengthen the bridge, and to enable the engineers remove the posted load limits.

TABLE OF CONTENTS

Executive Summary	I
Table of Contents	III
Part I: Flexural Strengthening of Four 76-Year Old T Beams with Various FRP Systems.....	1
Part II: Retrofit of a Three-Span Slab Bridge with FRP Systems – Testing and Rating	37
Implementation.....	64
Appendix A: Supporting Documents and Data for Part I	65
Appendix B: Supporting Documents and Data for Part II	100

FLEXURAL STRENGTHENING OF FOUR 76-YEAR OLD T BEAMS WITH VARIOUS FRP SYSTEMS– TESTING AND ANALYSIS

ABSTRACT

Fiber-Reinforced Polymer (FRP) plates and fabrics have emerged as viable systems for retrofitting of existing reinforced members with insufficient capacity. The results from previous research, conducted predominately on laboratory specimens, have been recently used to develop design guidelines. Detailed destructive testing of existing, aged members retrofitted with FRP systems is very limited. The reported research was conducted to examine the performance of four 76-year, deteriorated reinforced concrete beams retrofitted with external carbon FRP (CFRP) post-tensioning rods, bonded CFRP plates, bonded CFRP fabrics, and bonded CFRP plates with mechanical anchors, respectively. The various FRP systems studied in this research produced different failure modes and strength gains. Despite extensive deterioration and age of the beams, the retrofitted beams could develop and exceed the expected capacity computed based on available design guides. For cases where guidelines were not available, simple, yet effective, methods were developed to establish the capacity of the retrofitted beams.

Keywords: Beam, Carbon fabric, Carbon Plate, Deteriorated R.C. Beams, External Post-tensioning, Fiber Reinforced Polymer, Flexural Testing, Mechanical Anchorage, Retrofitting

RESEARCH SIGNIFICANCE

Available design guidelines for externally applied FRP composites have been developed primarily based on laboratory testing of newly cast specimens. The research presented in this paper provides information for examining the effects of existing deterioration in aged members on the effectiveness of FRP composites. Retrofitting and testing of four similar beams allowed a detailed evaluation of four different retrofitting schemes in terms of failure mode, ductility, and strength gain. The companion analytical studies offer design tools for cases where available guidelines do not provide a methodology for computing the capacity of the retrofitted members.

INTRODUCTION

As of August 2000, 167,993 of the 587,755 bridges in the national bridge inventory are judged to be structurally deficient, functionally obsolete, or both. With limited available funds and an increasing number of deteriorated, underrated, and overloaded bridges in the United States, an effective alternative to replacing bridges is needed. Economical retrofitting techniques appear to be one of the most viable choices. Typical retrofitting techniques involve the use of (a) external bonded steel plates, (b) steel or concrete jackets, (c) external post-tensioning, (d) bonded fiber reinforced polymer (FRP) plates or fabrics, or (e) externally applied FRP post-tensioning strands.

Fiber reinforced polymer plates, fabrics, or rods offer numerous advantages such as (a) structural benefits: FRP materials have very high strength, and have a higher strength/weight ratios than steel or concrete; hence, the strength and stiffness can be increased without a significant increase in the dead load, (b) life cycle benefits: FRP materials offer high resistance against corrosion and other elements; and (c) economic benefits: installation time and cost are less than the traditional retrofit techniques. Recognizing the benefits of FRP plates and fabrics as external flexural and shear reinforcement to revitalize the deteriorating infrastructure, a significant amount of research has been conducted in recent years to characterize the material properties and behavior of FRPs, to examine various issues related to behavior of members and systems strengthened with FRP, and to develop analysis and design methods for FRP reinforced concrete members (e.g., Neale, 2000). Taking advantage of the research data, design guidelines have been developed in the U.S., Canada, Europe, and Japan (e.g., ACI 440, 2000; fib, 2001). With the development of design guides and availability of research data demonstrating the viability of FRP, the engineering community has begun to embrace this new technology by using FRP composites in various projects around the world (e.g., CI, 1998). Considering the novelty of FRP composites and newness of the design guides, additional research is warranted to fill gaps in the available databases, to provide additional data for further refinements, to reaffirm the fledgling design guidelines, and to examine issues that have not yet been

considered. One such issue is the age of the members to be retrofitted. The previous studies have predominately focused only on performance of structures with relatively new concrete retrofitted with FRP composites. Therefore, bondability of FRP composites to aged members, and the effects of the existing cracks and damage due to years of environmental exposure and possible overloads have not been examined.

To investigate the performance of aged structures strengthened with FRP composites, four 76-year old T beams were used as test specimens. Each beam was initially loaded to develop 50% of the yield strain in the longitudinal bars. After establishing the benchmark data, the beams were unloaded and retrofitted by four different methods utilizing various FRP composite systems. Subsequently, each beam was loaded up to its ultimate limit state. Analytical models based on fundamental principles were used to compute the capacity of the beams before retrofitting, to evaluate the success of available methods to predict the behavior of structures retrofitted with FRP composites, to develop design models for cases where current guidelines are unavailable or inadequate, and to further understand the measured responses. The research program and relevant results are summarized in this paper.

DESCRIPTION OF TEST SPECIMENS

The test specimens consisted of four nominally 10-m long T beams removed from two bridges (FAI-37-2899 and FAI-37-2915) built in 1924. The bridges were on the same road and were close to each other; hence, all the beams had been exposed to essentially the same traffic load and environmental conditions. Details of the beams are shown in Fig. 1. Three of the longitudinal bars in the bottom most layer were 25.4x25.4 mm square bars, and the remaining 7 bars were 25.4-mm round bars. The bars had deformations according to the common practice of the time when the bridges were built. Based on reinforcing bar samples obtained from similar beams in the bridges, the material properties were measured according to ASTM A370. The average yield strength, ultimate strength, fracture strength, modulus of elasticity, and fracture strain were found to be 278 MPa, 512

MPa, 426 MPa, 166,600 MPa, and 31%, respectively. The longitudinal bars in the test beams had evidently corroded as suggested by rust stains on the concrete surface. At the conclusion of testing, corrosion of the bars was verified visually by exposing the bars. The concrete was a standard 1:2:4 mix that was typical for bridges built in the 1920's. Attempts to core the slab in all the beams failed because of the significant level of deterioration in the slab. A standard rebound hammer in conjunction with ASTM C805 was alternatively used to establish the concrete strength. The equivalent cylinder strength of each beam is summarized in Table 1.

OVERVIEW OF EXPERIMENTAL PROGRAM

The test program consisted of (a) the loading of each beam in as-is condition to develop 50% of the yield strain in the lowest longitudinal bars at the midspan, (b) unloading and retrofitting of each beam with various FRP systems, and (c) the load testing of each beam to produce large displacements and extensive damage.

Retrofit Method

Four different retrofit systems were used. A contractor specialized in retrofitting with FRP composites performed all the surface preparations and installations. The contractor made all the specific decisions about the details of various retrofit schemes. The concrete surface was deemed sound, and was not repaired. The contractor followed recommended standard surface preparation steps, including pressure washing of beams that were to be retrofitted with bonded FRP plates or fabrics. The material properties for various FRP systems are summarized in Table 2.

The clear span between the supports for Beam 1 was 9.91 m. This beam was retrofitted with four 9.5-mm external carbon FRP post-tensioning rods, two on each side of the web. The anchorage system is shown in Fig. 2. The anchorage systems were 4.1 m and 4.6 m from the centerline of the beam. Each rod was post-tensioned to 57.8 kN, which corresponded to 45% of the nominal ultimate capacity of the rods, to ensure a safety factor of 2.

In Beam 2, with a clear span of 9.96 m, a pair of 76.2-mm wide by 1.34-mm thick

unidirectional carbon fiber reinforced polymer (CFRP) plates was bonded to the bottom face of the web. The beam was retrofitted before it was placed in the test frame. Because of miscalculations about the final locations of the supports, the plates were extended farther than planned. One of the plates extended from the face to face of the supports. The second plate was terminated 216 mm away from the face of one support, and extended beyond the face of the other support by 216 mm. For this beam, ACI 440 guides (ACI 440, 2000) would require the plates be terminated at 708 mm away from the face of the supports. Hence, the plates in this beam had been extended significantly more than what current design guides would have required.

Beam 3 (clear span = 9.44 m) was wrapped with unidirectional carbon fabrics. The contractor followed typical steps for wet lay-up systems. Two 305-mm wide layers of fabric were bonded to the soffit of the web as longitudinal reinforcement. The fabrics were extended from the face to face of the supports; the fabrics could have been terminated at 916 mm from the face of the supports according to ACI 440 guides. Considering the age of the beam and its condition, the contractor extended the cut-off points to provide additional margin of safety against possible debonding. The web was also wrapped with two U-shaped layers of fabric as shear reinforcement throughout the entire clear span. The fabrics were extended to the bottom face of the flange on both sides of the web.

Retrofit of Beam 4 (clear span = 10 m) consisted of a pair 102-mm wide by 4.8-mm thick plates that were bonded to the soffit, and anchored at the ends as shown in Fig. 3. The 102-mm wide plates had unidirectional carbon fibers along the plate and biaxial E-glass at +/- 45 deg. Installation of the plates was similar to Beam 2. After allowing the epoxy to dry for 24 hours, 76.2 mm long A325 anchors were installed at each end. The anchors were 12.7 mm in diameter. The holes were drilled at not less than 152 mm on center with the first hole placed not closer than 36 mm from the ends of the plate. As seen from Fig. 3, the anchor bolts were staggered. The spacing between the anchor bolts had to be varied to avoid hitting the beam reinforcement. These bolts were primarily

intended to delay debonding of the FRP plates, and if possible, to ensure continued participation of the FRP plates after debonding. If anchor bolts had not been used, ACI 440 guides would specify cut-off points at 661 mm from the face of the support. As evident from Fig. 3, the plates extended beyond the east support, and were terminated at 171 and 203 mm from the face of the west support. The additional extension on the east side was due to miscalculations about the final location of the support. Considering the age and condition of this beam, the extra length of the FRP plates on the west side provided additional margin of safety against debonding.

Instrumentation and Testing Program

The test specimens were instrumented to (a) obtain load-deflection relationships at the quarter points and midspan; (b) monitor strain in the lowest longitudinal bars at the midspan; (c) strain profile through the depth at the midspan; (d) measure concrete surface strain on the web soffit at the quarter points; and (e) measure strains in each FRP plate at the midspan and quarter points in Beams 2 and 4, and strains on the fabric in Beam 3.

Each beam was initially loaded to produce 50% of the yield strain in the lowest longitudinal reinforcing bars. After retrofitting the beams, each beam was loaded to their ultimate limit state, which was arbitrarily defined as a midspan deflection of at least $L/115$, where L is the center-to-center span. Most beams were loaded beyond this level. The beams were loaded and unloaded several times before reaching the final target displacement to examine cyclic behavior of the retrofitted beams. The as-is beams were tested in a three-point bending setup. Due to scheduling issues, another reaction frame had to be used to test the beams after retrofitting. In the new test setup, the beams were subjected to two point loads located at 203 mm on either side of the beam centerline. The distance between the point loads is small in comparison to the span, and this setup is also equivalent to three-point bending. The slight differences between the two test setups were taken into account when the test results before and after retrofit program were compared. All the tests were conducted outdoors at a local prestressing yard. Additional details are provided elsewhere (Shahrooz

and Boy, 2001).

Considering that only one set of beams was available, the response of the as-is beams beyond the initial load levels had to be generated analytically. Having an understanding about the expected response of the as-is beams helped more detailed synthesis and understanding of the measured responses of the retrofitted beams. The analytical techniques used to generate the expected responses are discussed prior to presenting the measured results.

ANALYTICAL MODELING

The expected load-deflection relationships for the as-is and retrofitted beams were generated by double integration of the appropriate moment-curvature relationship along the length (Zhang and Shahrooz, 1999). This method has been found to reasonably replicate the actual behavior of under-reinforced flexural beams (Gillum et al., 1998). With the use of a computer program (BIAX, 1992), the necessary moment-curvature relationships were obtained by analyzing fiber models of the as-is and retrofitted beams. The measured dimensions (Fig. 1), except for the flange thickness, were used in establishing the fiber model. Field inspections indicated that the top portion of the flanges of all the test beams were deteriorated, often consisting of loose aggregates, to a level that could not be considered effective. Based on field measurements, the flange thickness in the fiber model was reduced by 25.4, 50.8, 38, 51 mm in Beams 1, 2, 3, and 4, respectively. The measured material properties were incorporated in the models. The nominal area of the reinforcing bars was reduced by 12% to account for the effects of corrosion as suggested in a previous study (Zwick et al, 1992).

For Beams 2, 3, and 4 that were retrofitted with CFRP plates or fabrics, generation of the moment-curvature relationships was essentially the same as that for the as-is beams. The CFRP reinforcement was incorporated in the fiber model as an extra layer of reinforcement (with the area equal to that of the CFRP) located at the elevation corresponding to half thickness of the CFRP. Perfect bond between the plates or fabrics and concrete was assumed in the model. Considering that CFRP reinforcement was assumed to work compositely with the substrate until fracture, the

generated load-deflection responses would give the upper bound response and capacity of the retrofitted beams.

TEST RESULTS

The results for each beam are presented and discussed separately. The performance of each beam is evaluated with respect to (a) load-deflection behavior, (b) stiffness characteristics, (c) mode of failure, and (c) strain distribution between the bonded FRP plates or fabrics and substrate.

Beam 1

Post-tensioning Force

The initial force in the instrumented rod immediately after release of the jacking force was measured to be 51.7 kN. Considering that each rod had been post-tensioned to 57.8 kN, the initial seating and relaxation loss is estimated to be 10.5%. Using a load cell, the variation of post-tensioning force in one of the rods was monitored for 73 days. The data presented in Fig. 4 suggest that the level of post-tensioning force fluctuates by about 1 kN as a function of temperature. The external post-tensioning system did not appear to experience additional losses beyond what was measured initially.

Stiffness

The initial slope of the measured load-midspan deflection curves before and after retrofitting (Fig. 5) was used to infer the flexural stiffness, EI . At the maximum initial load, the as-is beam experienced a number of new cracks as shown in the inset in Fig. 5. Some of the existing cracks also opened. Most of these cracks closed after unloading. The experimental data suggest that external post-tensioning increased the initial stiffness by about 9%. The exact value of the increase may be slightly more or slightly less because of the small differences in the locations of the neoprene pads (used as supports) in the as-is and post-retrofit tests, and possible changes in the stiffness characteristics of the pads due to the differences in the ambient temperatures (the as-is beam was tested in winter, whereas the retrofitted beam was tested in a hot summer day).

Capacity

Using the analytical results of the as-is beam, the moment corresponding to the strain measured in the longitudinal bar at the maximum measured deflection was obtained. This moment was used to back calculate what the as-is beam would have likely resisted had it been subjected to the same maximum measured deflection. This load was found to be 339 kN. At the maximum deflection, the retrofitted beam resisted a load of 388 kN; hence, external post-tensioning enhanced the capacity by 14%.

Modeling the external post-tensioning rods as tension ties, the capacity of the retrofitted beam was computed. The force measured in the instrumented rod prior to loading the beam (i.e., the target pre-stressing force minus 10.5% loss) was used in the analytical model as the tension tie force in all the rods. Based on this model, the capacity of the retrofitted model was computed as 380 kN, which is 2.3% less than the maximum measured load. A tension tie model appears to provide a reasonable method for computing the capacity of this beam.

Parametric Study

In an effort to examine whether the capacity could have been increased more than what was achieved, a parametric study involving increasing the post-tensioning force and/or lowering the anchor assembly was conducted. Three cases were considered, case (a): stress the rods to 75% of their ultimate capacity instead of 45% of the ultimate capacity, i.e., reduce the factor of safety to 1.2 instead of 2, but do not change the location of the anchors; case (b): lower the bottom carbon rod to 131 mm from the bottom of the web, and reduce the distance between the rods to 102 mm, but the rods are stressed to 45% of their ultimate capacity, i.e., the prestressing force used for Beam 1; and case (c): combine the higher post-tensioning force of case (a) and the lower position of the anchor system of case (b). The lower locations of the anchor system would not interfere with the beam longitudinal reinforcing bars. The additional force in case (a) would have increased the capacity by 1.2% over what was possible in Beam 1. For the same level of post-tensioning force in the rods in

case (b), 4% more capacity would have been possible by lowering the rods. If the rods were lower and were stressed to a higher load (i.e., case c), the capacity of the beam would have been 8% larger than what was achieved in Beam 1. Therefore, external post-tensioning would have likely increased the capacity of the concrete beam by 22%, instead of 14% in Beam 1, had the modifications of case (c) been implemented.

Beam 2

Stiffness

The stiffness of the beam before and after retrofitting was computed from the initial slope of the load-midspan deflection curves (Fig. 6), and by transformed section analysis in which standard techniques were used to transform the CFRP plates and reinforcing bars. Considering the condition of the beam, only the cracked section was considered. The change in stiffness is summarized in Table 3. Transformed section analysis indicates an increase of 4.2% in the stiffness in comparison to a 9% increase that was inferred from the measured load-midspan deflection curves. This difference is attributed to the slight variations in the test setup before and after retrofit, which would affect the inferred value of EI.

Behavior, Damage Pattern, and Mode of Failure

The crack pattern, condition of bond between the FRP plates and concrete, and mode of failure are illustrated in a number of insets in Fig. 6. At 335 kN ($\delta = 27.2$ mm where $\delta =$ midspan deflection), yielding of the instrumented longitudinal steel reinforcing bar at the midspan was detected. The FRP plates were bonded up to this point. However, at 357 kN ($\delta = 46.8$ mm), the FRP plates were apparently debonded as evident from the strain profile shown in Fig. 7a. Up to this load, the strain in the FRP plates was larger than the reinforcing bar strain, which suggests satisfactory bond transfer between the FRP plates and beam. Upon unloading (Point “A” in Fig.6), evidence of local debonding was visible. The north plate was found debonded 711 and 1345 mm to the east and

west of the beam centerline, respectively; and the south plate debonded 660 and 1041 mm to the east and west of the beam centerline, respectively. Local debonding extended further upon reloading, and at 360 kN ($\delta = 58.5$ mm) both of the plates debonded completely on the west side and fell (inset “b” in Fig. 6). The failure was apparently due to bond failure. The bond failure occurred at displacement ductility (defined as displacement at failure divided by the displacement at which the longitudinal bars yielded) was 2.15. Despite the age of the beam and its condition, the repair method was apparently successful in view of the displacement ductility, and the fact that debonding occurred after yielding of the bars. Loss of bond between the FRP plates and beam led to a sudden drop of 11% in the load carrying capacity. At point “B” (Fig. 6), local debonding of the plates that were still bonded to the beam was observed to have extended to 965 and 1143 mm to the east of the beam centerline for the south and north plates, respectively.

In spite of local debonding on either side of the midspan, the plates were still actively participating towards enhancing the capacity. Figs. 7b and 7c show the average strain in the FRP plates and concrete surface strain at the east and west quarter points, respectively. Up to complete debonding of the plates on the west side, the strains in the FRP plates continued to be larger than the concrete strain, which suggests adequate bond transfer. The strain in the FRP plates at the west quarter point reached a maximum of 3030 microstrains immediately before debonding. At this strain, the plates had developed 22% of their ultimate strength. After debonding on the west half of the beam, the plates at the east quarter point continued to work with the substrate as evident from the concrete strain and strain in the FRP plates (Fig. 7b). Bond transfer was apparently not uniform along the length. Throughout the test, up to complete debonding on the west half of the beam, the strains in the FRP plates on the west quarter point were between 1.5 to 2 times larger than their counterparts on the east quarter point. Immediately before complete debonding, the strain at the west quarter point became 6.5 times larger than the corresponding strain at the east quarter point.

Capacity

The nominal capacity of the retrofitted beam was computed based on the procedures outlined in ACI 440 guides (2000). The measured dimensions, except for the flange thickness as discussed previously, and material properties were used in the calculations. Considering that the beam was tested within a couple of months after installation of the CFRP plates, the environmental reduction factor recommended in ACI 440 guides, which is intended to account for the influence of long-term exposure to environmental conditions, was set to 1. The beam could reach and exceed the expected capacity by 30% despite its age and condition.

The expected load-deflection curves of the as-is and retrofitted beam are compared against the measured response in Fig. 6. The computed load-deflection curve reasonably matches the measured response up to the point at which the plates apparently debonded. Beyond this point, the analytical result, which does not account for debonding of the plates, tends to predict a larger capacity than the measured values. For example, at the deflection immediately before the plates were completely debonded on the western half of the beam, the measured load was 360 kN versus 373 kN from the analytical model. After full debonding of the plates on the west half of the beam, the measured load-deflection curve follows the computed curve for the as-is beam. In other words, after debonding of the plates on the west side, the beam behaved similar to the unretrofitted beam. Although the plates on the eastern half of the beam continued to work compositely with the substrate (see Fig. 7b), these plates could not enhance the capacity after debonding on the west half.

The retrofit scheme increased the capacity of the as-is beam by about 10% as indicated by comparing the maximum measured load versus the expected capacity of the as-is beam. The analytical load-deflection of the retrofitted beam suggests that the capacity of the beam could have been increased by another 15% if the plates had developed their ultimate strength. Bond failure on the west half of the beam prevented the beam from reaching the maximum possible capacity.

Beam 3

Stiffness

The stiffness gain after bonding of the longitudinal and transverse fabrics is summarized in Table 3. Similar to Beam 2, the increase in the stiffness based on the measured load-deflection curves is about twice that obtained from transformed section analysis. Slight changes in the way the beam was supported before and after retrofitting can explain this difference. In spite of questions regarding the exact value of stiffness gain, both the inferred and computed values of EI suggest that two layers of longitudinal and transverse CFRP fabrics in Beam 3 increased the stiffness more than what was possible by bonding two 76.2-mm CFRP plates in Beam 2.

Behavior, Damage Pattern, and Mode of Failure

In contrast to Beam 2, this beam did not exhibit a sudden mode of failure. The transverse and longitudinal fabrics began to crack gradually as the crack width in the substrate concrete widened. The fracture strain of the longitudinal and web fabrics is 85 and 25 times larger than the strain at which the concrete is expected to initially crack. Therefore, the fabrics did not fracture until the cracks had widened considerably. The first sounds of fabric fracturing were heard at 133 kN ($\delta = 5$ mm), followed by another set of fracturing sounds at 214 kN ($\delta = 6.8$ mm) and 329 kN ($\delta = 16.5$ mm), as identified in Fig. 8. These fractures were apparently localized since the load-deflection response of the beam was not affected. A larger portion of the longitudinal fabrics apparently fractured after reaching 378 kN ($\delta = 45.7$ mm) as evident by a drop in the load carrying capacity. After pushing the beam to a midspan deflection of 55 mm, the beam was unloaded. The insets in Fig. 8 suggest a relatively widespread fracturing of the web and longitudinal fabrics. Upon reloading, the regions where the fabrics had fractured continued to increase, but the fabrics essentially remained intact and prevented major spalling and damage of the concrete substrate. The beam was “intact” at the conclusion of testing despite having a permanent deflection of 110 mm (or

L/86). The strain gage on the reinforcing bar had malfunctioned, and as a result data regarding yielding of the longitudinal bars were not available. However, the trend of the load-deflection curve suggests that the drop in the load carrying capacity occurred after yielding of the longitudinal bars.

Capacity

The beam was able to reach and exceed the nominal capacity computed based on ACI 440 guides (2000), which was 337 kN. As explained for Beam 2, environmental exposure reduction factor was set equal to one in the calculations. The retrofit method was successful in terms of developing a load that was 12% larger than the expected capacity.

The analytical results provided a method for estimating the extent of fracturing in the fabrics. At the points marked by “■” in Fig. 8, the portions shown in the figure were assumed to have fractured, and the area of the fabric was reduced accordingly in the model. Up to point “c”, at which 203 mm width of the longitudinal fabric was assumed to have been lost, fracture of the transverse and longitudinal fabrics was limited to 102 mm on either side of the centerline of the beam. Beyond point “c”, the width of the remaining longitudinal fabric was not reduced further; however, loss of the transverse and a portion of the longitudinal fabric were gradually extended to 267 mm on either side of the centerline. At the maximum measured deflection, within 534 mm around the centerline of the beam, the transverse fabric was assumed to have fractured completely, and only 102 mm width of the longitudinal fabric was assumed to provide strength. Beyond this region around the centerline, the transverse fabrics and the entire width of the longitudinal fabrics were assumed to be intact. The spread of fractured fabrics assumed in the model corresponded reasonably to the field observations. The analytical model correlated well with the measured load-deflection curve, as evident from Fig. 8. The analytical model was not intended to replicate the exact sequence of fracturing of the fabrics at various locations, but it was meant to demonstrate that fracture of the transverse, and a portion of the longitudinal fabrics, was concentrated locally around the centerline. The gradual spread of fracturing

of the fabrics in the analytical model, and the observed mode of failure of Beam 3, point to a fundamental difference in the behavior of Beams 2 and 3. A significant amount of redistribution was possible in Beam 3 beyond the initial fracturing of the fabrics, whereas Beam 2 did not exhibit a similar behavior.

Comparing the measured load-deflection curve and that computed for the as-is beam indicates that at the conclusion of testing, despite local fracturing of the transverse and longitudinal fabrics around the beam centerline, the measured loads were larger than what the as-is beam could have likely resisted because of the continued participation of the fabrics that were intact. For example, at the maximum measured deflection, the load resisted by the retrofitted beam was 3% larger than the predicted load-carrying capacity of the as-is beam. For Beam 2, the load resisted by the retrofitted beam became essentially the same as the original beam after complete debonding of the plates on the west half.

Beam 4

Stiffness

The change in the flexural stiffness based on the value inferred from the load-midspan deflection, and from transformed section analysis, is compared in Table 3. Similar to Beams 2 and 3, the inferred value is about twice the computed value. The slight changes in the support conditions in the test setups before and after retrofit likely affected the measured responses and hence the inferred value of EI. The increase in stiffness predicted by either method is larger than the corresponding values for Beams 2 and 3, which is expected considering the larger thickness and width of the plates used in Beam 4.

Behavior, Damage Pattern, and Mode of Failure

Despite undergoing the largest deformations among all the test specimens and experiencing a significant amount of damage, the mechanical anchorage at the ends of the plates prevented a complete debonding of the plates. As seen from Fig. 9, the reinforcing bars at the midspan yielded at

300 kN ($\delta = 30.2$ mm, where δ is the midspan deflection). The strain profile at the midspan shown in Fig. 10a suggests initiation of local debonding of the plates around the midspan at an applied load of 311 kN. Upon unloading, the beam had a permanent deflection of 42 mm, and the beam had experienced major cracks as shown in the inset in Fig. 9. The north plates had debonded 1435 and 813 mm to the east and west of the beam centerline, respectively. A gap between the substrate concrete and the FRP plates at the midspan was visible (refer to the inset in Fig. 9). The plates debonded further after reloading. When the beam had a permanent deflection of 61 mm, the north plate had debonded to the location of the first anchor on the east side but no additional debonding was identified toward the west, and the south plate was debonded to 1778 and 1168 mm to the east and west side of the beam centerline, respectively. At the conclusion of testing, the beam had experienced major cracking and spalling (see the inset in Fig. 9). The north plate was completely debonded between the first set of anchors (those closer to the midspan) on the west and east sides, but it was still connected to the beam. The anchors had apparently prevented further debonding towards the supports. The south plate on the west side was debonded back to the first anchor, and it was debonded to the east quarter point. Despite extensive debonding, the plates continued to provide resistance as evident from the strains measured at the east and west quarter points (Figs. 10b and 10c).

Behavior of Anchored CFRP Plates

After local debonding of the plates, strain compatibility between the plates and beam was lost, and the strain in the plates dropped (Fig. 10a). Nevertheless, the plates continued to participate, albeit at a smaller level. The schematic deflected shape of the beam shown in Fig. 11 is used to explain the behavior of the anchored plates. After the plates debond between the anchor points, the beam curvature, and the beam rotation at the anchor points (θ_1 in Fig. 11) elongate the plates and produce tensile force. The component due to the curvature is appreciably smaller than that from the

beam rotation at the anchor points and may be ignored; hence, the elongation between the anchor points is taken as $\theta_1 h$, where h = distance from the neutral axis to the plates (Shahrooz and Boy, 2001). (The distance to the neutral axis is used to compute the elongation since the length of the beam along the neutral axis does not change, and corresponds to the original distance between the anchor points, L_1 . Moreover, the neutral axis for the uncracked section is used since the beam is not expected to crack at the anchor points.) The force in each plate is, thus, $AE \frac{2\theta_1 h}{L_1}$ where A = area of one plate and E = modulus of elasticity of the CFRP plates. Using basic principles, rotation θ_1 can be expressed in terms of the midspan deflection (δ). Therefore, the force in each plate (F) is $\frac{2AE}{L_1} h \frac{12\delta}{L^3} \left(\frac{L^2}{4} - a^2 \right)$ or $\frac{2AE}{L_1} h \frac{2\delta}{L}$ depending on whether the beam is assumed to be elastic or fully plastic (Shahrooz and Boy, 2001). Note that once a plate is debonded between the anchor points, the force in that plate is constant along its length. In Fig. 12, the force in one plate computed from these equations is compared against the measured average force in one plate (obtained by multiplying the area of one plate, the measured CFRP plate modulus of elasticity, and the average strain based on the measured data at the midspan and quarter points of the north and south plates). The analytical results based on elastic or full plastic behavior of the beam clearly bracket the measured forces. Considering that the beam was neither elastic nor fully plastic, the average force from the two equations is recommended. The resulting average force matches the experimental data remarkably well (Fig. 12), particularly at larger deflections when the plates had debonded over large distances. For smaller deflections, the average computed forces tend to be less than their experimental counterparts since strain compatibility would result in a larger force than that from the model, which assumes full debonding between the anchor points.

The aforementioned model may be used to explain the response of the plates before complete debonding between the anchor points. For this purpose, L_1 is viewed as the distance between the

points where the plate is bonded to the substrate. The model suggests that the force in the plate is inversely proportional to this distance; hence, this force should drop when plate debonding extends, and the force in the debonded region should equilibrate toward a single value over the debonded length. This behavior was observed experimentally. For example, at the midspan deflection of 88.5 mm the force (computed from the measured strains) at the east quarter point, midspan, and west quarter point of the south plate was 15, 124, 16 kN, respectively. Note that at the quarter points, the plate was bonded to the substrate, and the strain in the plate at these locations was governed by strain compatibility. However, when the deflection was increased to 88.7 mm, the forces changed suddenly to 93, 98, and 16 kN when the plate was debonded back to the east quarter point. The force between the beam centerline and east quarter point is essentially constant (within 5% of each other), and smaller than the force before debonding extended to the east quarter point. The model suggests this response. A similar behavior was observed when debonding extended to the west quarter point, and for the north plate. As a result of a series of such drops, the maximum tensile force in the north and south plate reached 35% and 38% of the load that would have fractured the plates. Upon unloading, at the final permanent deflection of 116 mm, the tensile strain in the north plate and south plate was 27% and 28% of the fracture strain, respectively. Therefore, the plates did not fracture and continued to participate towards increasing the capacity.

Capacity

The recommendations in ACI 440 guides do not provide specific procedures for calculating the capacity of bonded plates with mechanical anchors. The computed load-deflection curves of the as-is and retrofitted beam provided additional information for further synthesis of the observed behavior. At the maximum midspan deflection, the load resisted by retrofitted Beam 4 is 7% larger than the unretrofitted beam. The computed response of the retrofitted beam shows that 12% more load could have been resisted had the CFRP plates reached their ultimate capacity. Beyond the load at which the FRP plates would have fractured, the computed load-deflection response is, as expected,

identical to that of the as-is beam. As discussed previously, a series of local debondings along the length lowered the force in the plates; hence, the plates did not develop their ultimate capacity. Based on the developed analytical model, the plates, after complete debonding between the anchor points, would have reached their ultimate capacity at the midspan deflection of 440 mm (or $L/23$). Therefore, the beam could not realistically reach its full capacity corresponding to plate rupture. Although the beam resisted a load smaller than that corresponding to fracture of the plates, the beam performed better in terms of ductility and maintaining its load-carrying capacity. The beam developed a displacement ductility of slightly more than 5, and the load resisted by the beam did not decrease after reaching deflections as large as $L/65$. (The small decrease before the last unloading cycle (Fig. 10) is due to a slight pressure drop in the hydraulic system before releasing the load.). In contrast, if the plates had been bonded perfectly to the substrate, the beam would have developed a displacement ductility of 1.35, followed by a sudden drop in strength after fracture of the plates.

The flexural capacity of the retrofitted beam is essentially the sum of the capacity of the reinforced concrete section and the additional moment from the tension in the CFRP plates. For a given deflection, the force in the plates can be computed from the analytical model. The model becomes more reasonable after the plates debond over a larger portion of their length. Before this stage, however, the computed force is less than the actual value because the strain in the plates is governed by strain compatibility at the locations where the plates are bonded to the substrate. Therefore, the capacity of the retrofitted beam, as computed here, is less than the actual values for smaller deflections, when debonding is localized, and improves at larger deflections, when the plate debonding extends. For example, at the midspan deflection of 60, 80, 120, and 150 mm, the computed capacity is 318, 332, 360, and 379 kN, respectively versus the measured loads of 348, 353, 372, and 378 kN. Clearly, the model improves as plate debonding extends at larger deflections. Considering that the computed tension force in the plates is less than the actual values for small deflections, the method as described here provides a simple and conservative estimate of the

expected capacity. Additional studies are needed to develop a more comprehensive model that can capture the expected tension force in CFRP plates as local debonded lengths extend.

Comparison of Retrofitting Systems

The damage pattern and mode of failure of the beams clearly point to basic differences in the four systems. The CFRP fabrics bonded to Beam 3 prevented major spalling and damage of concrete that was observed in the other beams. The system used in Beam 3 was the most redundant as local fracturing of the fabrics around the beam centerline did not influence the overall behavior as the fabrics away from the midspan remained intact and could still provide resistance. A similar redundancy was clearly not evident for Beam 2 as local debonding of the CFRP plates led to eventual debonding along one half of the beam. After debonding, the response was similar to the unretrofitted beam. Beams 1 and 4 did not exhibit any major, sudden failure mode similar to Beams 2 and 3 because the basic mechanism behind the success of these beams, i.e., the anchorage of the CFRP rods in Beam 1 or the bolts at the ends of CFRP plates in Beam 4, did not fail. Clearly, these beams could be subjected to large midspan deflections ($L/116$ in Beam 1 and $L/65$ in Beam 4) without any failure. However, if the anchorage in either Beam 1 or 4 had failed, the failure would have likely been catastrophic because of the sudden release of the stored energy in the CFRP rods in Beam 1 or the bolted CFRP plates in Beam 4.

The analytical results in Figs. 5, 6, 8, and 9 indicate that the capacity of Beams 1, 2, 3, and 4 was enhanced by 14.2%, 9.9%, 9.2%, and 17.5%, respectively after retrofitting. The retrofit system used for Beams 1 and 4 increased the capacity the most. However, loss of anchorage in these beams would have led to a sudden and violent mode of failure. The anchorage details used in these beams were successful to prevent such a catastrophic failure mode.

SUMMARY AND CONCLUSIONS

Four 76-year old reinforced concrete T-beams were retrofitted with a different system employing carbon fiber polymer reinforced (CFRP) composites to investigate the ability of different

FRP systems to strengthen aged members with substantial deterioration. The systems used in this project were (a) external post-tensioning system with CFRP rods, (b) bonded CFRP plates, (c) bonded CFRP fabrics, and (d) bonded CFRP plates with mechanical anchors at the ends of the plates. The experimental data were augmented with analytical results to better understand the observed behavior, particularly when visual data or the measured data were insufficient. The analytical studies were also used for parametric studies, and developing the expected capacity of the as-is and retrofitted beams. Based on the presented data, the following observations and conclusions are drawn.

1. Despite significant deterioration in the beams, the retrofitted beams could develop and exceed the expected capacities computed from current guidelines for externally bonded FRP systems. The poor quality of concrete, however, apparently lowered the bond strength between CFRP plates and substrate. As a result, the plates in Beam 2 were debonded after developing only 22% of their ultimate strength.
2. The external CFRP post-tensioning rods in Beam 1, and anchored CFRP plates in Beam 4 resulted in the largest strength gain, and did not exhibit an appreciable loss of strength at large deflections. The anchor system in Beam 1 and anchors at the end of CFRP plates in Beam 4 were adequate to develop sufficient forces in the rods or anchored plates. If the anchor system in either beam had failed prematurely, the mode of failure would have been catastrophic, as large amounts of energy stored in the rods or plates would have been released suddenly. If adequate measures are taken to prevent anchorage failure, the systems used in Beams 1 and 4 apparently offer the best retrofitting option, particularly for members with extensive deterioration since these systems do not rely on the quality of bond between FRP plates and substrate.
3. Beam 3, with bonded longitudinal and transverse CFRP fabrics, displayed the highest level of redundancy. Fracturing of the fabrics, after widening of cracks, spread gradually to regions away from the midspan; hence, loss of strength was rather gradual. At large deflections (exceeding 1/100

of the span length), the fabrics could still enhance the capacity despite local fracturing at several locations. Although this system did not increase the capacity as much as external post-tensioning or bonded CFRP plates with mechanical anchorages, the use of bonded fabrics appears to be a viable choice for deteriorated members as bond to deteriorated substrate appears to be less critical.

4. The measured global responses of the retrofitted beams and/or their capacity can be correlated reasonably well through the use of relatively simple analytical models. These models can be used as effective design tools when current design guidelines do not provide specific recommendations about a particular retrofitting system.

ACKNOWLEDGEMENTS

The Ohio Department of Transportation and the Federal Highway Administration under contract number 14719(0) sponsored the study reported herein. The contents of this paper reflect the opinion the views of the authors who are solely responsible for the facts and accuracy of the data presented herein. It does not necessarily reflect the views or policies of ODOT or FHWA, and does not constitute a standard, specification, regulation, or recommendation. The authors acknowledge Messrs. Vikram Dalal and Brad Fagrell at ODOT. Testing of the beams was conducted at Prestressed Services, Inc. (PSI) in Melbourne, Kentucky with tremendous help from Mr. Don Bossie and his crew. The technical support personnel and many current and former graduate students at the University of Cincinnati Infrastructure Institute were instrumental in the successful completion of this project.

REFERENCES

ACI 440, "Guide for the Design and Construction of Externally Bonded FRP Systems for Strengthening Concrete Structures", Draft, American Concrete Institute, 2000

Concrete International, American Concrete Institute, Vol. 20, No. 6, 1998, pp. 22-58.

fib, "Design and Use of Externally Bonded FRP Reinforcement (FRP EBR) for Reinforced Concrete Structures," Final Draft, Progress Report of *fib* EBR group, International Concrete Federation.

Gillum, A.J., Cole J., Turer A., Shahrooz B.M., “Bond Characteristics of Portland Cement Overlays on Sealed Existing Bridge Decks”, Report No. UC-CII 98/02, Cincinnati Infrastructure Institute, 1998.

Neale, K.W., “FRPs for structural rehabilitation: a survey of recent progress”, *Progress in Structural Engineering and Material*, John Wiley & Sons, Vol. 2, Issue 2, 2000, pp. 133-138.

Shahrooz B.M. and Boy S., “Retrofit of Existing Reinforced Concrete Bridges with Fiber Reinforced Polymer Composites,” Report No. UC-CII 01/01, Cincinnati Infrastructure Institute, 2001.

Wallace, J.W., “BIAX – A Computer Program for the Analysis of Reinforced Concrete and Reinforced Masonry Sections”, Report No. CU/CEE-92/4, Clarkson University, 1992.

Zhang W., Shahrooz B.M., “A Comparison Between ACI, AISC, and Analytical Methods for Concrete-Filled Tubular Columns”, *ASCE Structural Journal*, 125(11)(1999): 1213-1223.

Zwick M., Aktan A.E., Miller R., Shahrooz B., Heckenmueller M., Ho I., Hrinko W., Toksoy T, “Nondestructive and Destructive Testing of a Reinforced Concrete Slab Bridge and Associated Analytical Studies,” Report No. UC-CII 92/02, Cincinnati Infrastructure Institute, 1992.

Table 1 Equivalent Cylinder Compressive Strength (MPa)

Beam	Web	Flange
1	53	20
2	46	19
3	45	17
4	44	23

Table 2 Material Properties for Various FRP Systems

(a) Carbon Fiber Rod and Plates

CFRP System	F_u (MPa)	E (MPa)	Fracture Strain (%)
9.5-mm rod*	2,069	137,900	1.50%
76.2 mm plate	2,289	155,052	1.48%
102 mm (Bolted plate)	585	53,095	1.10%

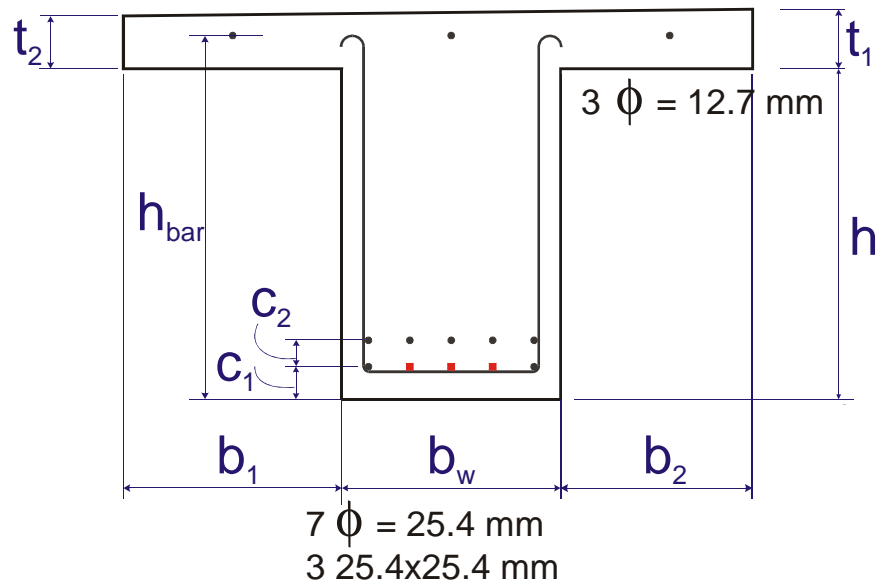
(b) Two Layers of Carbon Fabric Sheet

Fabric Orientation	F_u (kN/mm)	E (kN/mm)	Fracture Strain (%)
Longitudinal	1.30	117.3	1.11%
Transverse	0.031	9.69	0.32%

* Published properties for 9.5-mm rod are shown here. Properties for other systems were measured.

Table 3 Change in EI After Retrofitting

Beam	From P- δ	Cracked Transformed Section
2	9.0%	4.2%
3	9.3%	4.8%
4	14.2%	6.7%



Beam	b_1	b_w	b_2	h	t_1	t_2	h_{bar}	C_1	C_2
1	419	419	375	591	152	146	654	63.5	50.8
2	422	410	378	587	152	152	654	63.5	50.8
3	362	616	381	616	140	102	654	114	50.8
4	397	408	454	565	152	140	622	63.5	50.8

Figure 1 Dimensions and Reinforcement of T Beams

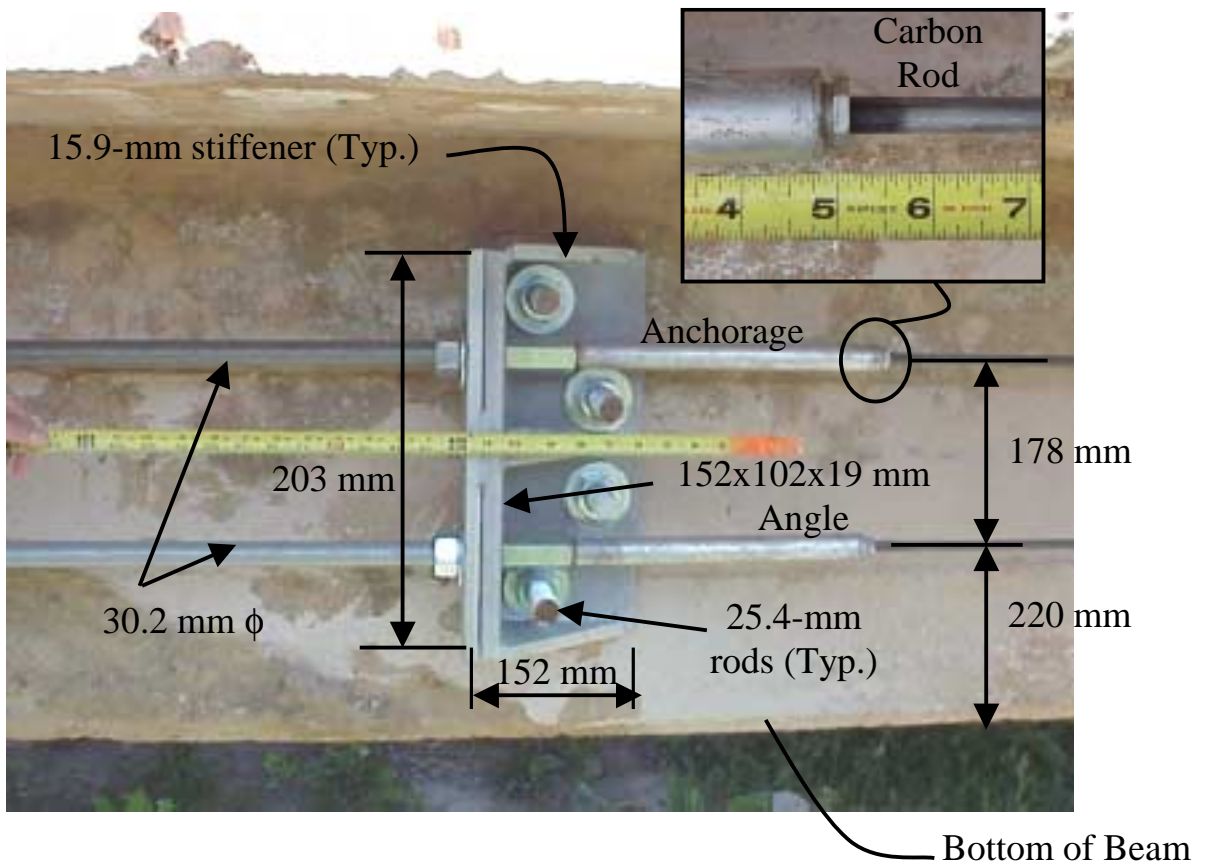


Figure 2 Elevation Views of Anchor System in Web of Beam 1

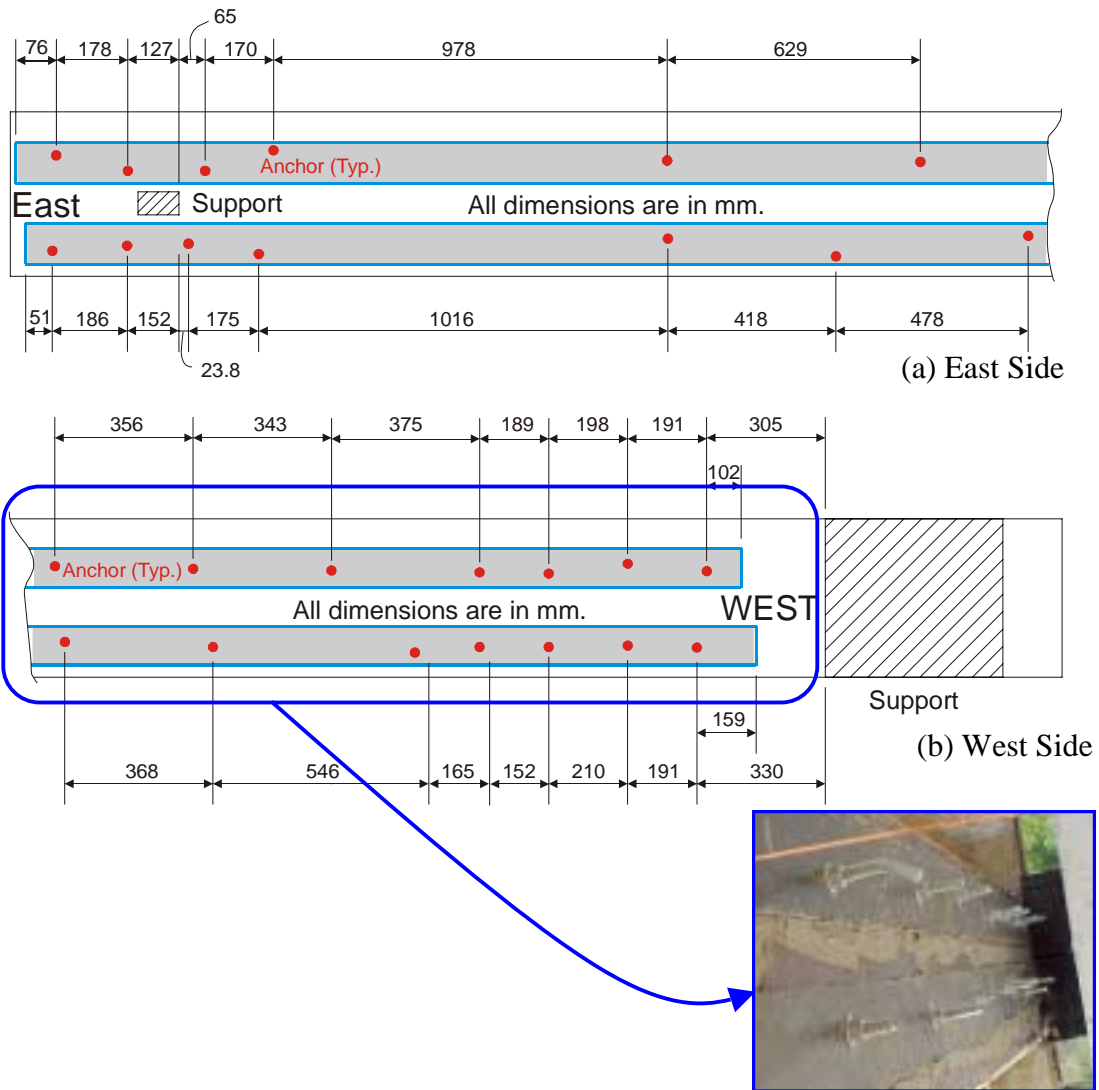


Figure 3 Bottom Views of Mechanical Anchorage in Beam 4

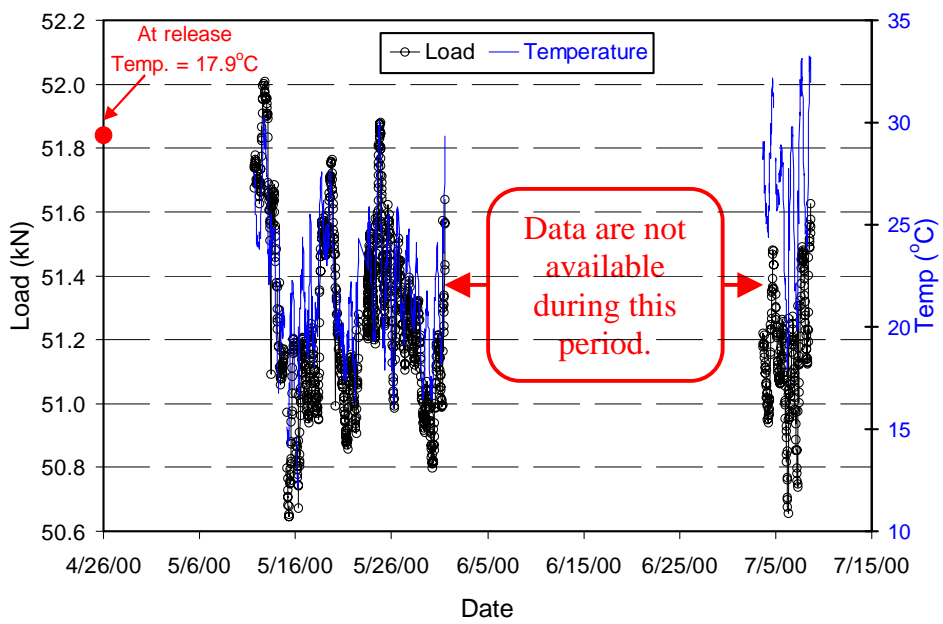


Figure 4 Variation of Pre-stressing Force in CFRP Rod over Time

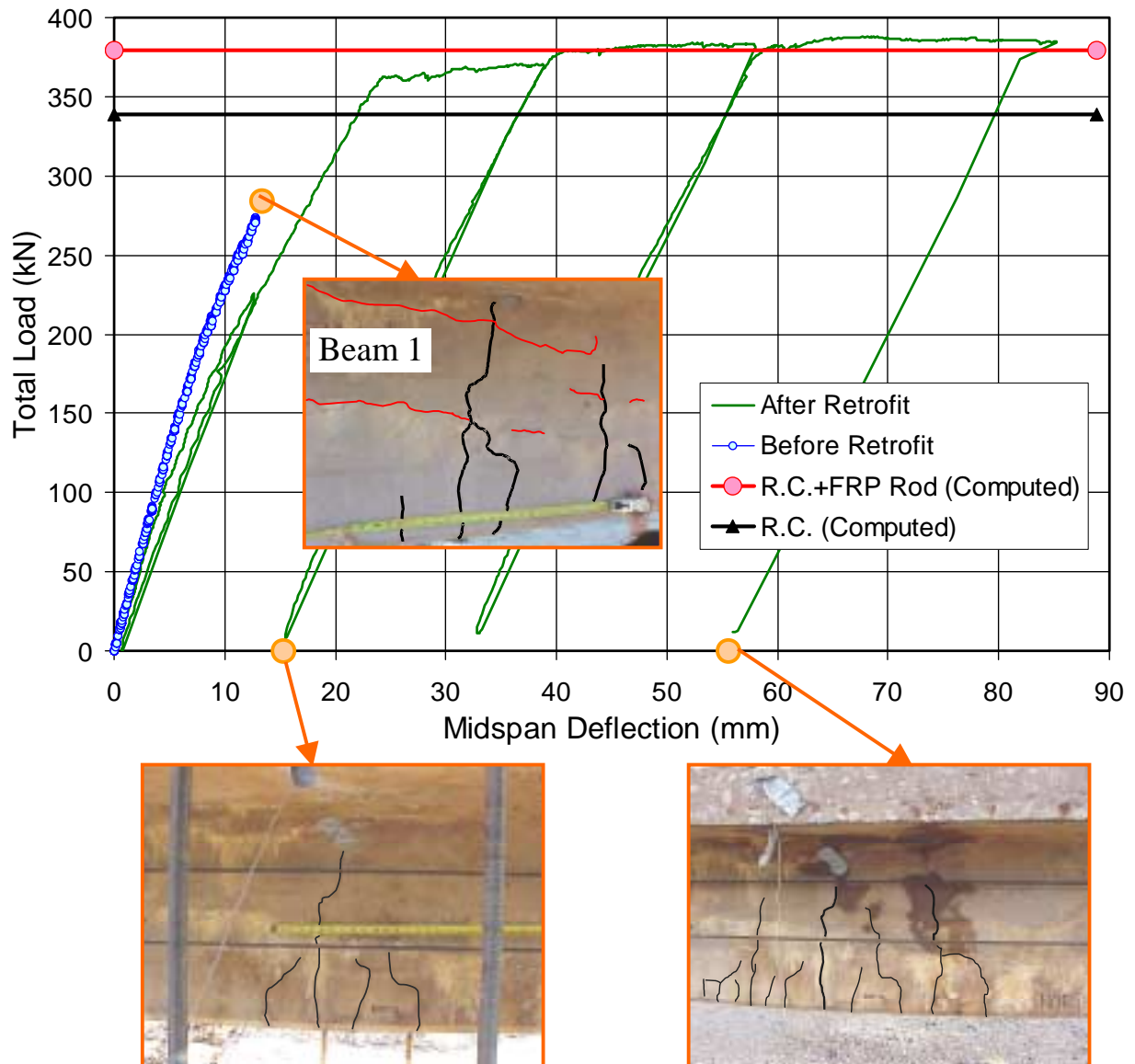


Figure 5 Load-Midspan Deflection and Damage Pattern in Beam 1

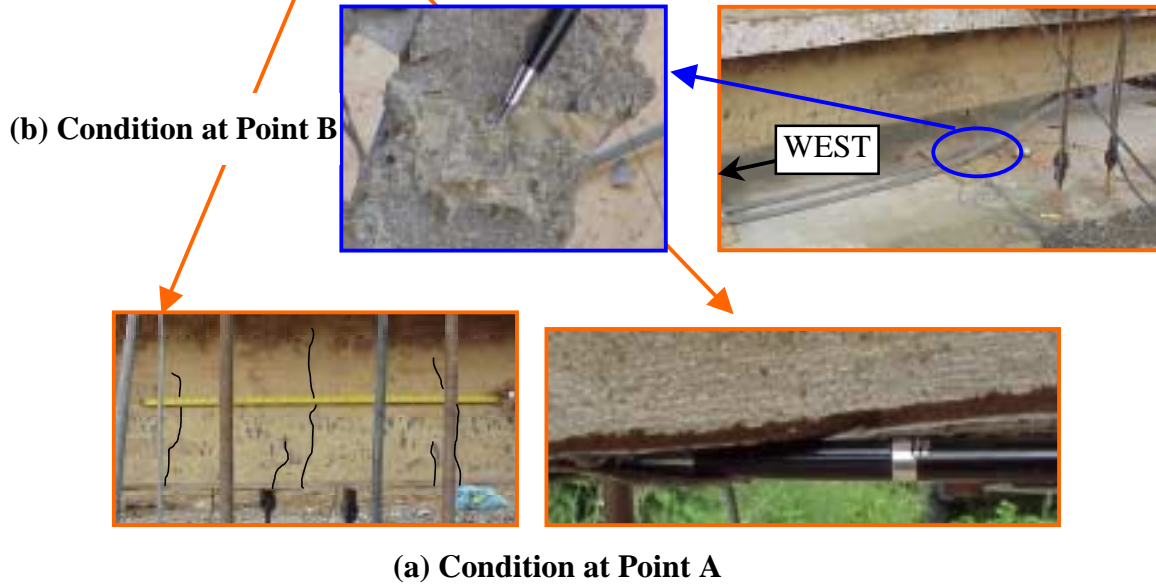
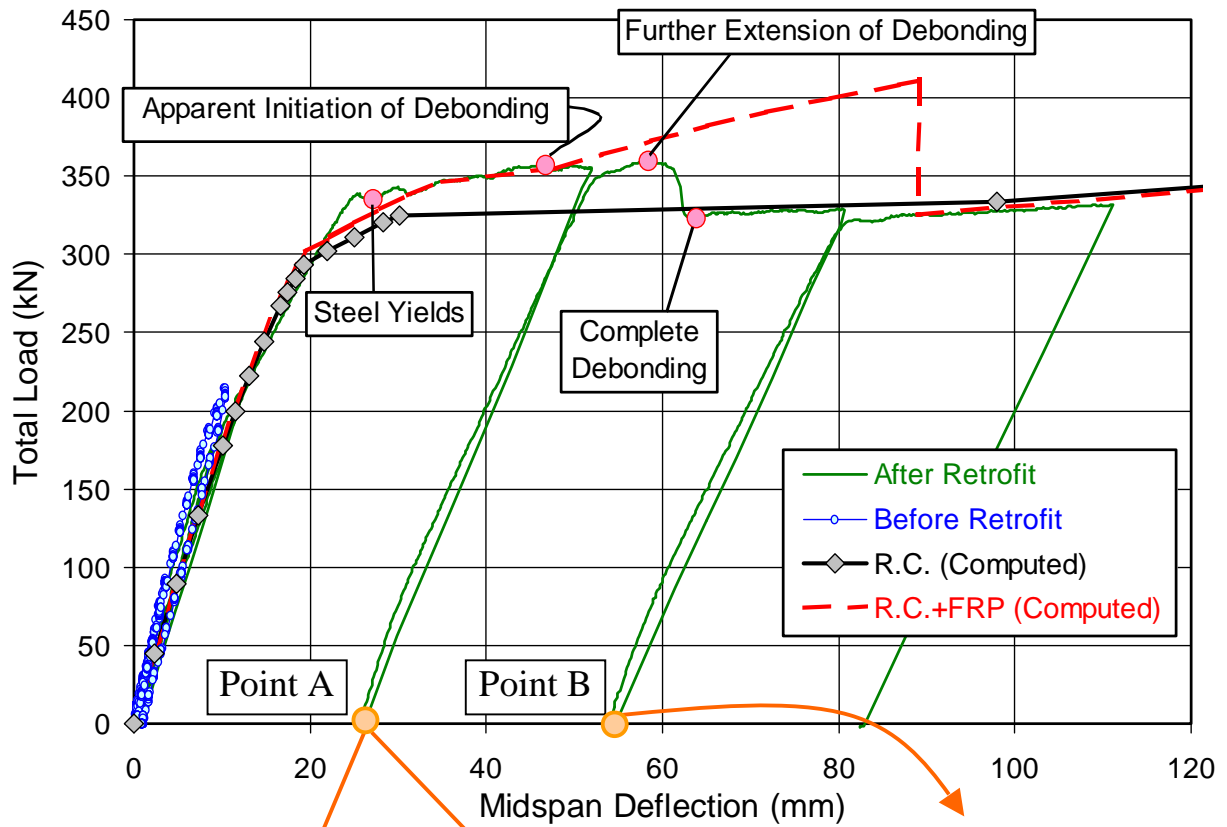
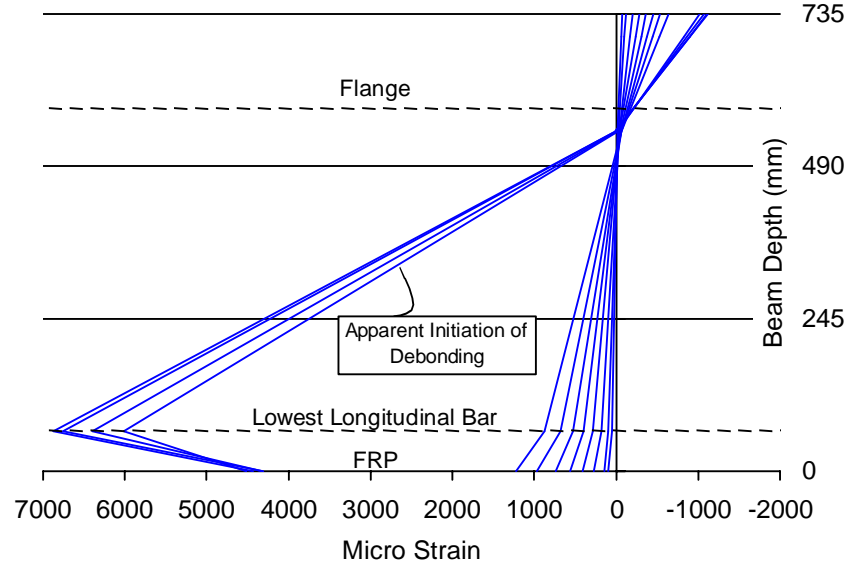
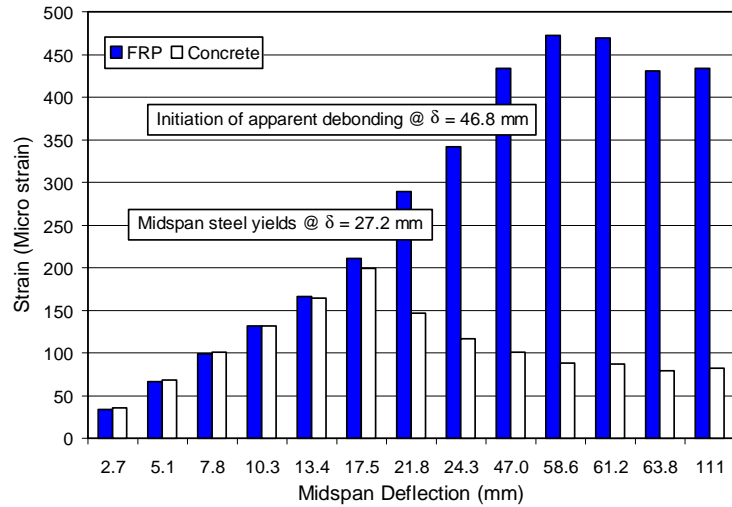


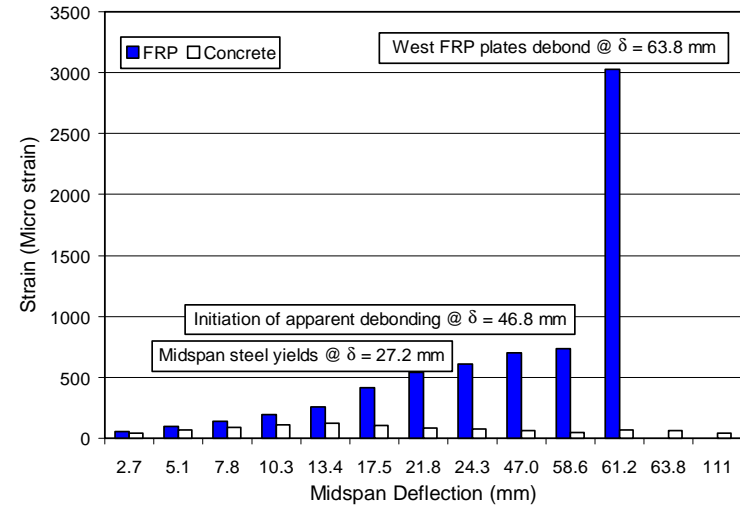
Figure 6 Load-Midspan Deflection Curve and Observed Damage in Beam 2



(a) Strain Profile at Midspan



(b) Concrete v.s. FRP Strain – East Quarter Point



(c) Concrete v.s. FRP Strain – West Quarter Point

Figure 7 Distribution of Strains in Beam 2

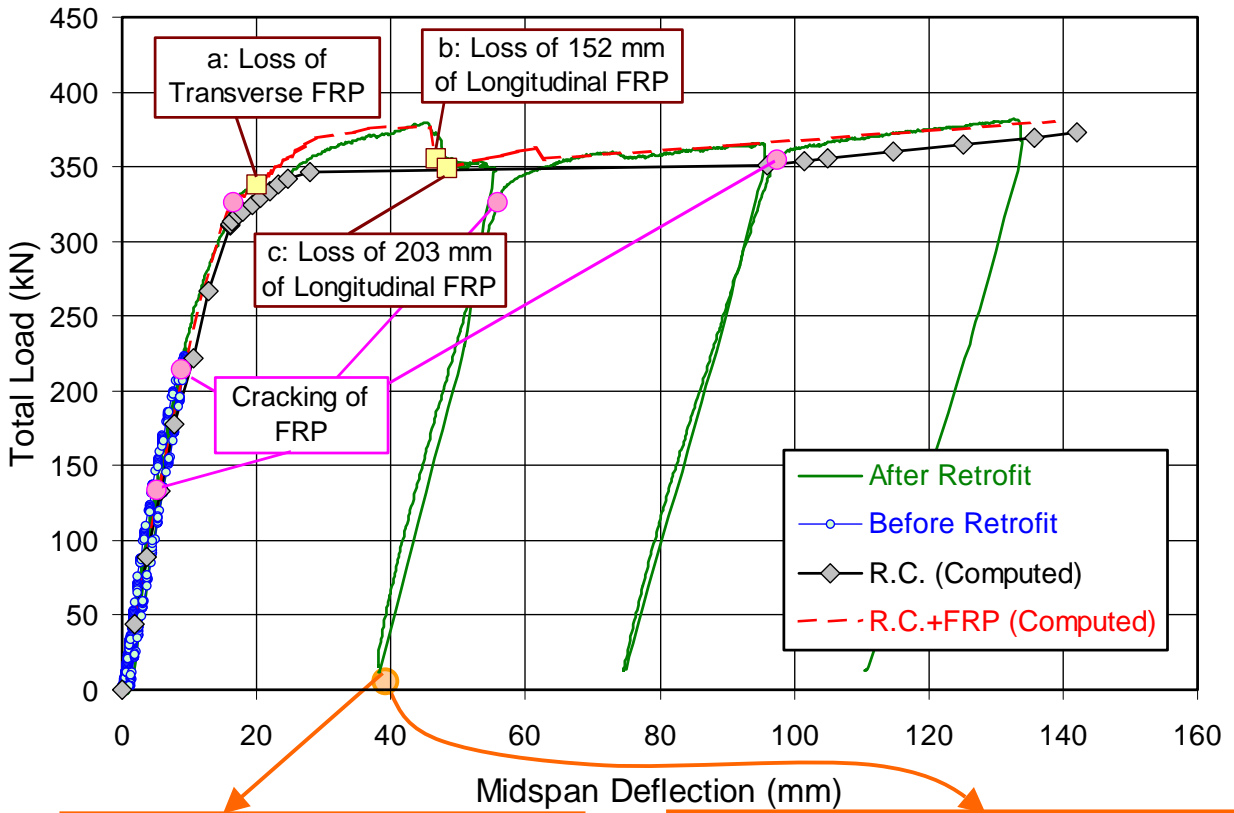


Figure 8 Load-Deflection and Damage Pattern in Beam 3

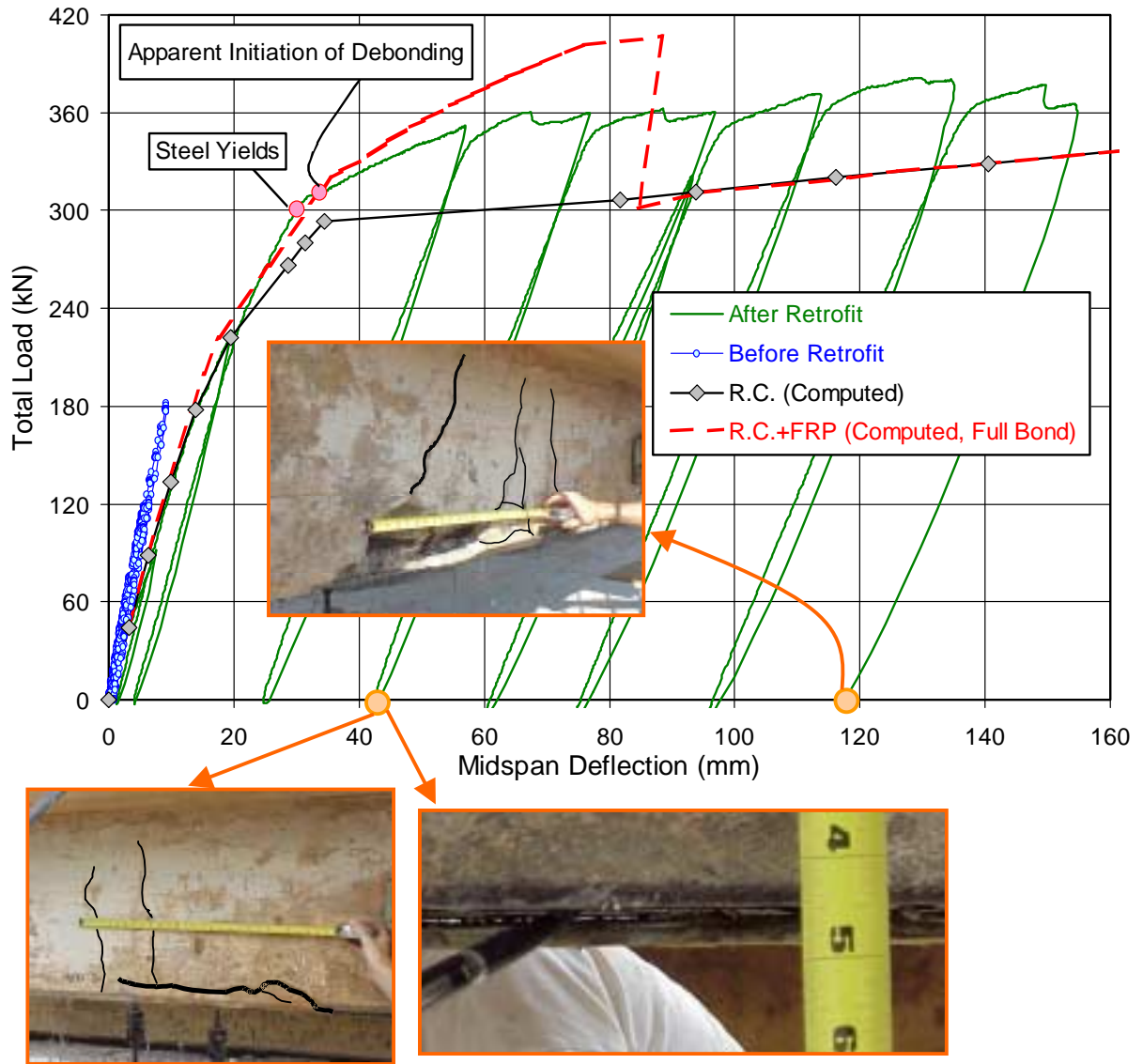
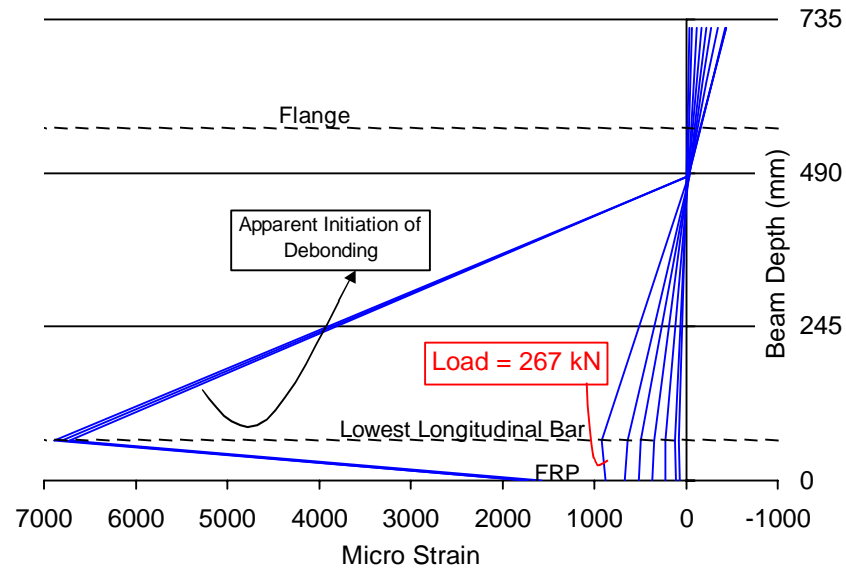
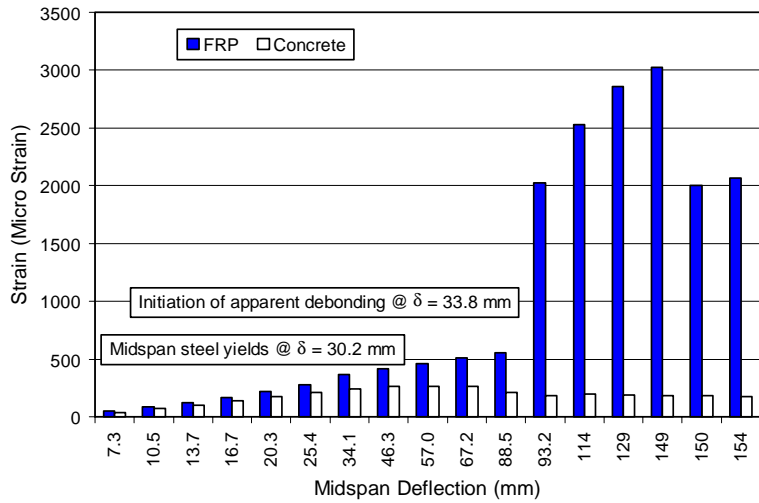


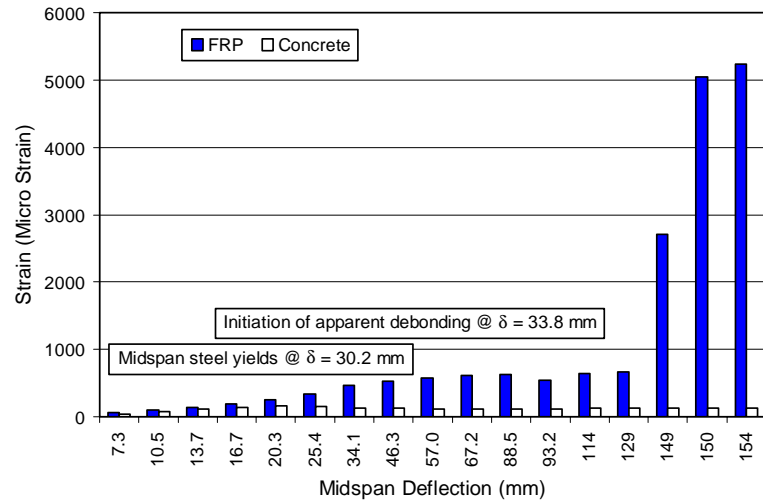
Figure 9 Load-Deflection and Damage Pattern – Beam 4



(a) Strain Profile at Midspan



(b) Concrete v.s. FRP Strain – East Quarter Point



(c) Concrete v.s. FRP Strain – West Quarter Point

Figure 10 Distribution of Strains in Beam 4

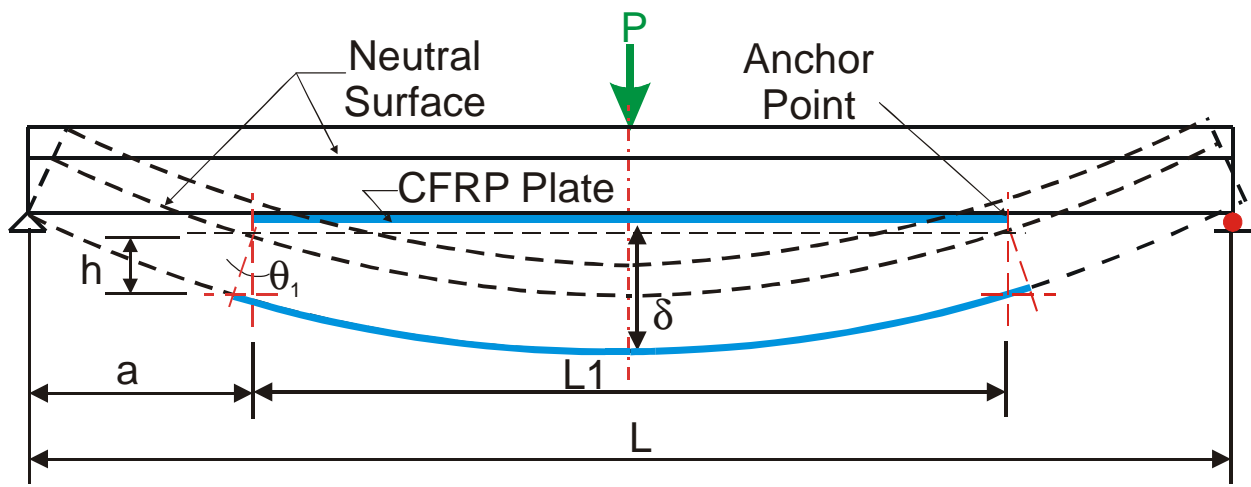


Figure 11. Elongation of CFRP Plates

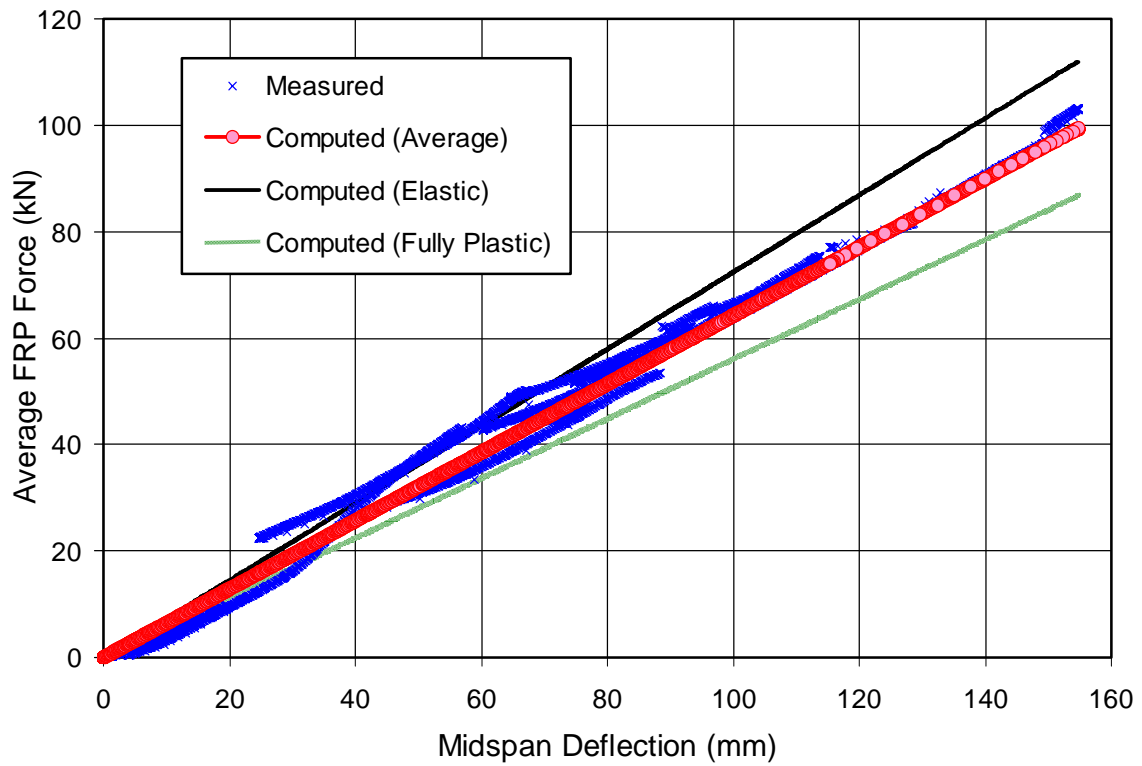


Figure 12. Measured v.s. Computed Tension Force in CFRP Plates

Retrofit of a Three-Span Slab Bridge with FRP Systems – Testing and Rating

ABSTRACT

A 45-year old, three-span reinforced concrete slab bridge with insufficient capacity was retrofitted with 76.2 and 127-mm wide bonded carbon fiber reinforced polymer (FRP) plates, 102-mm wide bonded carbon FRP plates with mechanical anchors at the ends, and bonded carbon FRP fabrics. The use of four systems in one bridge provided an opportunity to evaluate field installation issues, and to examine the long-term performance of each system under identical traffic and environmental conditions. Using controlled truckload tests, the response of the bridge before retrofitting, shortly after retrofitting, and after one year of service was measured. The stiffness of the FRP systems was small in comparison to the stiffness of the bridge deck, and accordingly the measured deflections did not noticeably change after retrofitting. The measured strains suggest participation of the FRP systems, and more importantly the strength of the retrofitted bridge was increased. A detailed three-dimensional finite element model of the original and retrofitted bridge was developed and calibrated based on the measured deflections. The model was used to more accurately predict the demands needed for computing the rating factors. The addition of FRP plates and fabrics led to a 22% increase in the rating factor and corresponding load limits. During a one-year period, traffic loading and environmental exposure did not apparently affect the performance of the FRP systems. In view of the increased capacity and performance of the FRP systems, load limits were removed and normal traffic was resumed. Future tests are necessary to monitor the long-term behavior of the FRP systems.

INTRODUCTION

As of August 2000, about 29% of the bridges in the National Bridge Inventory database have been identified as structurally deficient, functionally obsolete, or both. Many of these bridges fail to comply with current design codes, cannot resist traffic loads that are larger than the original design loads, and exhibit signs of deterioration due to years of service. If the inadequacies are structural, effective retrofit and strengthening systems can typically alleviate the need for other drastic options such as weight limit posting or total replacement. Therefore, the service life of a large number of the existing bridges can be extended.

Among various strengthening methods, the ones that use Fiber-Reinforced Polymer (FRP) composites are appealing as they have a high tensile strength, low weight, and high resistance to corrosion. Bridges can, therefore, be retrofitted more efficiently than if conventional systems, such as bonding steel plates, or steel or concrete jacketing, are used. The engineering community has recognized the advantages of FRP systems in recent years as evident from a large body of research (ACI 440, 2001 has a comprehensive bibliography of key previous research on the use of FRP materials for strengthening of concrete structures), by the development of design recommendations (e.g., ACI 440, 2001; fib, 2001), and application of such systems in a number of projects (e.g., CI, 1998). Additional demonstration projects are, however, necessary to provide more data regarding field performance of bridges retrofitted with FRP systems, highlight the advantages of such systems to the engineering and transportation communities, further examine issues related to field installation techniques, and evaluate the long-term durability of FRP systems under actual live loads and environmental exposures. For this purpose, the research reported in this paper was conducted. The research involved retrofitting of a reinforced concrete slab bridge, which had been posted due to inadequate

capacities, and field-testing of the as-is bridge, shortly after strengthening, and after one year of service. Four FRP systems were used in order to examine issues related to field installation of each system under similar constraints, and to explore the performance of the four systems under identical traffic and environmental conditions. The bridge was rated before and after retrofitting, and the load limits were removed after a detailed evaluation of the capacity of the retrofitted bridge and its performance. Various aspects of the research along with a number of important observations and results are summarized in this paper.

TEST BRIDGE

The research project revolved around a three-span reinforced concrete slab bridge (CLI-380-0032) built in 1955. The spans are 6.71, 8.38, and 6.71 m, the roadway is 9.75 m wide, and the slab is 298 mm thick (Fig. 1a). The slab is thicker near the edges along the entire length (Fig. 1b). The bridge has a 70° skew. The piers consist of 470-mm thick walls. The slab-abutment and slab-pier connections consist of standard 191 mm long by 63.5 mm deep shear keys. The slab reinforcement is shown in Fig. 1c. Photographs of the bridge are shown in Fig. 1(f)-(g). The material properties of the reinforcing bars and concrete were assumed, as no samples were available for testing. Considering the age of the bridge, the yield strength of the reinforcing bars was assumed to be 276 MPa, as suggested by ODOT rating guidelines (Section 900, 2000). A number of previous studies (e.g., Shahrooz et al., 1994a) suggest that the actual concrete compressive strength for bridges built around the same time is approximately 55.2 MPa. For capacity calculations, the concrete compressive strength was conservatively taken as 20.7 MPa, but was assumed to be 55.2 MPa in the analytical models intended to correlate the measured responses.

The bridge was generally in good condition with the exception of minor cracks on the

under side of the slab in the midspan, mostly along the construction joint in the centerline of the roadway. The bridge had been posted because of insufficient capacity of the slab.

RETROFIT SYSTEMS

In an effort to increase the capacity of the bridge and remove the posted load limits, the bridge was strengthened by FRP composites. Four different systems, supplied by one manufacturer, were incorporated in order to examine the performance of various systems under identical traffic and environmental conditions. The locations and photographs of the FRP systems are shown in Fig. 2. The systems included: (a) bonded 76.2-mm wide x 1.33-mm thick carbon plates spaced at 305 mm on center; (b) bonded 127-mm wide x 1.90-mm thick carbon plates spaced at 457 mm on center; (c) one layer of 305-mm wide carbon fabrics covering the entire north east of span 3; and (d) 102-mm wide x 4.83-mm thick carbon plates, spaced at 305 mm on center, with bolts at the ends. The 76.2-mm and 127-mm wide plates as well as the fabrics had unidirectional carbon fibers. The 102-mm wide plates had unidirectional carbon fibers and E-glass fibers at +/- 45 degrees. Following the procedures outlined in ASTM D3039, the strength, modulus of elasticity, and fracture strain of each system were obtained by the research team based on 4 tensile specimens for each system. The coefficient of variation of the measured properties was at most 5%, and testing of additional samples was deemed unnecessary. These values are summarized in Table 1.

Installation Procedure

The FRP systems were installed by a contractor specialized in retrofitting with FRP. In consultation with engineers at the Ohio Department of Transportation (ODOT), the contractor selected the layout and types of the retrofitting systems so that four different systems can be incorporated in one bridge.

The following steps were followed to prepare and install the FRP systems:

1. The concrete surface was cleaned with high-pressure steam to ensure that the surface was free of all dirt, oil, and debris. The surface was allowed to dry so that it would be free of apparent moisture before applying the FRP plates or fabrics.
2. The locations of various FRP composite systems were marked on the concrete surface.
3. Using paint rollers, an epoxy primer was applied to the prepared surface. The primer was allowed to dry for at least 30 minutes before proceeding with the next steps.
4. For the FRP plates, these steps were followed:
 - a. The surface of the carbon FRP plates was cleaned with a degreaser.
 - b. A structural epoxy was mixed in accordance with the manufacture's directions, and was applied to the concrete surface with a V-notched trowel. The epoxy filled any voids and uneven surfaces.
 - c. The same structural epoxy was applied to the plates by using a V-notched trowel. Starting at one end and moving along the length, the plates were installed. Using a roller, enough pressure was applied to press out any excess epoxy and trapped air pockets. The excess epoxy was cleaned.
 - d. For the 102-mm bolted plates, the structural epoxy was allowed to dry for 24 hours before installing the anchors. Four 76.2-mm long A325 anchor bolts were installed at 152 mm on center, with the first anchor placed at 76.2 mm from the end of the plate. The anchors were 12.7 mm in diameter. The anchors were staggered approximately 6.35 mm from the centerline of the plate.

5. For the fabrics, a heavy layer of a saturating epoxy was applied by using a paint roller. After unrolling, each 305-mm wide segment of the fabric was pressed into place at the center toward each end. Precautions were made to keep the fabric tight and wrinkle free. A heavy layer of the saturating epoxy was applied over the fabric. A fabric roller was used to remove any trapped air pockets, and to work the saturating epoxy into the fabric. A similar procedure was followed for all the 305-mm wide strips until the entire region was covered. The individual strips of fabric, in the transverse direction, were next to each other and did not overlap. The length of the fabrics was selected to avoid longitudinal splices. After waiting for approximately 30 minutes, a finishing coat of saturating epoxy was applied to protect the fabrics against ultra violet light, and to enhance their appearance.

EXPERIMENTAL PROGRAM

The bridge was instrumented and tested before retrofitting, shortly after installation of the retrofitting systems, and after one year of service. The initial tests established a number of critical benchmark responses of the bridge, while the other sets of tests provided information regarding the participation of the FRP systems. The bridge was instrumented as shown in Fig. 3 to measure concrete surface strains at 20 locations, vertical deflections of the slab at 20 locations, and strains in the FRP systems at 3 locations (SG21, SG22, and SG23 in Fig. 3b). The strain gages on the FRP systems were installed close to the locations where the maximum concrete surface strain in each span had been measured during testing of the unretrofitted bridge. The suite of instruments was distributed to measure adequate responses from all the regions with different retrofit systems.

Two standard ODOT loaded dump trucks were used for testing, each truck weighed about

132 kN. These two-axle trucks are 140 mm long between the center of the front and back axle, 80 mm wide between the centers of the front two tires, and 80 mm wide between the centers of the back four tires. The exact weight of each truck was measured for each phase of the testing program. Based on a number of previous studies dealing with similar trucks (e.g., Shahrooz et al. 1994a, Miller et al., 1994), the distribution of the total weight between the front and back axles was established. Seven truck positions were selected to produce (a) maximum positive moment in span 1, (b) maximum positive moment in span 2, (c) maximum positive moment in span 3, (d) maximum negative moment at pier 1 with the trucks located in the north lane, (e) maximum negative moment at pier 1 with the trucks located in the south lane, (f) maximum negative moment at pier 2 with the trucks located in the north lane, and (g) maximum negative moment at pier 2 with the trucks located in the south lane. (Refer to Fig. 2 for the location of various spans and piers.)

TEST RESULTS AND INTERPRETATION

Attempts were made to ensure that the trucks would be positioned at the same locations during various tests within reasonable tolerances. Variations in the truck weights were, nevertheless, inevitable; the weights changed by as much as 9% between various tests. The measured responses (deflections and strains) had to be first normalized so that the differences due to changes in the truck weights would be eliminated, and comparison of the data from different tests would be meaningful. The normalization procedure is presented before discussing the experimental data.

Normalization Procedure

One method for normalizing the measured data is to multiply the data by a factor $N = r_2/r_1$ where N = normalization factor, r_1 = response (deflection or strain) at a given point under a

given load case, and r_2 = response at the same point under a different load in the same load case. Separate normalization factors were obtained for each load case. The normalization procedure for a given load is explained as follows. Additional details regarding the normalization method are provided elsewhere (Shahrooz et al., 1994b).

1. A linear elastic three-dimensional finite element model of the bridge was constructed by using a computer program called SAP2000 (1998). As shown in Fig. 4, the slab, piers, and abutments were modeled by shell elements with 6 degrees of freedom at each node. The thickness of the slab along the edges was increased to simulate the edge “beams”. Rotational springs along the three axes were introduced at all the nodes joining the slab shell elements to the abutment/pier shell elements. The spring constants were fine tuned so that the computed deflection profiles and those measured before the bridge was retrofitted would match as closely as possible. The constants for all the rotational springs were found to be 16,948 kN-m/rad.

The same rotational spring constants were used in the analytical model of the bridge after retrofitting. Modeling of the bridge after retrofitting was essentially the same as that before the bridge was strengthened; however, the stiffness of the slab had to be modified to account for the effects of the FRP systems. Different regions of the slab with various FRP systems were transformed into equivalent concrete sections in order to compute the appropriate properties of the shell elements. For the FRP systems with individual plates spaced at 305 or 457 mm on center, the stiffness properties of the slab per 305-mm width of the slab were computed and used in the model in lieu of discrete modeling of the regions of the slab with and without FRP plates.

2. The analytical model of the bridge after retrofitting was subjected to the truck weights

measured during the pre-retrofit tests. The computed deflections at the instrumented locations form the values of r_2 in the normalization equation. Analyzing the same model with the truck weights measured during each of the post-retrofit tests form the corresponding values of r_1 in the normalization equation for each of the post-retrofit tests.

3. The normalized deflections for each of the post-retrofit tests were obtained by multiplying the experimental data and the appropriate normalization factor, $N = r_2/r_1$, corresponding to each instrumented location. A single set of normalization factors was used for the deflections and strain gages by assigning the same factor for a deflection point and the strain gage located close to that point.

This normalization approach had essentially the effect of “translating” all of the measured data to what they would have been had the truck weights remained identical to those used for testing of the bridge before retrofitting. Note that it was unnecessary to normalize the values obtained for the before-retrofit tests.

Test Results

Representative normalized deflection profiles, along each instrument line, are shown in Fig. 5. The results in this figure are for the load case indented to produce the maximum moment in the middle span. Similar deflection profiles for the other truckload tests are provided elsewhere (Shahrooz and Serpil, 2001). The deflections measured shortly after retrofitting are generally smaller than the corresponding values during the before-retrofit tests, but a similar trend is not seen at all locations for the tests conducted after one year of service. These differences may be interpreted as signs of degradation of the FRP systems' effectiveness; however, visual inspections do not suggest initiation of debonding or deterioration of the FRP systems. More plausible reasons for the observed changes in the deflected profiles are: (a) the

trucks could not be positioned at exactly the same positions during the three series of tests, slight variations in the truck positions would alter the measured deflections; (b) the displacement transducers have a resolution of ± 0.0762 mm, and the differences in the measured deflections are within this resolution; and (c) the deflected shapes shown in Fig. 5 were normalized, as described above, based on a finite element model that did not exactly reproduce the measured deflections at all locations, slight differences in the computed and measured deflections would impact the normalization factors. In view of these reasons and the measured responses, the contribution of the FRP systems towards enhancing the stiffness of the bridge cannot be assessed conclusively. The overall flexural stiffness of the deck is significantly larger than the stiffness of the FRP systems. Transformed section analyses indicate that 76.2-mm plates, 102-mm bolted plates, 127-mm plates, and carbon fabrics increase the flexural stiffness of the concrete deck by only 1.5%, 2.5%, 1.8%, and 1.7%, respectively. Therefore, the FRP systems are not expected to have a major impact on the overall stiffness of the bridge, and the small enhancements from the FRP systems were apparently masked by the reasons discussed above.

The impact of retrofitting systems on the performance of the bridge is perhaps better illustrated by comparing a number of strains on the concrete and FRP systems. In Fig. 6, the maximum measured strains in the FRP systems (SG21, SG22, and SG23) are compared to the corresponding concrete strains. The maximum strains plotted in Fig. 6 are from different tests, but the strains for the FRP and concrete are from the same tests, e.g., the data for SG15 and SG22 are from truckload test 1, which was intended to produce the maximum moment in the middle span, while the data for SG8 and SG23 are for truckload test 2, which aimed at producing the maximum moment in Span 3 (refer to Fig. 2 for the location of Span 3). After installation of the FRP systems, the concrete strain at all locations dropped, e.g., at location SG15, where the

largest strain in the slab was measured, the concrete strain was reduced by about 34%. (Note that the strain gages used in this project would measure strains within +/- 1 micro strain.) This trend points to the participation of the FRP systems toward resisting the applied live loads. The strains in the FRP systems measured shortly after retrofitting and after one year of service did not change significantly as shown in Fig. 6; the small differences in the two sets of strain data are attributed to slight variations in the exact positions of the trucks during the two tests. Field inspections do not suggest possible local debonding that would lead to changes similar to those observed in Fig. 6. Therefore, the participation of the FRP systems toward strengthening of the slab did not change after one year of service.

The strains measured during the truckload tests are small, e.g., the maximum strains in concrete and FRP systems are about 0.004% and 0.0025%, respectively. Clearly, the loads from the two trucks used for testing did not produce large demands in the bridge; the maximum concrete strain was about one quarter of that causing cracking, and the FRP systems were strained to only 0.64% of the “usable strain” at which the capacity of the bridge with FRP systems is computed (ACI 440, 2001). The small strains do not imply that the FRP systems cannot increase the overall strength of the bridge and its rating factors because (a) the loads for the truckload tests do not represent those used for rating, and (b) capacity of members strengthened with FRPs is computed based on strength design approach in which significantly larger strains are used in the calculations, as discussed next. The small strains in the FRP systems suggest that the bond between FRP systems and concrete would not be a major concern for service loads.

IMPACT OF RETROFITTING ON RATING FACTORS AND LOAD LIMITS

Using relatively simple modeling techniques, the bridge had been rated by ODOT

engineers and found to be inadequate, and load limits had been posted. To reaffirm the original rating factors, a more detailed model of the as-is bridge, which was calibrated based on the measured responses, was constructed and used to calculate the demands in the bridge. A similar detailed model was also used for computing the demands in the retrofitted bridge as part of rating of the retrofitted bridge. After a brief description of the analytical model, the rating factor and the resulting load limits are presented and discussed.

Analytical Model

A three-dimensional elastic finite element model of the bridge was constructed (Fig. 4). The model is the same as that used for computing the normalization factors. The thickness of the slab, abutments, and piers in the model was based on field measurements. The concrete compressive strength was taken as 55.2 MPa. Through the use of this model, reasonable correlation of the measured deflection profiles was possible as evident from representative results shown in Fig. 7. The model was used to calculate the live and dead load moment and shear demands. As discussed previously, the truckload tests did not subject the bridge to large demands; however, the experimental data were vital for calibrating detailed analytical models for the original and strengthened bridge.

Rating Procedure

All the applicable provisions in AASHTO (2000) and ODOT rating specifications (Section 900, 2000) were followed to calculate the rating factors and the associated load limits. The calibrated analytical model was used to generate the influence lines for negative moments at the abutments and piers, positive moments at the midspan of each span, and shear at the abutments and midspan of each span. Using the influence lines, the critical location of the applicable loads (HS20-44, 2F1, 3F1, 4F1, and 5C1 (see Table 2 for truck dimensions and axle

weights), and lane loading) was identified. Two trucks, one in each lane, were used in the analyses. The trucks were assumed to travel in the same or opposite directions in order to compute the largest demands. Clearly, the availability of the calibrated analytical model allowed a more accurate calculation of the demands. The capacity of the un-retrofitted bridge was established by standard techniques (AASHTO, 1996). The capacity of the slab with FRP systems was computed based on an available set of guides for design of externally bonded FRP systems (ACI 440, 2000). All the applicable specifications for strain compatibility between FRP laminates and substrate concrete, environmental durability reduction factors, and other reduction factors as well as serviceability considerations recommended in ACI 440 were followed to compute the capacity of the slab with various FRP systems. Based on the strain compatibility requirements of ACI 440, a maximum “usable strain” of 0.39% was used in capacity calculations. For the FRP systems with individual plates spaced at 305 or 457 mm on center, the strength per 305-mm width of the slab were computed and used in the calculations in lieu of distinguishing between the capacity of different regions of the slab with and without FRP plates. The two-way action of the slab was ignored when computing the capacities of the original and the retrofitted bridge for simplicity and because the FRP systems had unidirectional carbon fibers.

Both inventory level and operating level rating factors (R.F.) and load limits were computed according to $R.F. = \frac{C - A_1 D}{A_2 L (1 + I)}$, in which C = capacity at a given section computed from AASHTO strength design approach or from ACI 440 guide specifications, D = dead load moment or shear without any load factors, L = live load moment or shear without any load factors, I = impact factor which is 0.3 for the bridge under consideration, $A_1 = 1.3$, and $A_2 = 2.17$ and 1.3 for inventory level rating and operating level rating, respectively.

Rating Factors and Load Limits

The controlling rating factors and corresponding load limits before and after retrofitting for various types of loading are summarized in Tables 2 and 3. Note that the rating factors were controlled by the positive moment in the middle span. The experimental data also suggest the largest strains, which are directly related to the moment in the slab, occur in the middle span (refer to Fig. 6).

The rating factor for the original bridge was governed by HS20-44 truck loading. The operating and inventory level rating factors for the original bridge were 1.45 and 0.87, respectively. The load limits for Ohio legal loads are 150, 213, 257, and 383 kN for 2F1, 3F1, 4F1, and 5C1, respectively before retrofitting the bridge. Note that these values are about 8% larger than the corresponding values posted on the bridge (133, 204, 240, and 356 kN for 2F1, 3F1, 4F1, and 5C1, respectively).

After retrofitting, the rating factors and associated load limits were increased by about 22%. The rating factor was once again controlled by HS20-44 truck loading. The critical operating and inventory level rating factors became 1.77 and 1.06, respectively. Therefore, the retrofitting scheme was successful in enhancing the capacity of the bridge, rating factor, and load limits. Considering the reported enhancements in the overall capacity, the posted load limits were removed.

SUMMARY AND CONCLUSIONS

In an effort to strengthen a three-span reinforced concrete slab bridge, which had been posted because of small rating factors, and remove the load postings, the bridge was strengthened with FRP systems. The FRP systems included 76.2 and 127-mm wide carbon bonded plates, 102-mm wide carbon bonded plates with anchors at the ends, and bonded carbon fabrics. This

project also provided a unique opportunity to examine the long-term performance of four FRP systems under identical environmental conditions and loading, and to evaluate field installation issues for each system. For this purpose, detailed truckload tests were conducted to obtain benchmark responses of the original bridge, shortly after installation of the FRP systems, and after one year of service. The measured data proved useful for calibration of a relatively detailed three-dimensional finite element model of the bridge. The calibrated model was used to calculate the demands as part of establishing the rating factors and associated load limits for the as-is and retrofitted bridge. Based on the experimental and analytical studies, the following general conclusions and observations are made.

1. The participation of the FRP systems towards enhancing the overall stiffness of the bridge was small, and could not be conclusively seen for the level of loads used for testing. After retrofitting, concrete strain in the slab dropped as the FRP systems participated toward resisting the applied live loads. The participation of the FRP retrofitting scheme was most pronounced at the location with the highest moment demands.
2. After one year of service, the effectiveness of the FRP systems, as gauged by the measured strains in the FRP systems, did not essentially change from that obtained shortly after installation of the FRP systems. Additional testing of the bridge in the future along with inspection of the FRP-concrete bond quality, and condition of the FRP plates and fabrics would provide valuable data regarding the long-term performance of four FRP systems under identical environmental exposures and loading.
3. The retrofitted bridge achieved larger rating factors and load limits than the corresponding values for the original bridge. Retrofitting with the FRP systems led to a 22% increase in the load carrying capacity of the bridge. The FRP systems proved to be a simple, yet effective,

method to strengthen the bridge, and to enable the engineers remove the posted load limits.

ACKNOWLEDGEMENTS

The Ohio Department of Transportation and the Federal Highway Administration under contract number 14719(0) sponsored the study reported herein. The contents of this paper reflect the opinion the views of the authors who are solely responsible for the facts and accuracy of the data presented herein. It does not necessarily reflect the views or policies of ODOT or FHWA, and does not constitute a standard, specification, regulation, or recommendation. The authors acknowledge Messrs. Vikram Dalal, Brad Fagrell, Stefan Spinosa, and Amjad Waheed at ODOT for their valuable assistance in various aspects of the reported project. The technical support personnel and many current and former graduate students at the University of Cincinnati Infrastructure Institute were instrumental in the successful completion of this project.

REFERENCES

ACI 440, "Guide for the Design and Construction of Externally Bonded FRP Systems for Strengthening Concrete Structures", Revised 10-26-2001, American Concrete Institute, 2001.

AASHTO – *Manual for Condition Evaluation of Bridges-1994*, American Association of State Highway and Transportation Officials, Washington, D.C., 2nd Ed., 2000.

AASHTO – *Standard Specifications for Highway Bridges*, American Association of State Highway and Transportation Officials, Washington, D.C., 16th Ed., 1996.

Concrete International, American Concrete Institute, Vol. 20, No. 6, 1998, pp. 22-58.

fib, "Design and Use of Externally Bonded FRP Reinforcement (FRP EBR) for Reinforced Concrete Structures," Final Draft, Progress Report of *fib* EBR group, International Concrete Federation.

Miller R.A., Aktan A.E., Shahrooz B.M.: "Destructive Testing of a Decommissioned Concrete Slab Bridge," *Journal of the Structural Division*, ASCE, 120(7)(1994): 2176-2198.

SAP 2000 – *Integrated Finite Element Analysis and Design of Structures*, Computers and Structures, Inc., Berkeley, California, 1998.

Section 900 – *Structure Load Rating*, Ohio Department of Transportation, Columbus, Ohio, April 2000, pp. 9.1-9.11.

Shahrooz B.M., Miller R.A., Saraf V.K., Godbole B.: "Behavior of R.C. Slab Bridges During and After Repair," *Transportation Research Record*, 1442(1994a): 128-135.

Shahrooz B.M., Miller R., Saraf V., Godbole B.: "Strength Continuity of Deteriorated Continuous Slab Bridges," *Report No. UC-CII 94/01*, Cincinnati Infrastructure Institute, 1994b.

Shahrooz B.M. and Serpil B., "Retrofit of Existing Reinforced Concrete Bridges with Fiber Reinforced Polymer Composites," *Report No. UC-CII 01/01*, Cincinnati Infrastructure Institute, 2001.

Table 1 Measured Material Properties of Various FRP Systems

(a) Carbon Fiber Plates

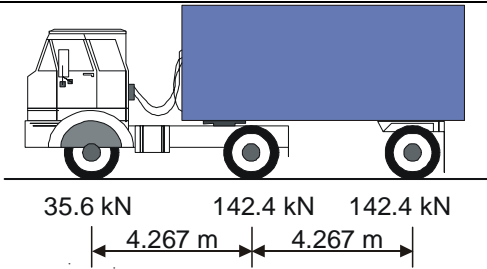
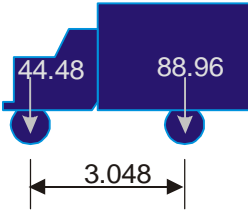
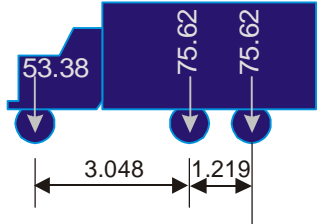
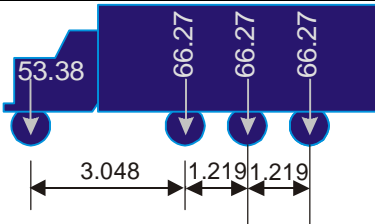
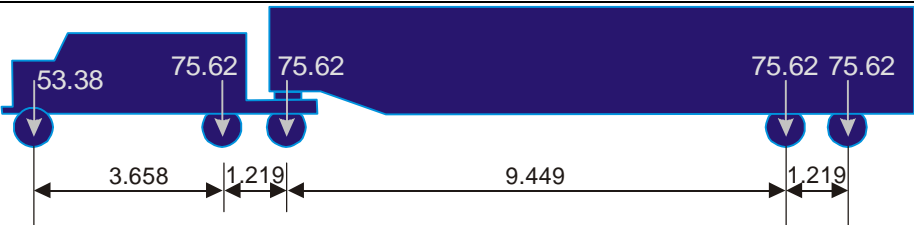
CFRP System	Thickness mm	F_u (MPa)	E (MPa)	Fracture Strain (%)
76.2 mm plate	1.33	2,289	155,052	1.48%
127-mm plate	1.9	1,117	116,514	0.96%
102 mm (Bolted plate)	4.83	585	53,095	1.10%

(b) One Layer of Carbon Fabric Sheet

F_u (kN/mm)	E (kN/mm)	Fracture Strain (%)
0.547	58.5	0.93%

Table 2 Rating Factors and Load Limits – Operating Level

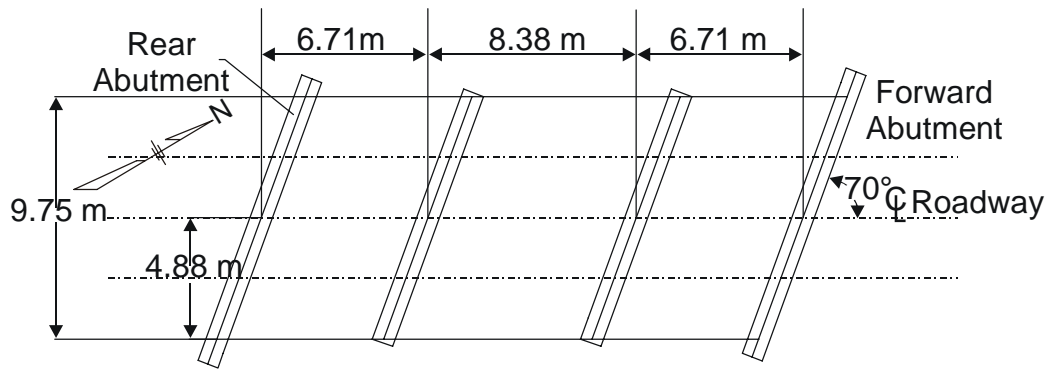
*Trucks 2F1, 3F1, 4F1, and 5C1 are Ohio Legal Loads, and are used for load rating.
 *See ODOT Rating Specifications (Section 900, 2000).

Load	Before Retrofitting		After Retrofitting		
	R.F.	Load Limit (kN)	R.F.	Load Limit (kN)	
	HS20-44	1.45	232	1.77	283
	2F1 [*]	2.24	150	2.74	183
	3F1 [*]	2.09	213	2.55	260
	4F1 [*]	2.14	257	2.61	313
	5C1 [*]	2.15	383	2.63	467
Lane Load	2.12	318	2.58	388	

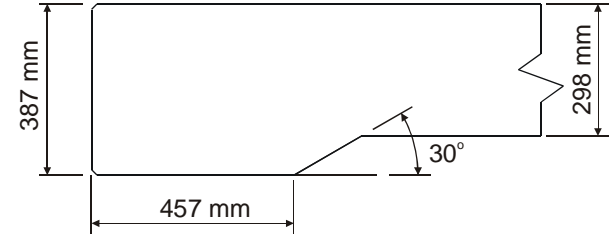
All truck weights and dimensions are in kN and m, respectively.

Table 3 Rating Factors and Load Limits – Inventory Level

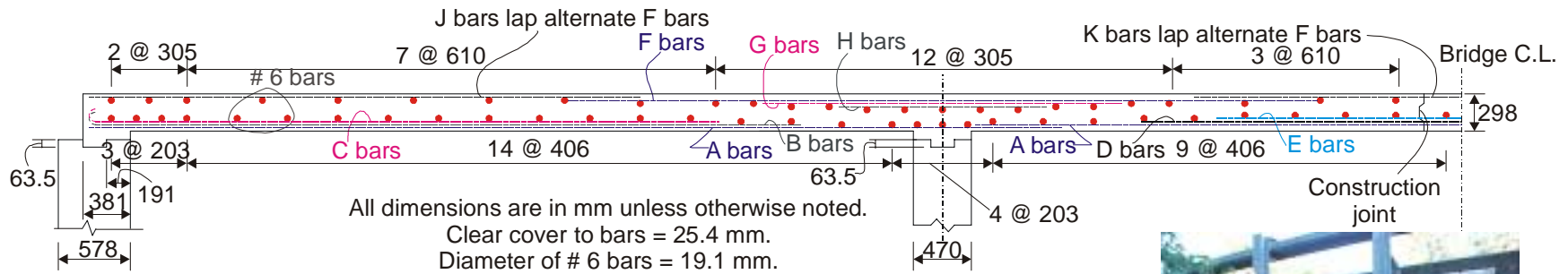
Load	Before Retrofitting		After Retrofitting	
	R.F.	Load Limit (kN)	R.F.	Load Limit (kN)
HS20-44	0.87	139	1.06	169
Lane Load	1.27	190	1.55	233



(a) Plan View



(b) Edge "Beam"



All dimensions are in mm unless otherwise noted.
Clear cover to bars = 25.4 mm.
Diameter of # 6 bars = 19.1 mm.

(c) Reinforcement

Bar	Diameter (mm)	Spacing (mm)	Length (m)
A	22.2	318	7.85
B	22.2	635	5.74
C	22.2	635	5.08
D	22.2	635	5.44
E	22.2	635	4.42
F	25.4	318	5.64
G	25.4	635	2.72
H	25.4	635	1.68
J	19.1	635	4.45
K	19.1	635	4.32

(d) Bar Sizes



(e) Overall View of Bridge



(f) Slab-Pier Connection



(g) Bottom View of Midspan

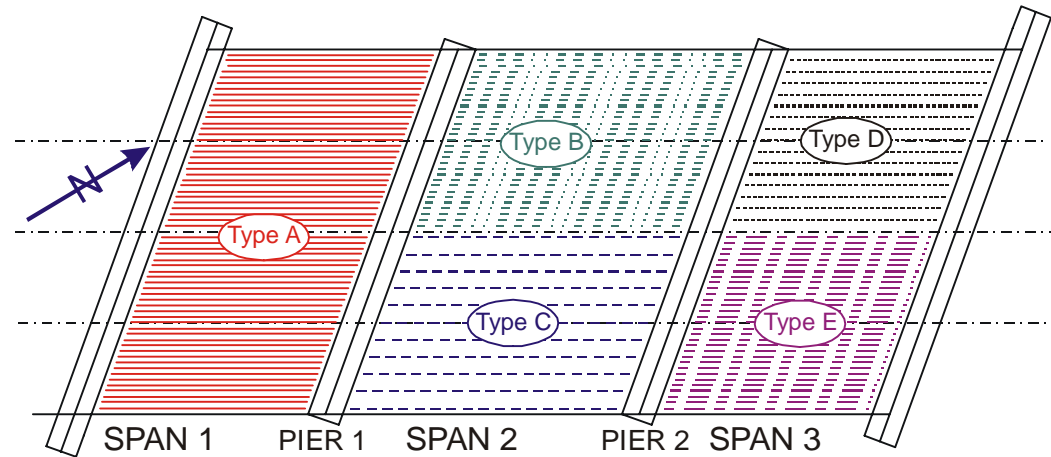
Figure 1. Details of Test Bridge



(a) Bonded CFRP Plates



(b) Bolted CFRP Plates

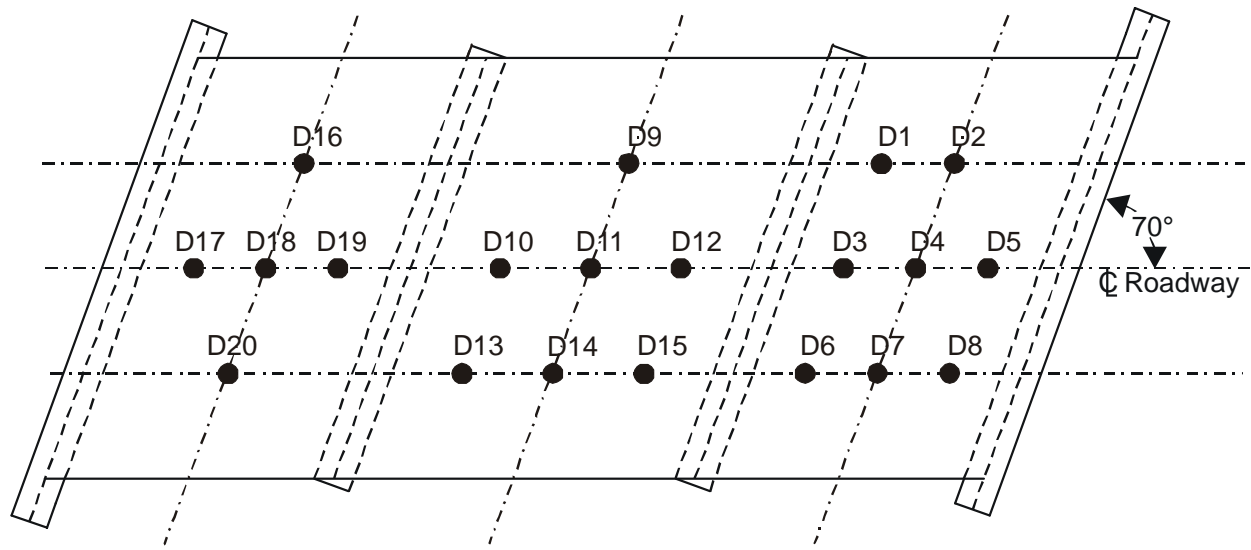


- Type A: 76.2 mm x 5.49 m CFRP Plates @ 305 mm O.C. (32 Plates)
- Type B: 76.2 mm x 7.16m CFRP Plates @ 305 O.C (16 Plates)
- Type C: 127 mm x 7.16 m CFRP Plates @ 457 mm O.C. (10 Plates)
- Type D: 305 mm x 5.49 m CFRP Fabric @ 305 mm O.C. (16 Fabric Pieces)
- Type E: 102 mm x 5.49 m CFRP Bolted Plates @ 305 mm O.C. (16 Plates)

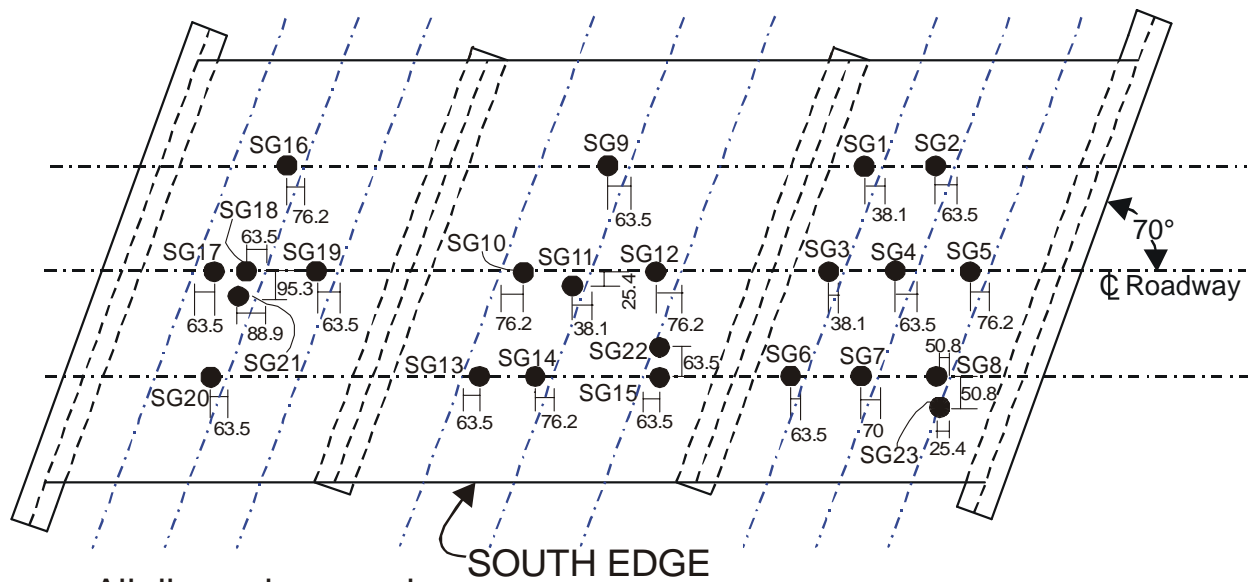


(c) CFRP Fabrics

Figure 2. Locations and Photographs of Various FRP Systems



(a) Locations of Displacement Transducers



All dimensions are in mm.

SG21, SG22, & SG23: on FRP systems

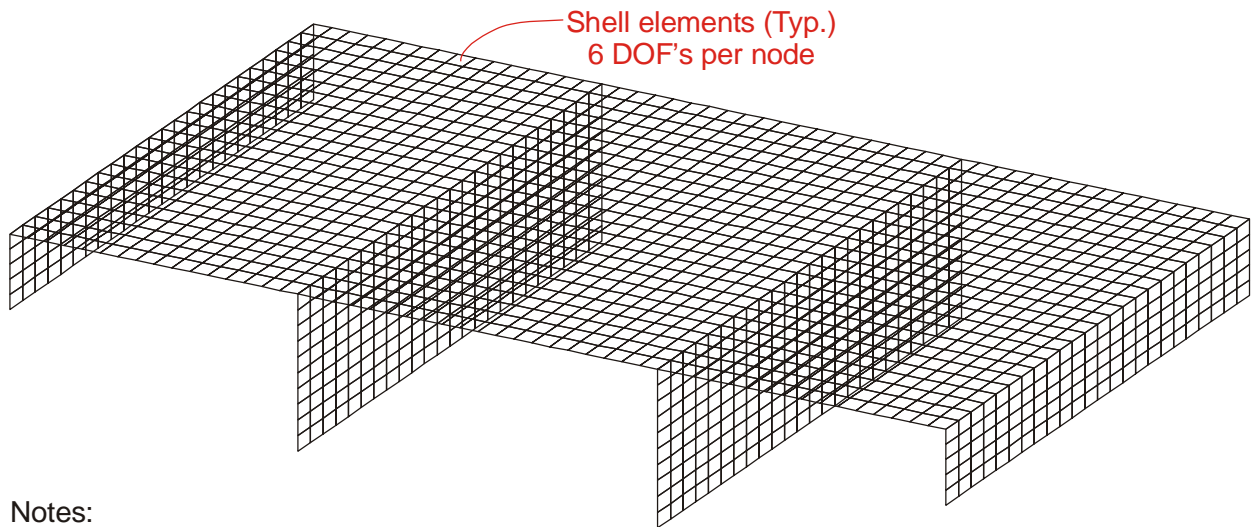
SG21 on the 15th 76.2-mm plate from the south edge

SG22 on the 6th 127-mm plate from the south edge

SG23 on the 7th 102-mm bolted plate from the south edge

(b) Locations of Strain Gages

Figure 3. Instrumentation Plan



Notes:

1. All DOF's are fixed at the base of abutment and pier elements.
2. Rotational springs in x, y, and z with $K_{\theta} = 16,948 \text{ kN-m/rad}$. were used at all adjacent nodes in the slab shell elements and in the abutment/pier shell elements.
3. Translations in x, y, and z directions are the same at all adjacent nodes in the slab shell elements and in the abutment/pier shell elements.

Figure 4. Three-Dimensional Model of Bridge

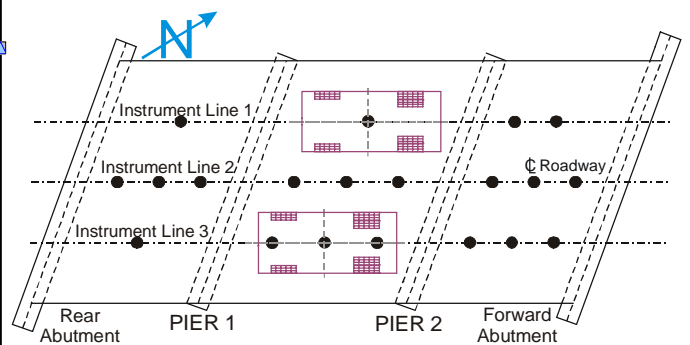
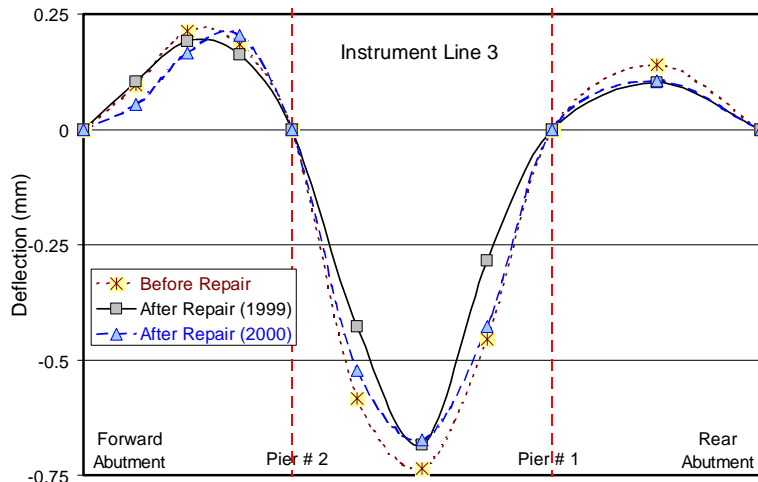
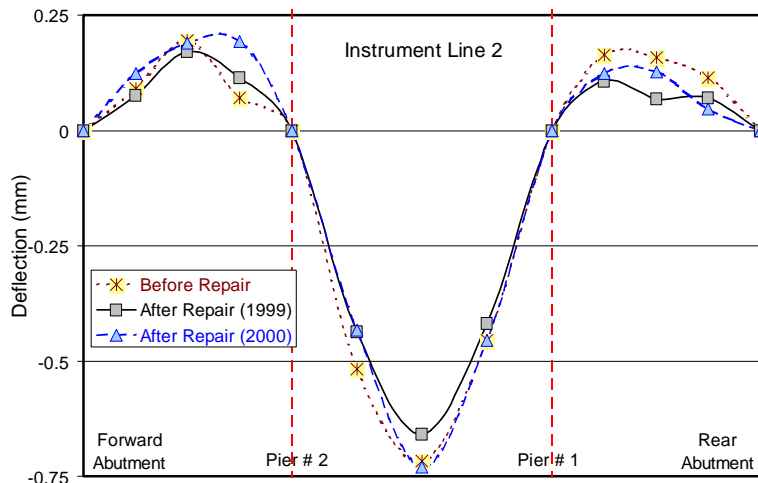
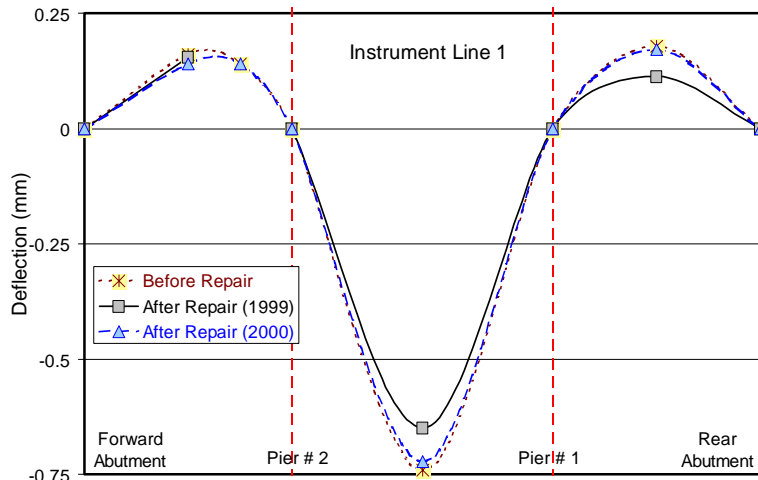
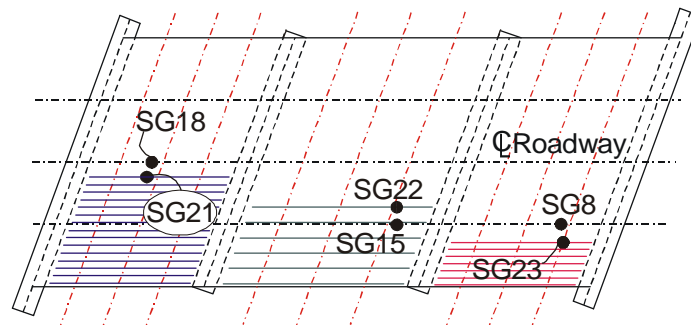


Figure 5. Representative Deflection Profiles for Truck Load Test No. 1



FRP Systems are shown partially.
 SG21, SG22, & SG23: on FRP systems
 SG21 on the 15th 76.2-mm plate from the south edge
 SG22 on the 6th 127-mm plate from the south edge
 SG23 on the 7th 102-mm bolted plate from the south edge

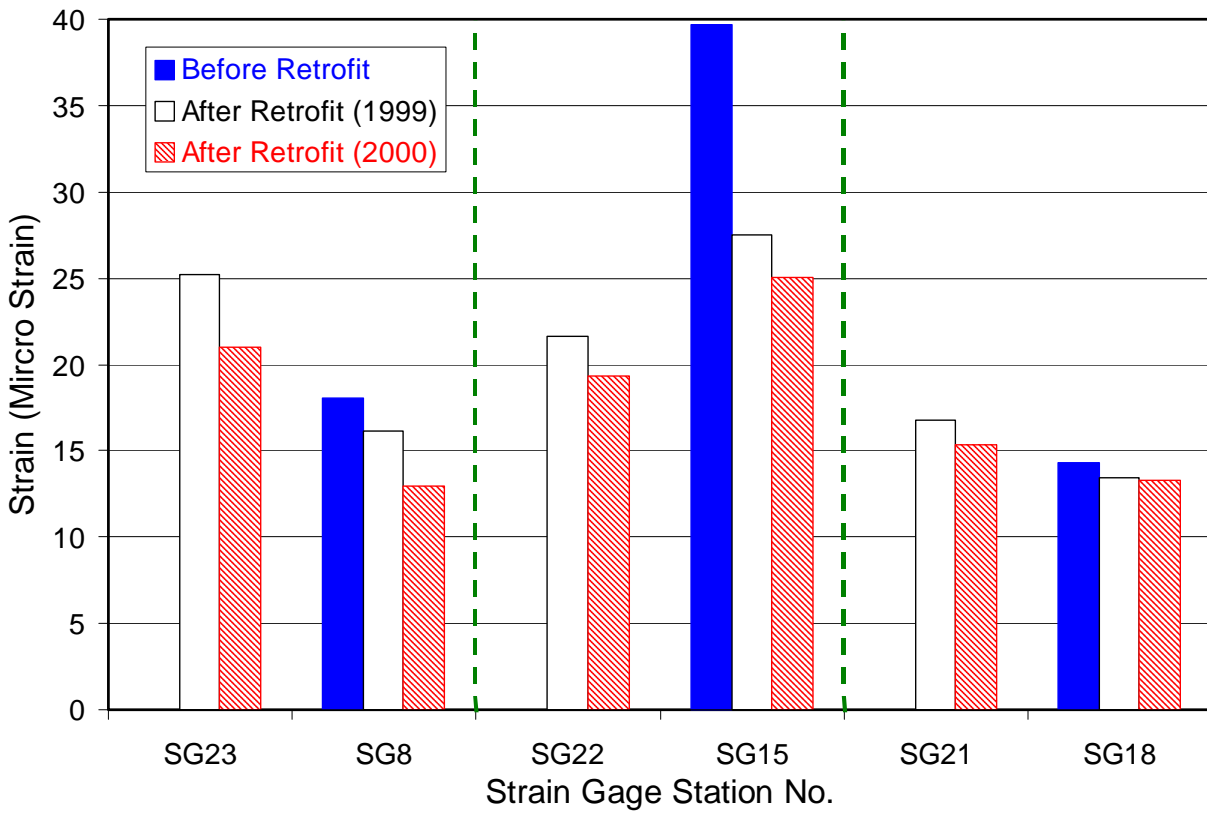
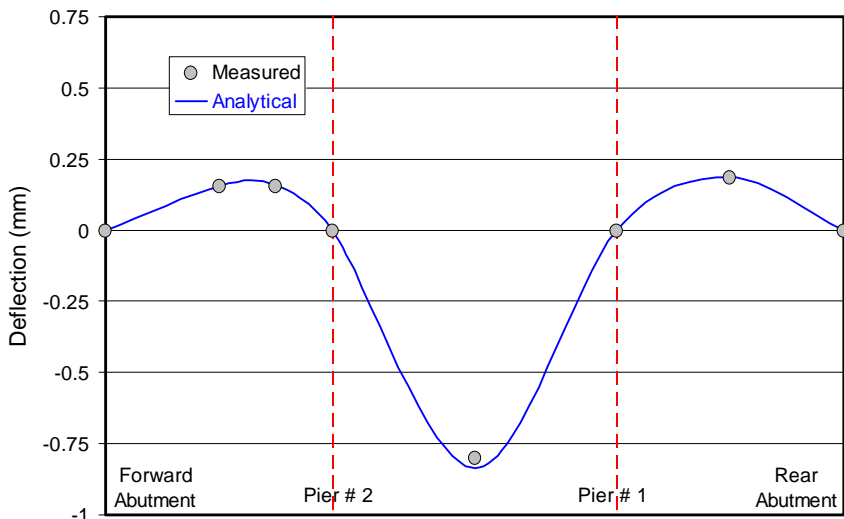
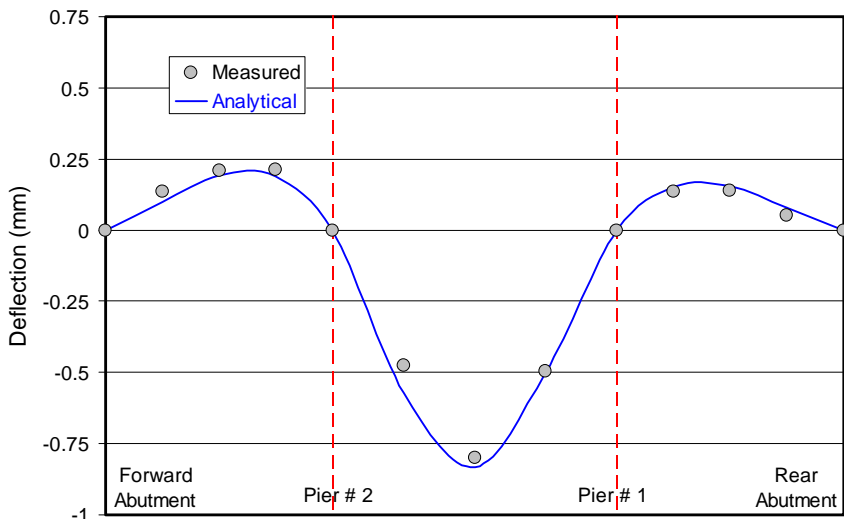


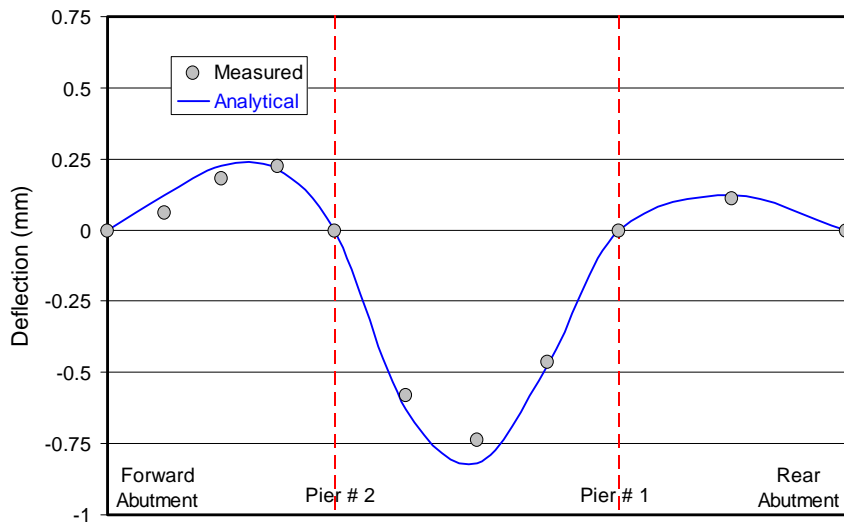
Figure 6. Maximum Strains in Slab and FRP Systems Measured During Various Tests



(a) instrument line 1



(b) instrument line 2



(c) instrument line 3

Fig. 7 Calculated Versus Measured Deflections

Implementations

Based on this two-part research, the following implementations are recommended.

1. The beams in FAI-37-2899 and FAI-37-2915 could have effectively been retrofitted with externally applied fiber reinforced polymer (FRP) composites. For old bridges with questionable concrete quality, bonded plates with mechanical anchors are recommended as such plates provide the best ductility. Members with mechanically anchored FRP plates will retain their capacity even if overload conditions debond the plates from the substrate concrete over a significant portion of the bond length. The Ohio Department of Transportation's engineers are highly recommended to consider externally bonded FRP composites for future strengthening of existing bridges.
2. The use of FRP composites to strengthen CLI-380-0032 proved to be very effective. The rating factor of the retrofitted bridge was increased by 22%. The FRP systems demonstrated that deficient bridges can simply, yet effectively, be strengthened in an effort to remove the posted load limits. The research results have been conveyed to ODOT District 8 in order to remove the load postings. The University of Cincinnati research team, in collaboration with ODOT engineers, was successful for strengthening a bridge that serves a major community in Ohio.

APPENDIX A:
Supporting Documents and
Data for Part I

Table A.1 Equivalent Cylinder Compressive Strength (MPa)

Beam	Web	Flange
1	52.8	19.7
2	46.2	19.1
3	45.0	17.4
4	44.1	22.5

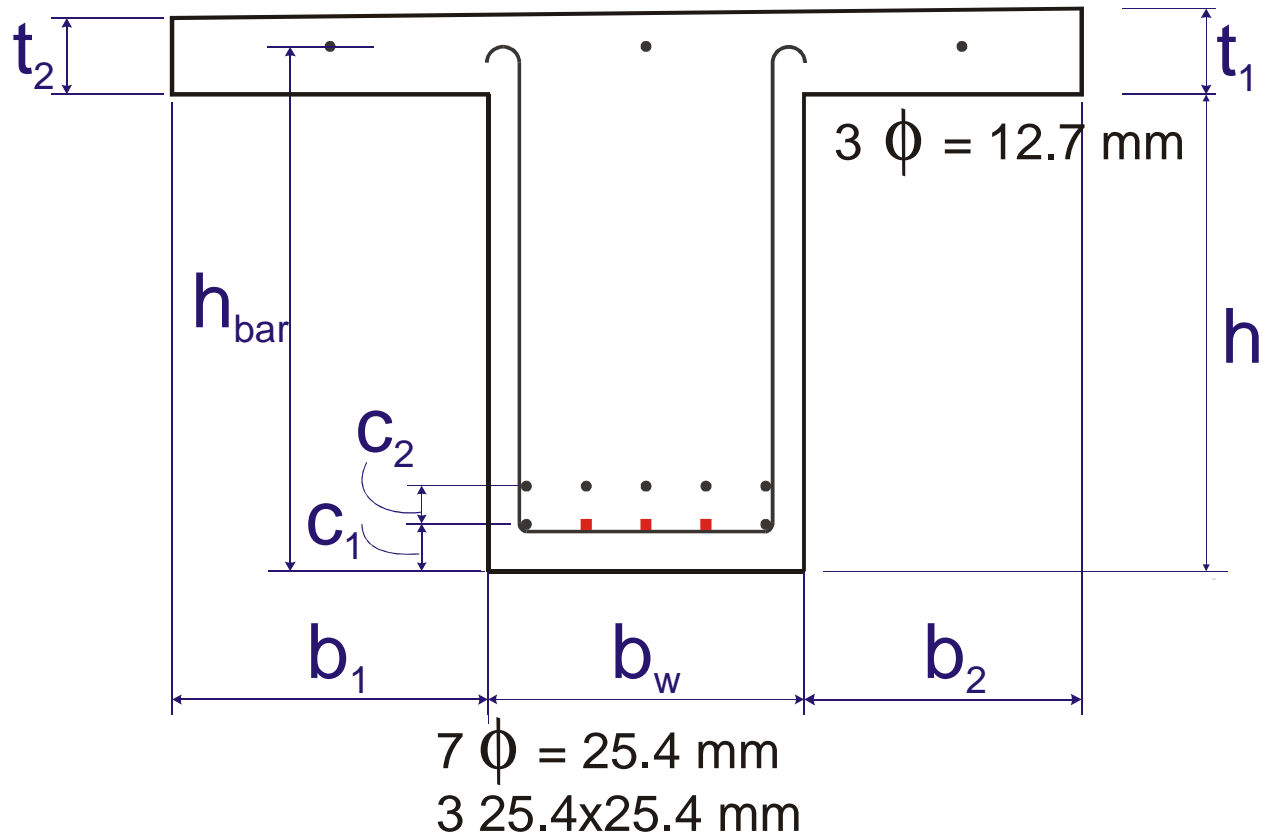
Table A.2 Measured Properties for Fiber Reinforced Plates and Sheets

(a) Carbon Fiber Plates

Nominal Plate Width (mm)	Sample I.D.	F _u (MPa)	E (MPa)	Fracture Strain (%)
76.2	1	2245	----	
	2	2253	----	
	3	2199	----	
	4	2460	155052	
	Average	2289	155052	
102 (Bolted)	1	631	50938	
	2	633	54832	
	3	563	----	
	4	526	----	
	5	542	53515	
	6	607	----	
	7	611	----	
	8	567	----	
	Average	585	53095	

(b) Two Layers of Carbon Fabric

Fabric Orientation	Sample I.D.	F _u (kN/mm)	E (kN/mm)	Fracture Strain (%)
Longitudinal	1	1.341	----	
	2	1.264	----	
	3	1.285	118.4	
	4	1.327	116.2	
	Average	1.304	117.3	
Transverse	1	0.0336	----	
	2	0.0332	9.618	
	3	0.0263	9.770	
	Average	0.0310	9.694	

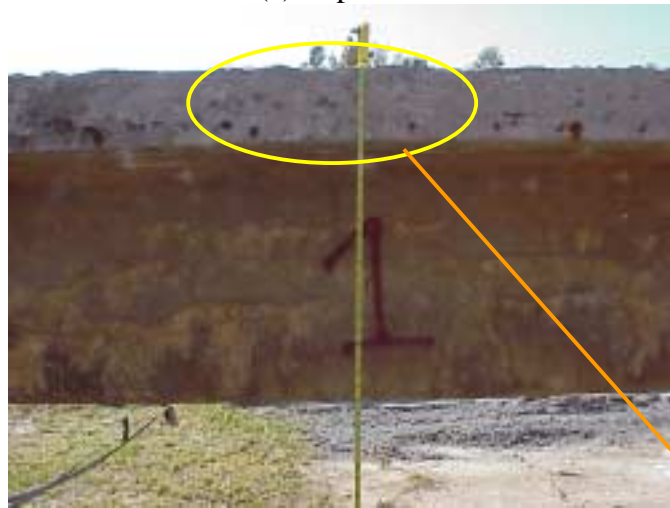


Beam	b_1	b_w	b_2	H	t_1	t_2	h_{bar}	C_1	C_2
1	419	419	375	591	152	146	654	63.5	50.8
2	422	410	378	587	152	152	654	63.5	50.8
3	362	616	381	616	140	102	654	114	50.8
4	397	408	454	565	152	140	622	63.5	50.8

Figure A.1 Cross Section of T Beams



(a) Top View



(b) Side View



Figure A.2 Existing Damage and Crack – Beam 1

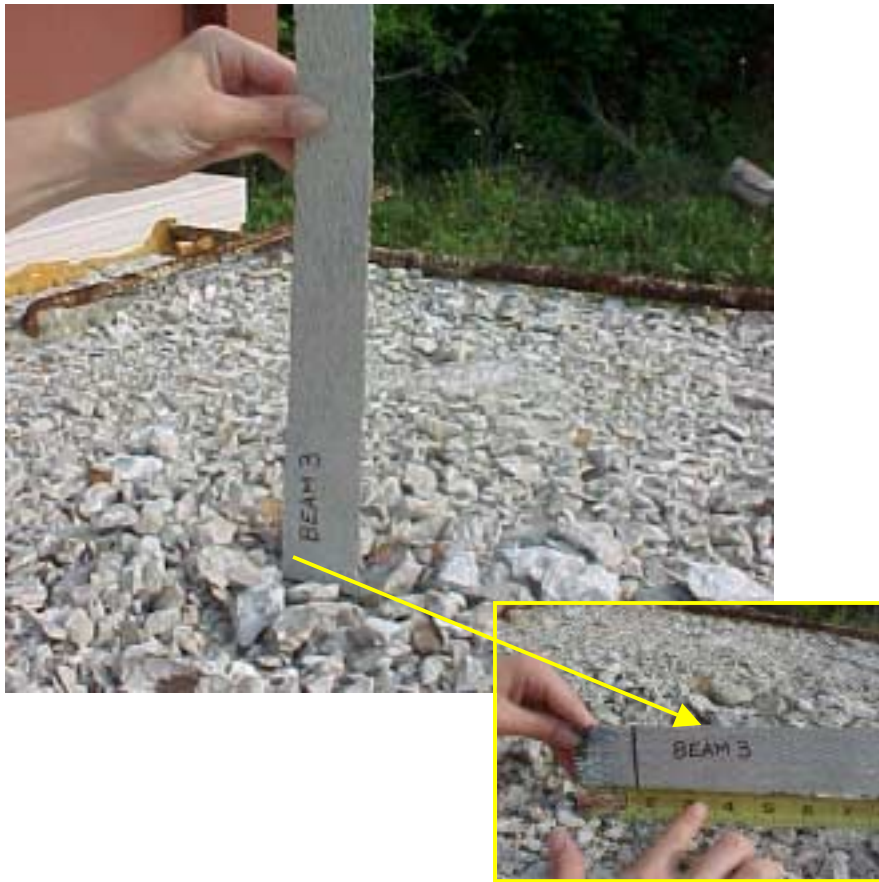


(a) Top View



(b) Side View

Figure A.2 (Cont.) Existing Damage and Crack Pattern – Beam 2



(a) Top View



(b) South Side



(c) North Side

Figure A. 2 (Cont.) Existing Damage and Crack Pattern – Beam 3



(a) Top View



(b) Side View

Figure A. 2 (Cont.) Existing Damage and Crack Pattern – Beam 4



Piece of rusted
bar that came off

(a) Slab Bar

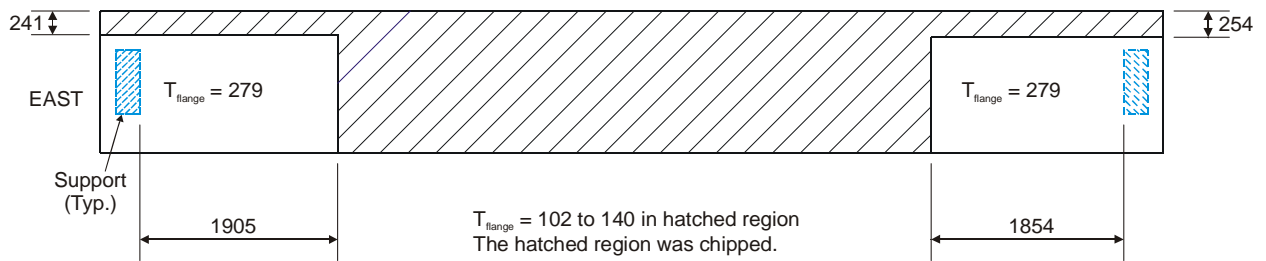


(b) Bottom Longitudinal Bar

Figure A.3 Typical Corrosion in Reinforcing Bars



(a) Condition as delivered



(b) Top View of Beam Showing Flange Thickness After Chipping



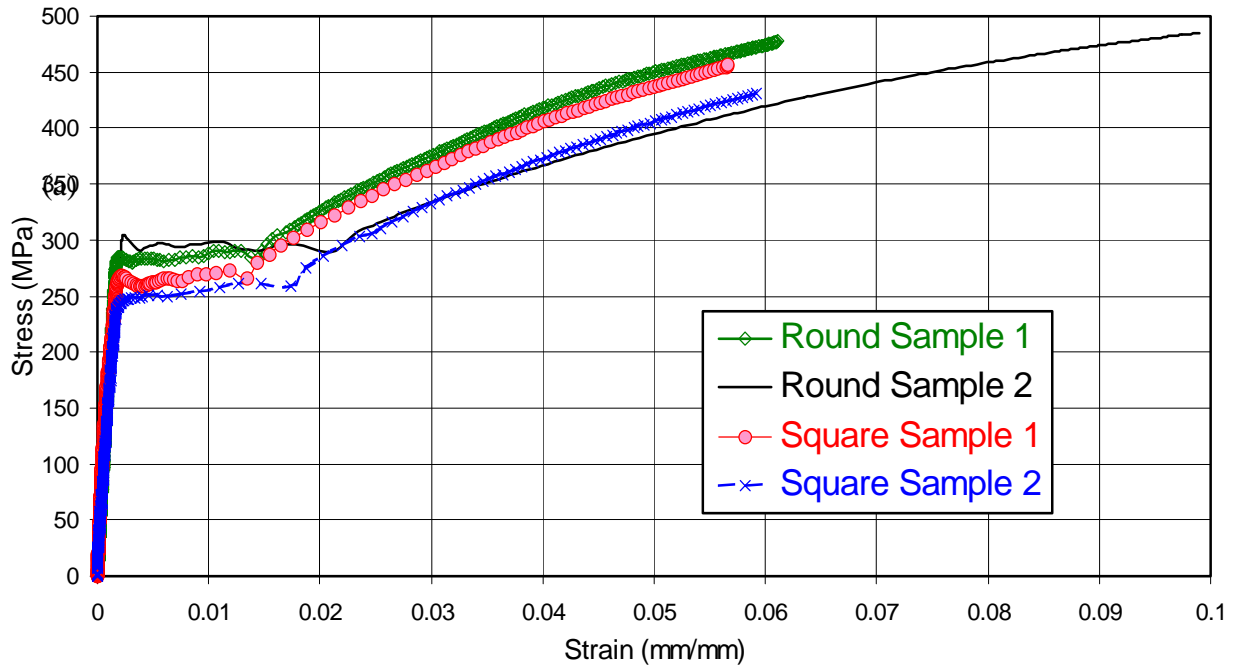
Looking West



Looking East

(c) Photos of Flange After Chipping

Figure A. 4 Flange in Beam 3



(a) Stress-Strain Curves

Specimen	F_y (MPa)	F_u (MPa)	F_f (MPa)	E_s (MPa)	ϵ_f (%)
Round # 1	288	554	479	181375	32.3
Round # 2	293	504	421	136742	31.9
Square # 1	269	502	408	209506	28.0
Square # 2	261	487	395	138775	31.5

F_y = Yield strength; F_u = Ultimate Strength; F_f = Fracture Stress
 E_s = Modulus of Elasticity ϵ_f = Fracture Strain

(b) Summary of Critical Properties

Figure A.5 Measured Properties of Steel Reinforcing Bars in T Beams

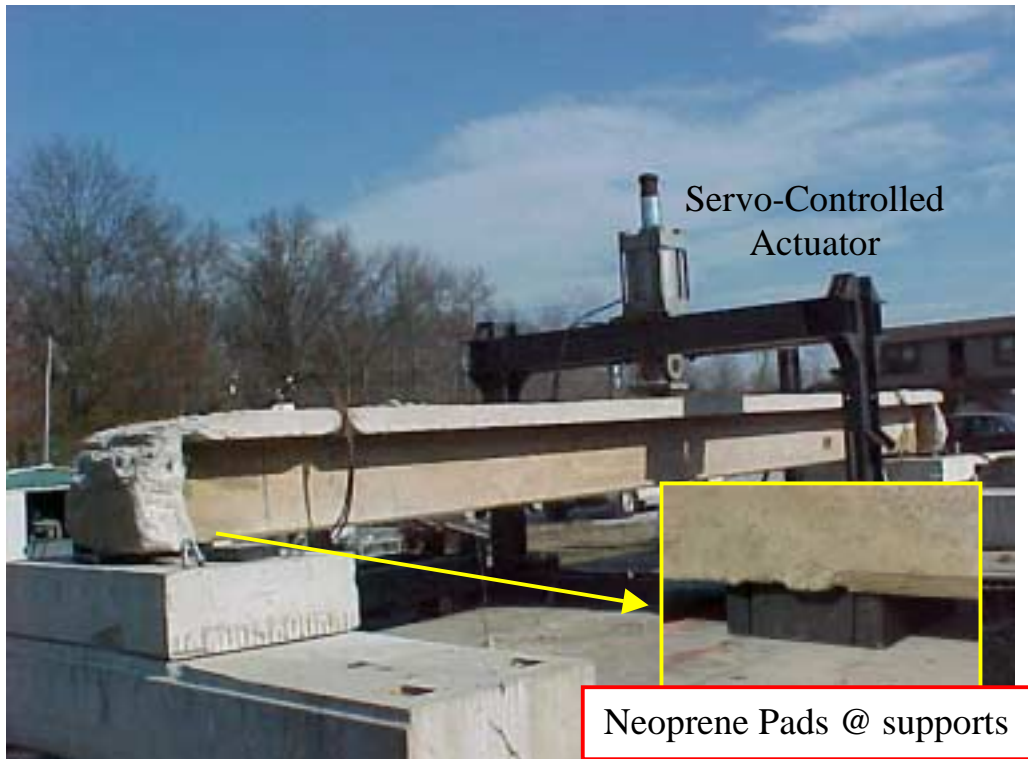
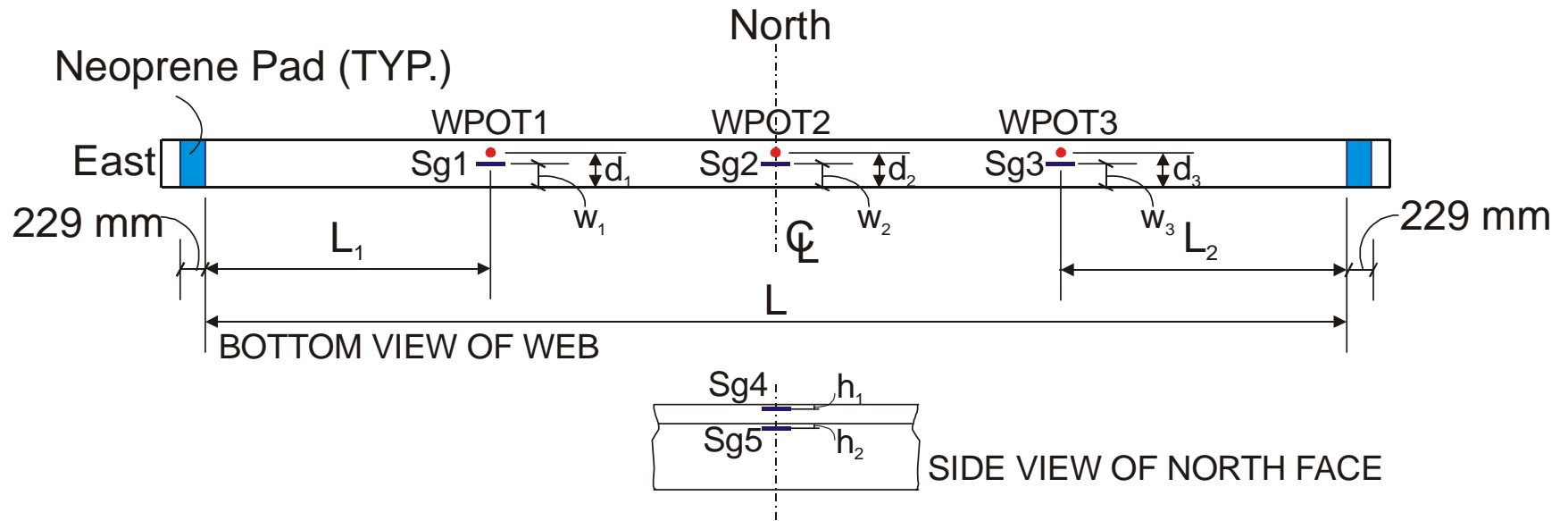


Figure A.6 Test Setup Before Installation of FRP Systems



Beam	L	L_1	L_2	w_1	d_1	w_2	d_2	w_3	d_3	h_1	h_2
1	9906	2477	2477	210	254	216	305	210	248	38.1	44.5
2	9957	2488	2496	167	205	192	205	195	205	50.8	60.3
3	9436	2559	2359	311	248	324	219	298	356	50.8	69.9
4	10008	2502	2502	222	231	204	128	223	160	76.2	77.8

Notes:

For Beam 2, Sg1 was 28.6 mm to the east of WPOT1.

For Beam 3, Sg2 was 31.8 mm to the west of WPOT2.

Sg2 was on reinforcing bar.

Figure A.7 Instrumentation Before Installation of FRP Systems



(a) Strain Gage on Reinforcing Bar at Midspan



(b) Strain Gage on Concrete Surface at Quarter Points



(c) Displacement Transducer at Midspan and Quarter Points

Figure A.8 Pictures of Various Instruments Before Installation of FRP Systems

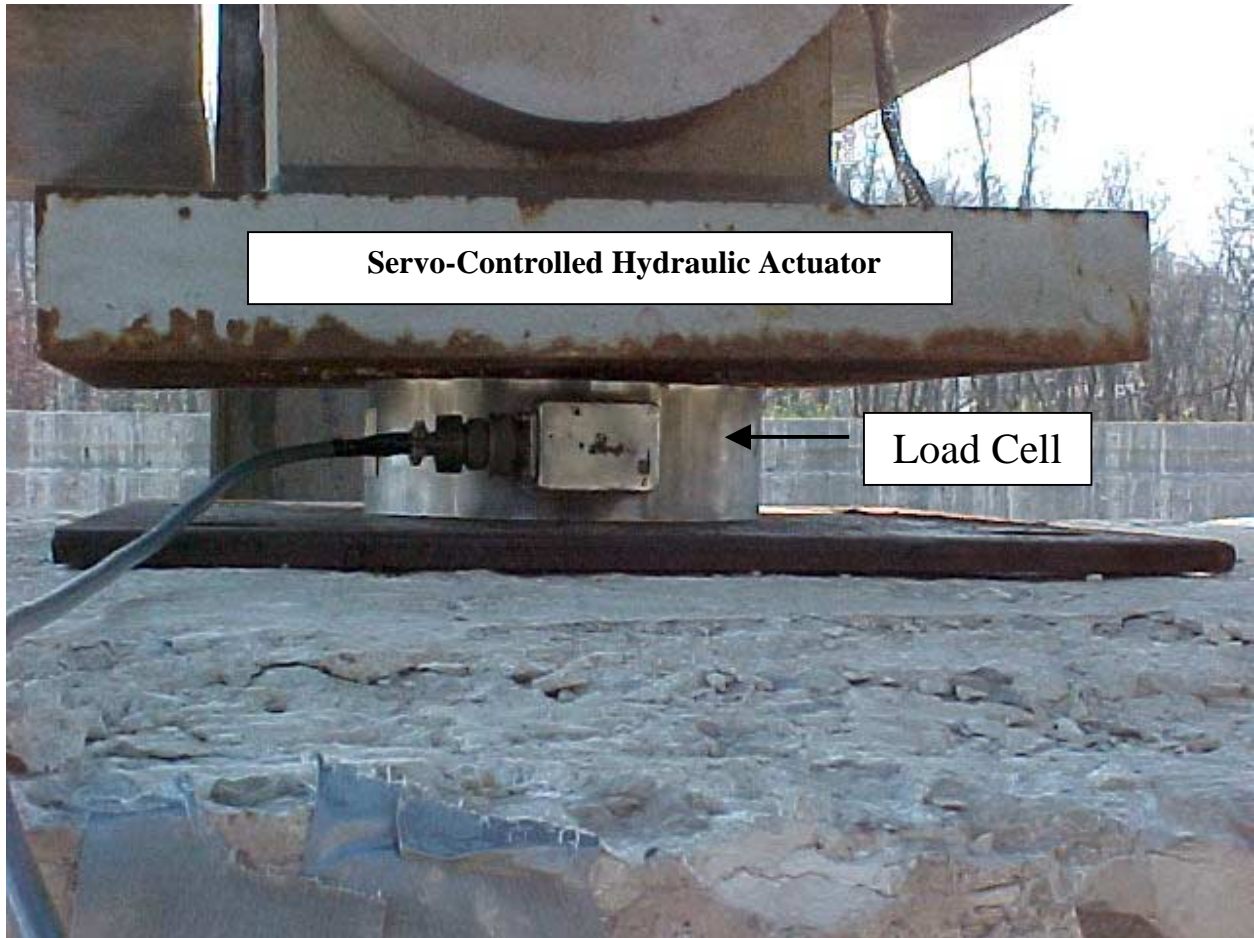


Figure A.9 Picture of Load Cell in Test Setup Before Installation of FRP

Application Procedures for Various FRP Systems

- **76.2-mm Bonded Plates**

1. Clean the concrete surface with high-pressure steam. Repair any deteriorated or spalled areas of the concrete to ensure that concrete surface is of good sound condition. The surface must be roughened to a coarse sandpaper texture either by sandblasting, shotblasting, or scarifying with a toothed grinder. The surface must be cleaned of all dirt and debris, and be free of all apparent moisture.
2. Mark the locations of the plates.
3. Apply FRS Epoxy Primer to the prepared surface by using a paint roller. Allow primer to dry for a minimum of thirty minutes. Mix the FRS Structural Epoxy in accordance with the manufacturer's directions, and apply a layer of FRS Structural Epoxy to the prepared concrete surface using a 3.175-mm v-notched trowel. The epoxy must fill any voids and uneven areas.



Application of Structural Epoxy on Primed Surface

4. Cut all FRS material to required lengths.
5. Clean the sanded side of the FRS plates with a degreaser (i.e., acetone or MEK) and allow to dry before applying epoxy.
6. Apply FRS Structural Epoxy using a 3.175-mm v-notched trowel to the sanded side of the FRS plate. Install the plate by starting at one end and moving along the length of the plate until complete. Apply enough pressure to press out any excess epoxy and trapped air pockets. Remove any excess FRS Structural Epoxy. The epoxy gains 90% of its bond strength within the first 48 hours. Bracing or wedging with lumber is typically not required, as 76.2-mm plates do not problems with sagging.



Installation of FRP plate

- **102-mm Bolted Plates**

1. Clean the concrete surface with high-pressure steam. Repair any deteriorated or spalled areas of the concrete to ensure that concrete surface is of good sound condition. The surface must be roughened to a coarse sandpaper texture either by sandblasting, shotblasting, or scarifying with a toothed grinder. The surface must be cleaned of all dirt and debris, and be free of all apparent moisture.
2. Mark the locations of the plates.
3. Apply FRS Epoxy Primer to the prepared surface by using a paint roller. Allow primer to dry for a minimum of thirty minutes. Mix the FRS Structural Epoxy in accordance with the manufacturer's directions, and apply a layer of FRS Structural Epoxy to the prepared concrete surface using a 3.175-mm v-notched trowel. The epoxy must fill any voids and uneven areas.
4. Cut all FRS material to required lengths.
5. Clean the sanded side of the FRS plates with a degreaser (i.e., acetone or MEK) and allow to dry before applying epoxy.
6. Apply FRS Structural Epoxy using a 3.175-mm v-notched trowel to the sanded side of the FRS Bolted Plate. Install the Bolted Plate by starting at one end and moving along the length of the Bolted Plate until complete. Apply enough pressure to press out any excess FRS Structural Epoxy and trapped air pockets. Remove any excess epoxy. The epoxy gains 90% of its bond strength within the first 48 hours. Shoring or wedging with lumber is typically necessary for the 102-mm plates due to their thickness and weight.



Shoring of 102-mm FRP Plates

7. Allow the FRS Structural Epoxy 24 hours to dry. After 24 hours, drill and install the anchors at the specified locations. Install a minimum of four A325 by 76.2 mm long anchors at each end of the 102-mm plates. The anchors must be at least 12.7 mm in diameter. The holes should be drilled at not less than 152 mm on center with the first placed not closer than 36 mm from the ends of the plate. Stagger the anchor bolts.

- **Bonded Fabrics**

1. Clean the concrete surface with high-pressure steam. Repair any deteriorated or spalled areas of the concrete to ensure that concrete surface is of good sound condition. The surface must be roughened to a coarse sandpaper texture either by sandblasting, shotblasting, or scarifying with a toothed grinder. Corners to be wrapped must be rounded to a minimum of 19.1-mm diameter. The surface must be cleaned of all dirt and debris, and be free of all apparent moisture.
2. Apply FRS Epoxy Primer to the prepared surface by using a paint roller. Allow primer to cure for a minimum of thirty minutes. Fill all voids and uneven areas with the FRS Structural Epoxy.
3. Apply a heavy layer of the FRS Saturating Epoxy using a paint roller. After unrolling the FRS Fabric, press it into place at the center and move toward each end. The Fabric must be kept tight and wrinkle free. Apply a heavy layer of FRS Saturating Epoxy over the fabric. Use Fabric rollers to remove any trapped air pockets, and work the saturating epoxy into the Fabric. Wait approximately 30 minutes and apply an additional coat of saturating epoxy. Repeat if additional layers of fabric are required.

- **Post-tensioning with Smooth Rods**

1. Mark the locations at which the anchor bracket will be attached to the web.



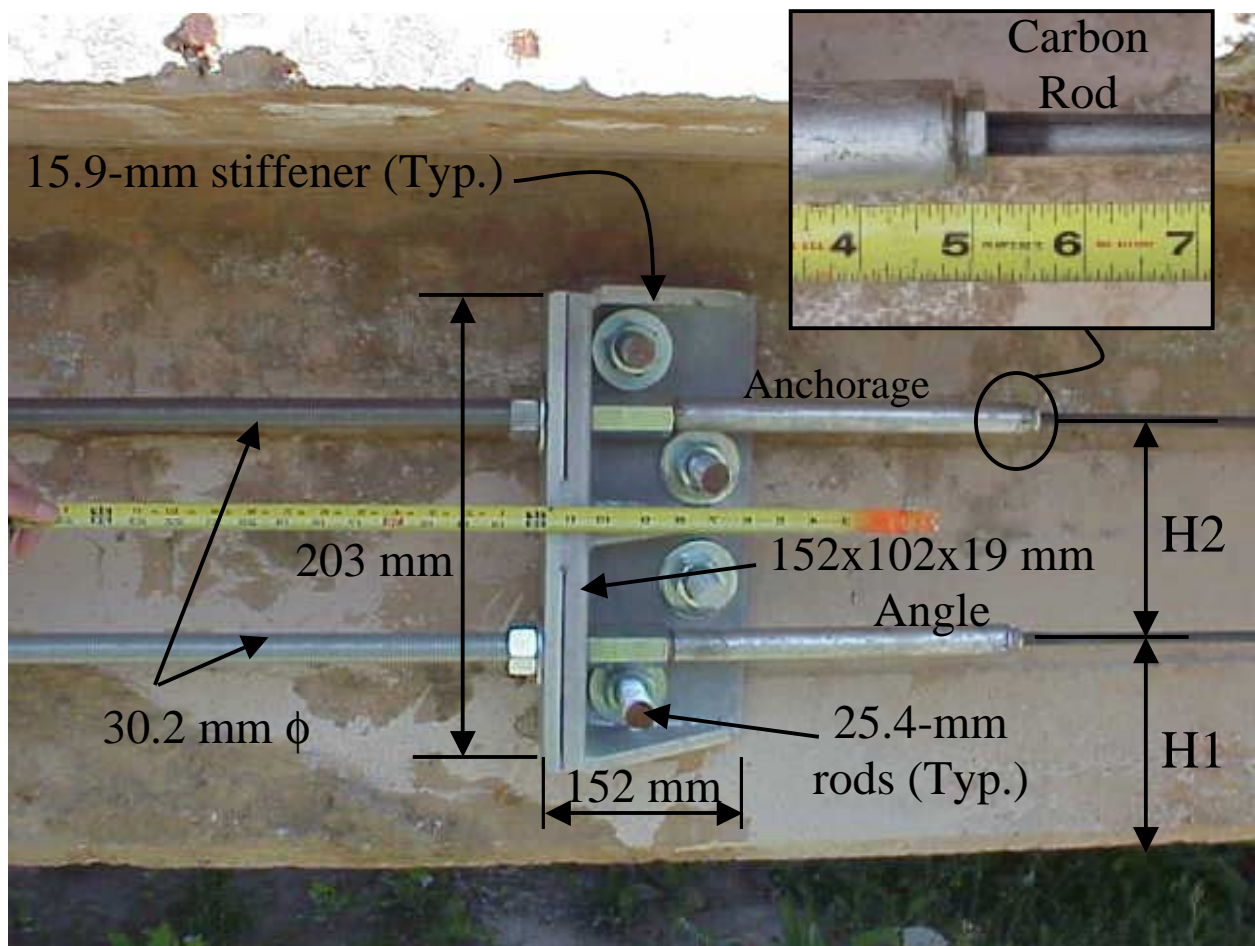
2. Drill holes through the web.



3. Bolt the anchor brackets (one on each side of the web) at each end of the beam.

4. Connect the smooth rod with anchors to the anchor bracket and pull each rod to 45% of the ultimate capacity of the system. Load the rods 50% of the final load on one side of the side of the web, load the rods on the other side of the web to 100% of the final load, and then go back to the first side and load to 100% of the final load.

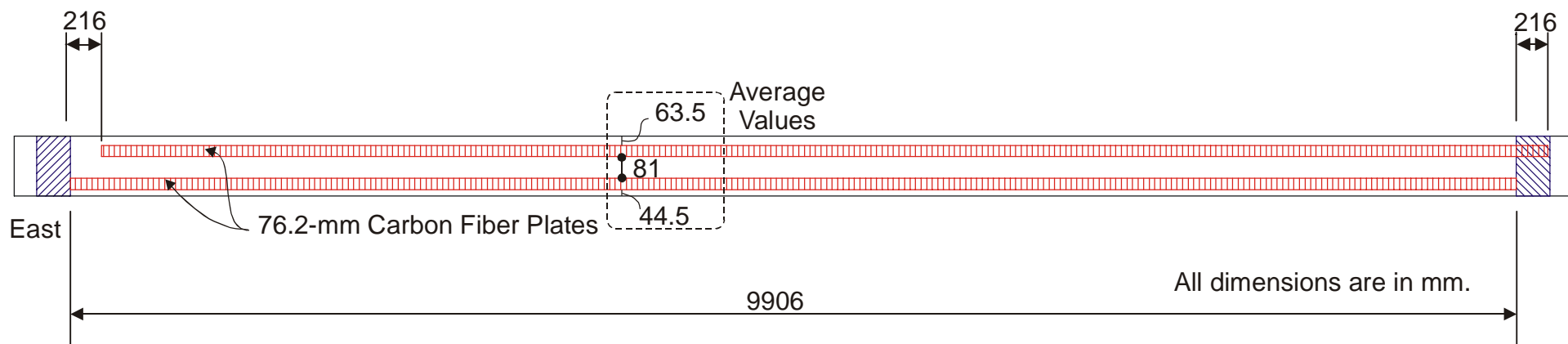




Location	H1 (mm)	H2 (mm)
North Face – East Anchor	216	178
North Face – Middle	229	178
North Face – West Anchor	216	178
South Face – East Anchor	219	178
South Face – Middle	222	178
South Face – West Anchor	216	178

East anchors were 4,560 mm from the center line.
 West anchors were 4,064 mm from the center line.

Figure A.10 Anchor System in Beam 1



(a) General Layout of FRP Plates



W1 = 38.1 to 50.8 mm
 W2 = 79.4 to 82.3 mm
 W3 = 63.5 mm

(b) Photograph of 76.2-mm Bonded Plates

Figure A.11 Bottom View of Beam



(a) Overall View

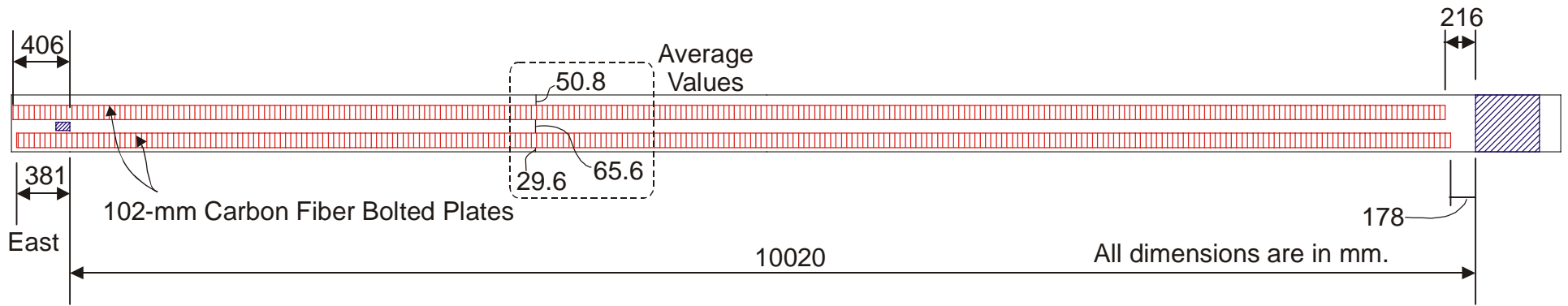


(b) View of Bottom of Web

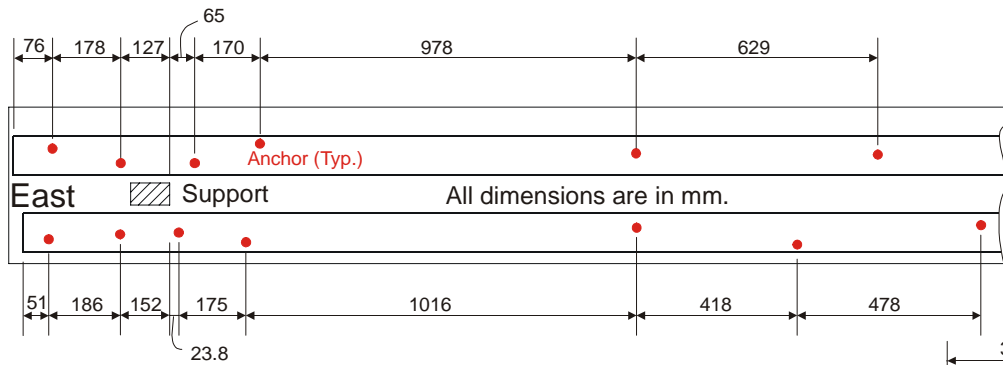


(c) View of Web Reinforcement

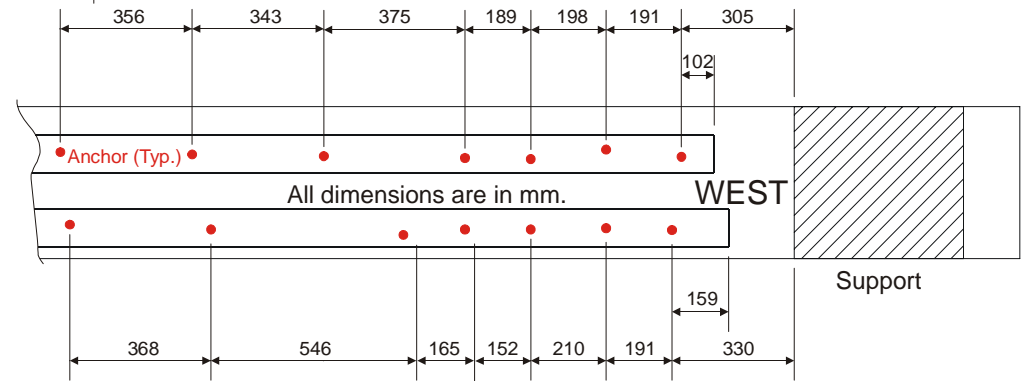
Figure A.12 Longitudinal and Web Fabric in Beam 3



(a) General Layout of FRP Plates



(b) Bolt Spacing – East Side



(c) Bolt Spacing – West Side

Figure A.13 Bottom View of Beam 4



(a) East Support

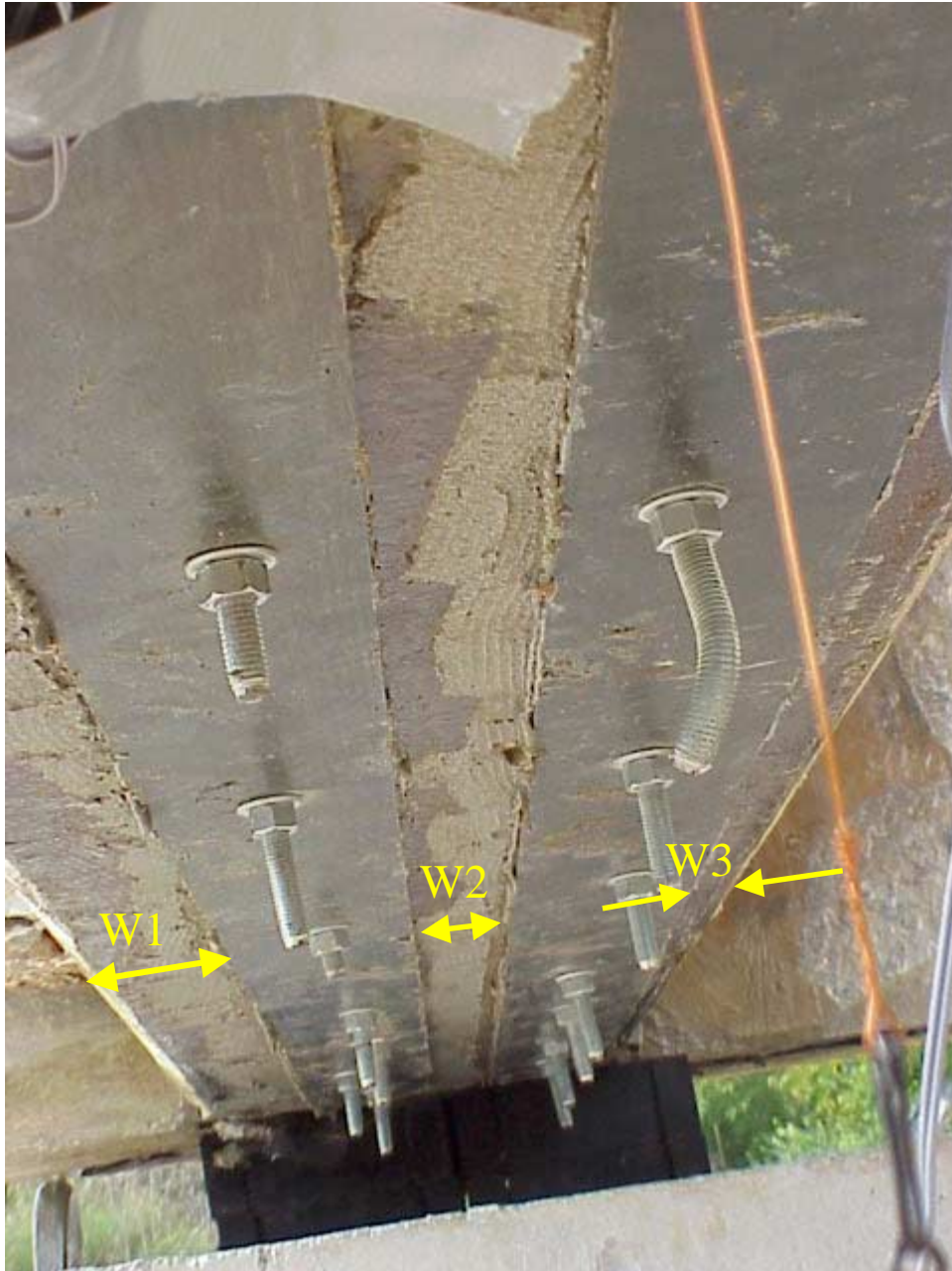


(b) West Support



(c) Overall View of Bolts

Figure A.14 Photographs Showing Supports and Anchor Bolts in Beam 4



W1 = 25.4 to 76.2 mm
W2 = 50.8 to 76.2 mm
W3 = 19.1 to 44.5 mm

Figure A. 15 Locations of Bolted Plates in Beam 4

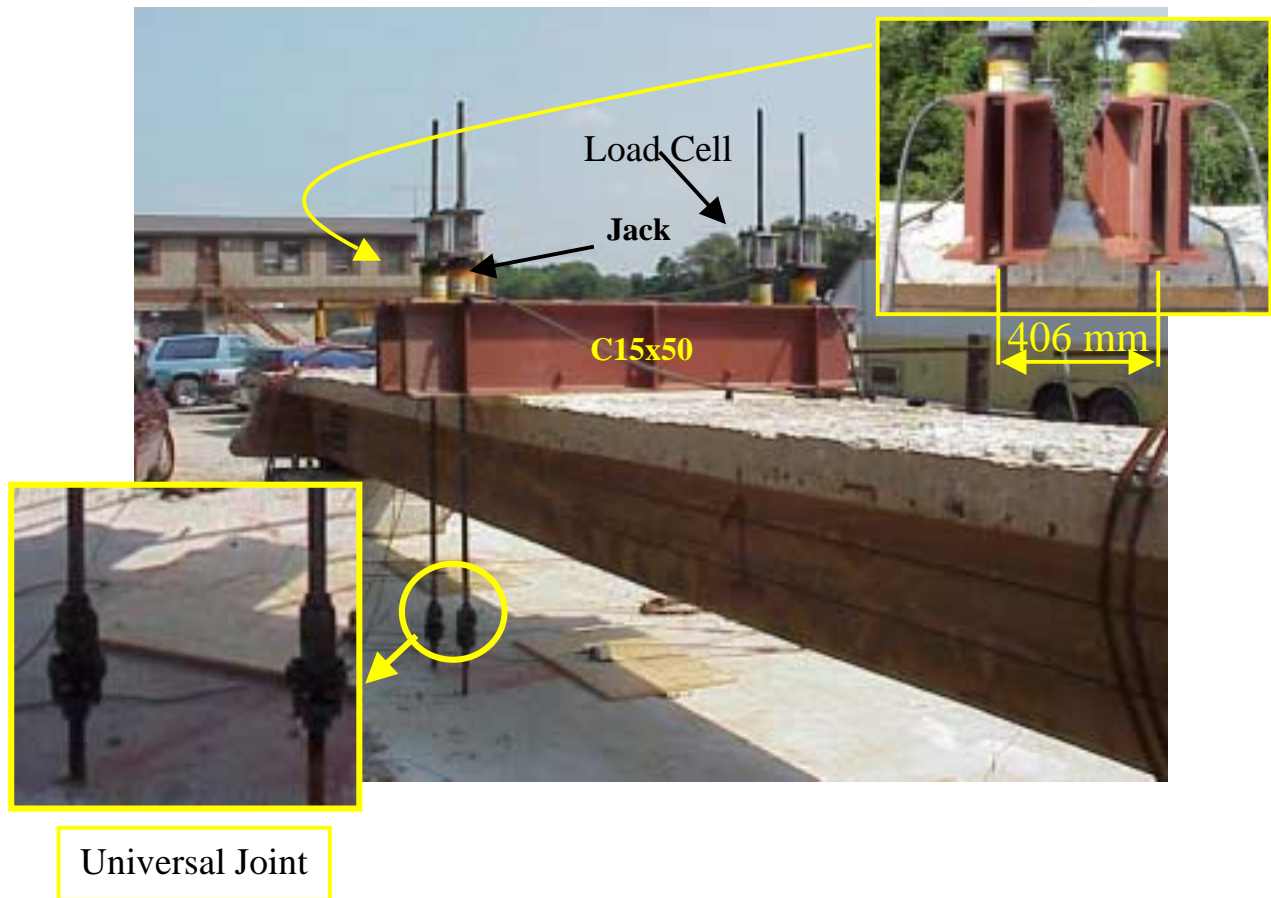


Figure A.16 Test Setup After Installation of FRP Systems

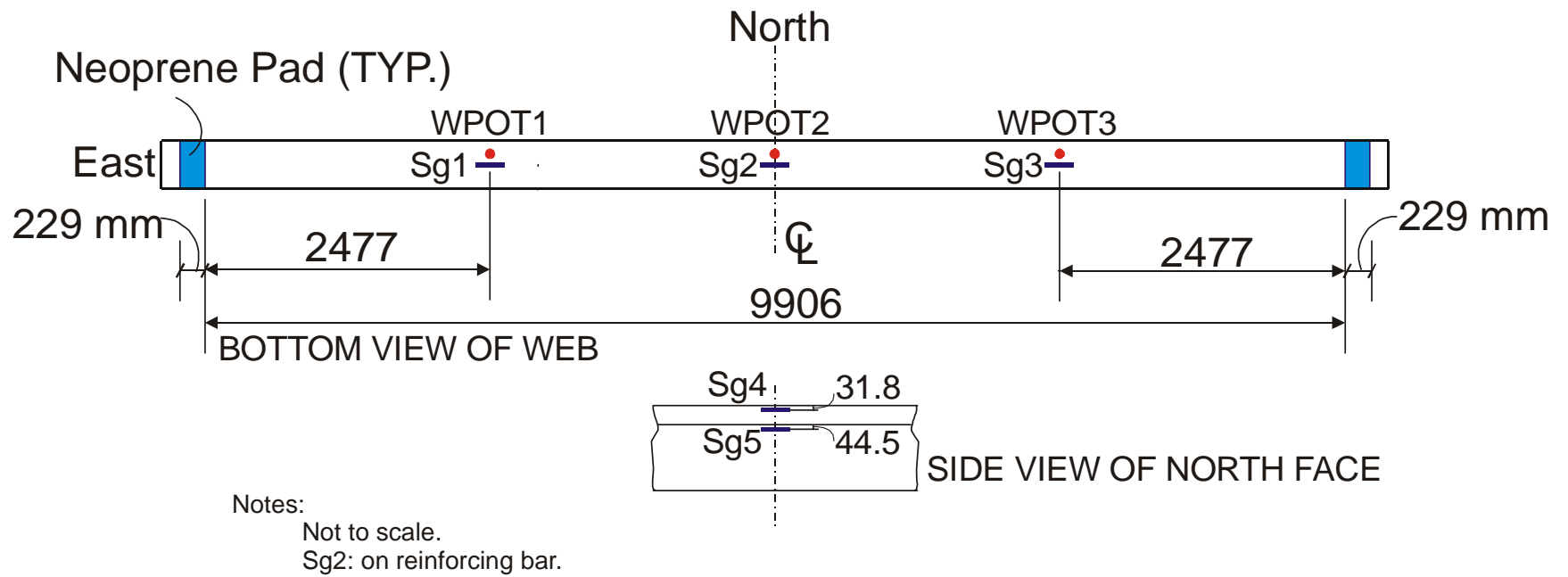
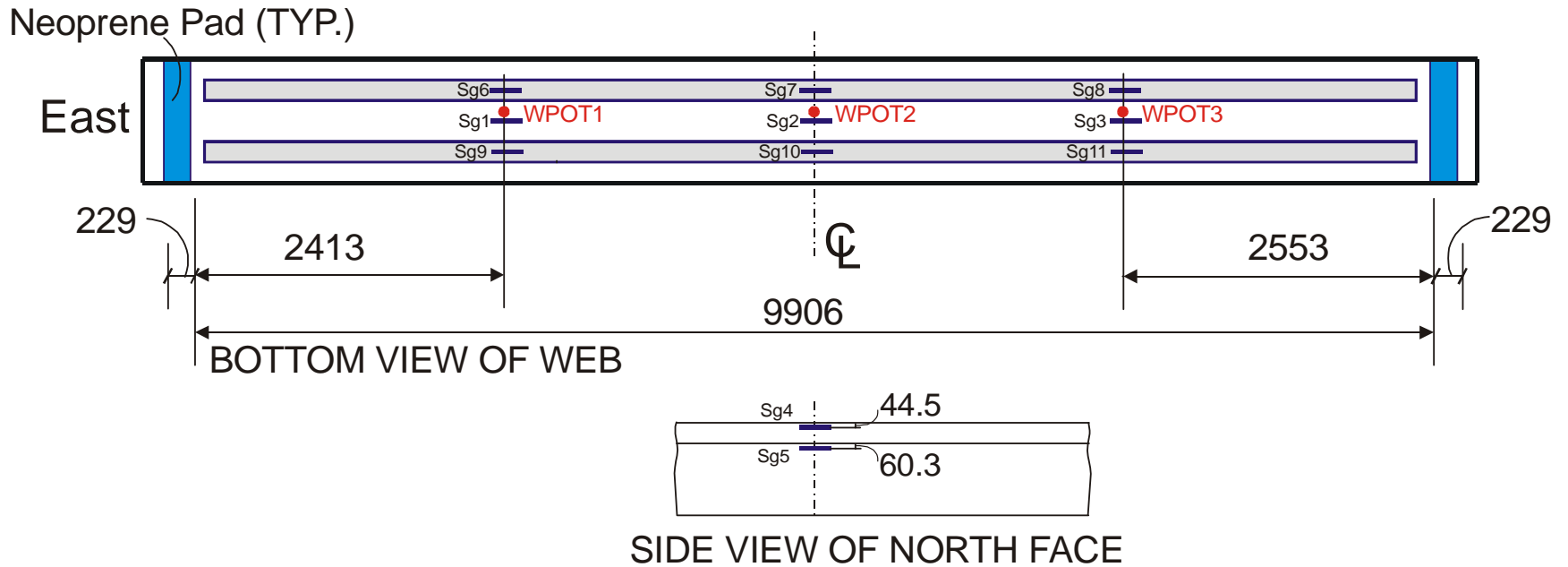


Figure A.17 Instrumentation for Beam 1 After Installation of FRP Systems



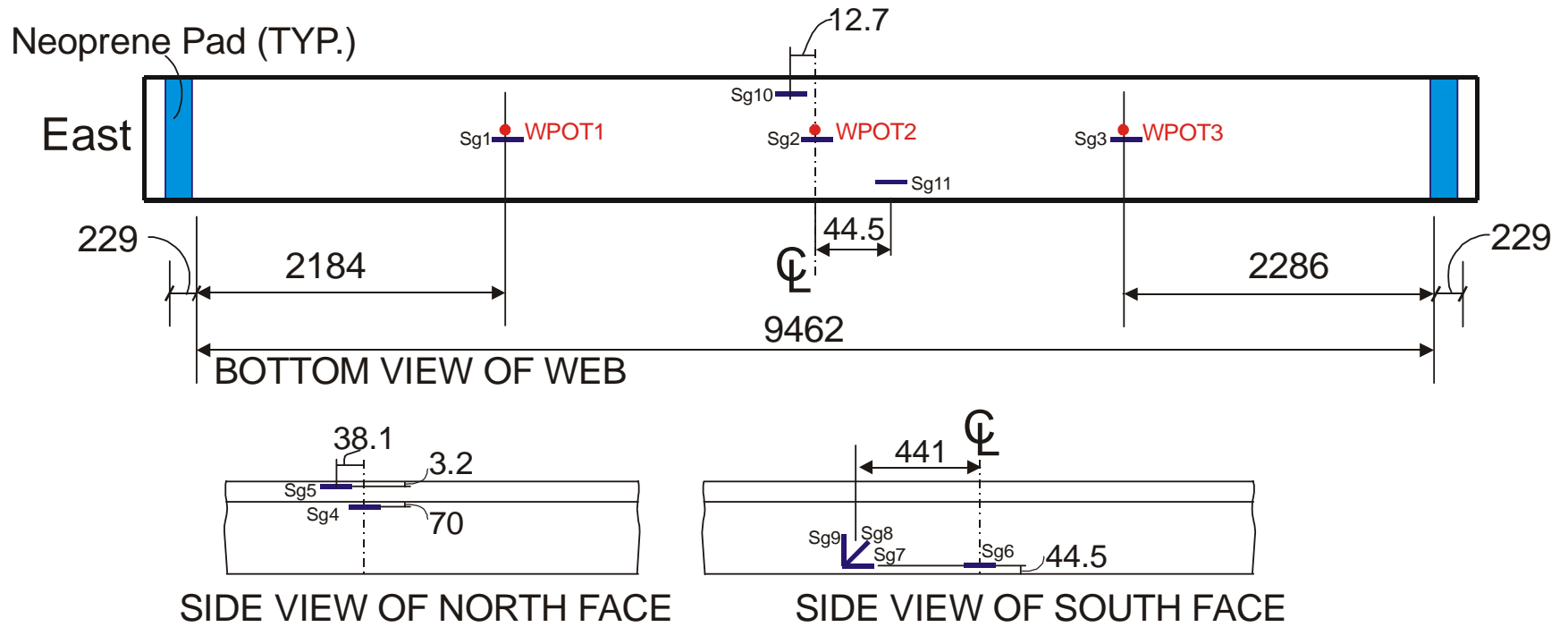
Notes:

Not to scale.

The shown extents of FRP plates do not correspond to the actual values.

Sg2: on reinforcing bar.

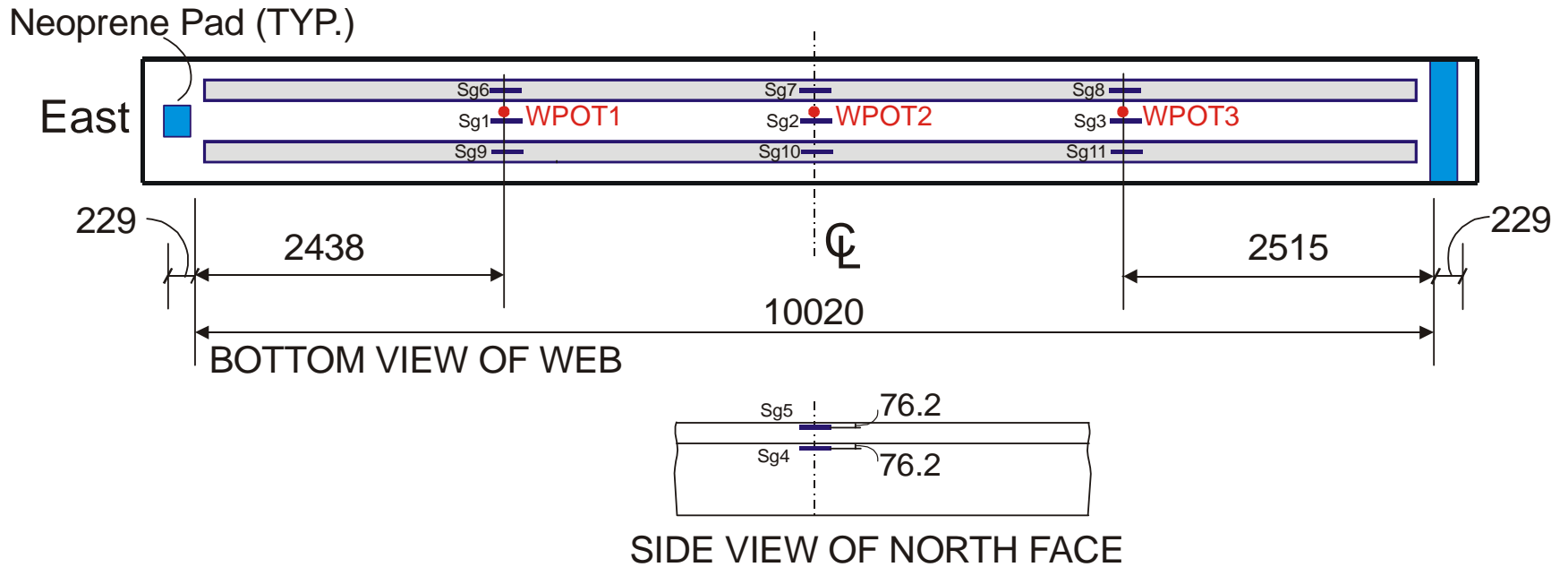
Figure A.18 Instrumentation for Beam 2 After Installation of FRP Systems



Notes:

- Not to scale.
- Sg2: on reinforcing bar.
- Sg1 and Sg3: on concrete surface under longitudinal fabric.
- Sg10: on transverse fabric on the bottom.
- Sg11: on longitudinal fabric on the bottom.

Figure A.19 Instrumentation for Beam 3 After Installation of FRP Systems



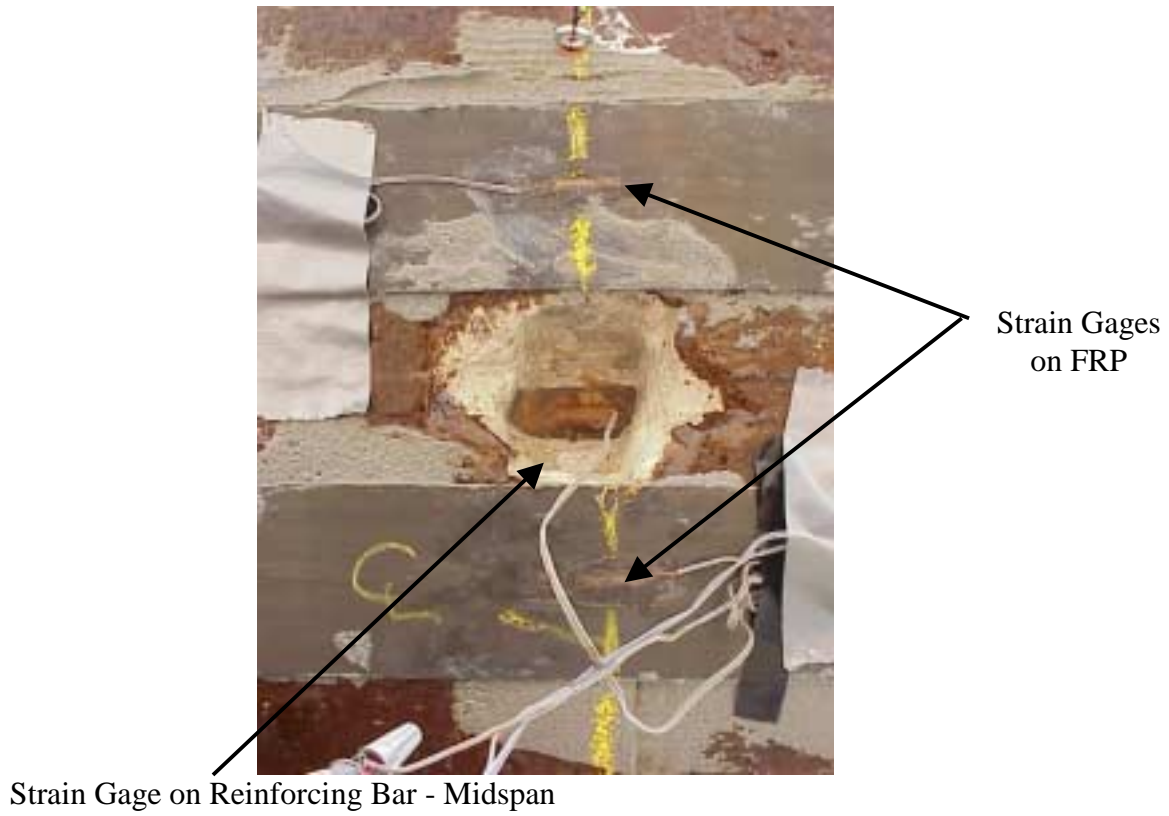
Notes:

Not to scale.

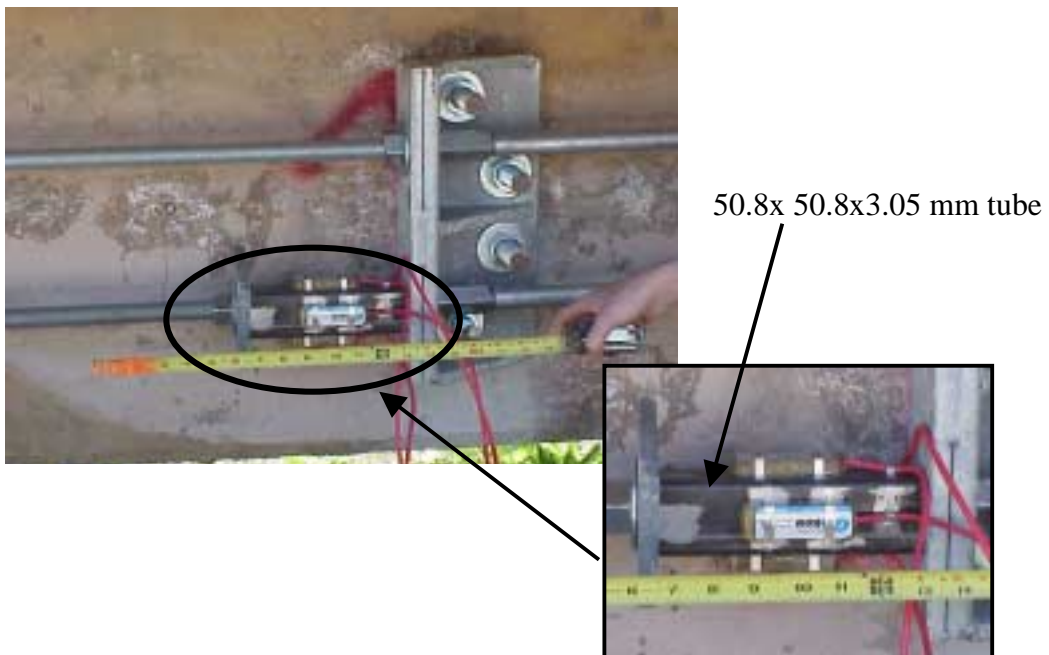
The shown extents of FRP plates do not correspond to the actual values.

Sg2: on reinforcing bar.

Figure A.20 Instrumentation for Beam 4 After Installation of FRP Systems

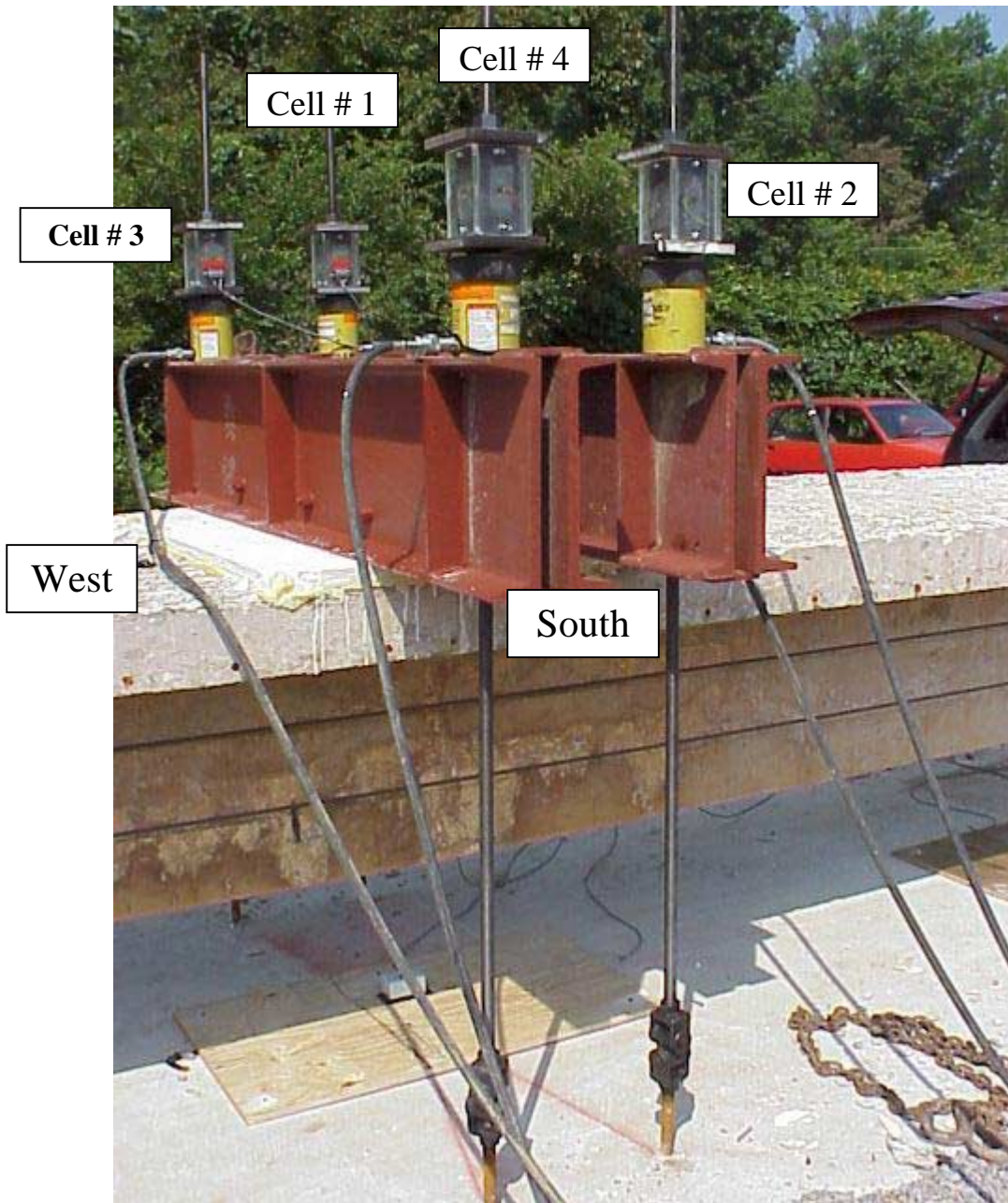


(a) Strain Gages on Steel and FRP



(b) Load Cell for Monitoring of Loss of Pre-Stressing Force in Beam 1

Figure A.21 Pictures of Additional Instruments After Installation of FRP Systems



(c) Location of Load Cells

Figure A.21 (Cont.) Pictures of Additional Instruments After Installation of FRP Systems

Calculation of Force in Tension Tie

Refer to the figure shown below. In this figure, the deflections are magnified for illustration purposes.

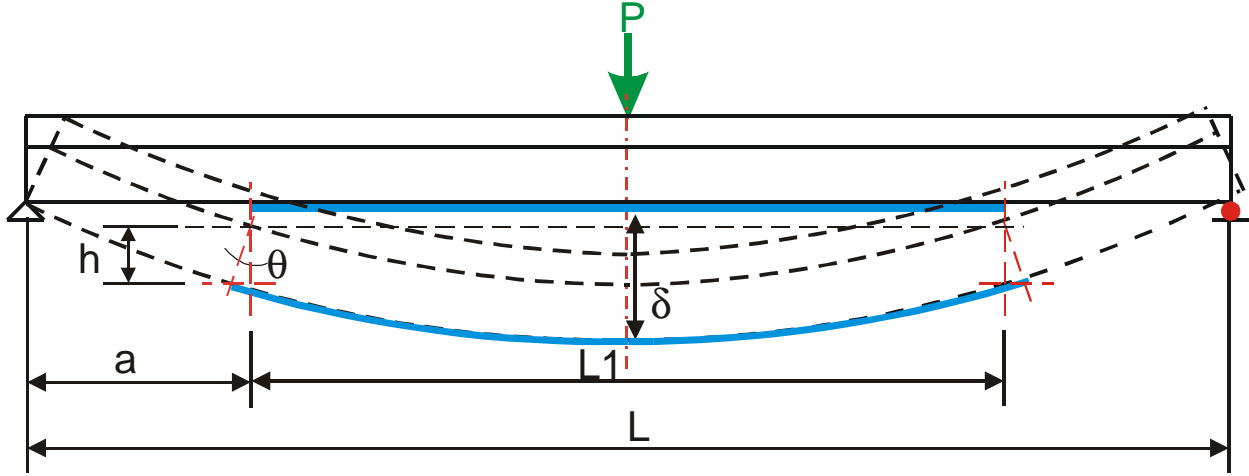


Figure 1

Assume that a second-degree parabola represents the equation of the elastic curve, i.e., $y=ax^2+bx+c$. By imposing the boundary conditions of @ $x=0: y=0$, @ $x=0.5L: y=\delta$, and @ $x=0.5L: dy/dx=0$, this equation is simplified to $y = -\frac{4\delta}{L^2}x^2 + \frac{4\delta}{L}x$. After the beam deforms, the

length of the bottom fiber on half of the beam is obtained from $\int_0^{0.5L} \sqrt{1 + \left(\frac{4\delta}{L} - \frac{8\delta}{L^2}x\right)^2} dx$. After

integration, this equation becomes $\frac{L}{4} \sqrt{1 + 16\left(\frac{\delta}{L}\right)^2} - \frac{1}{16\left(\frac{\delta}{L^2}\right)} \ln \left[-\frac{4\delta}{L^2} + \sqrt{1 + 16\left(\frac{\delta}{L}\right)^2} \right]$.

The strain in the CFRP plates as a result of beam curvature is computed based on the new length. From this strain, the force in the CFRP plates can be obtained easily as the plates remained elastic. The ratio of the computed CFRP force to the measured force is plotted in Figure 2. As seen from this figure, the contribution of beam curvature is small. At the largest deflection, corresponding to $L/65$ where L is the span length, the force in the CFRP plates due to the beam curvature is 16% of the total measured force. The relationship between the force in CFRP plates from the beam curvature and midspan deflection for Beam 4 can be simplified as $F = 0.0007\delta^2 + 0.0002\delta$ (see Figure 3), in which F = force in the CFRP plates in kN and δ is the midspan deflection in mm. Considering the small coefficients and the maximum contribution due to beam curvature is 16% (Figure 2), this component is ignored in the rest of the derivations.

Another component that elongates the CFRP plates is the rotation of the beam at each anchor point (θ_1). Based on Figure 1, the elongation of the CFRP plates at each anchor point is $\theta_1 h$ where h is the distance from the neutral axis to the bottom fiber, and θ_1 is the rotation of the beam at the anchor points. The distance to the neutral axis is used to compute the elongation since the length of the neutral axis does not change. The total elongation of the CFRP plates is

$2\theta_1 h$. The resulting strain in each CFRP plate is $\frac{(L1 + 2\theta_1 h) - L1}{L1} = \frac{2\theta_1 h}{L1}$.

The rotation at each anchor point is related to the midspan deflection according to the following equations.

$$\delta = \frac{PL^3}{48EI}$$

$$\text{Elastic: } \theta_1 = \frac{P}{4EI} \left(\frac{L^2}{4} - a^2 \right) \quad \text{Fully Plastic: } \theta_1 = \frac{2\delta}{L}$$

$$\therefore \theta_1 = \frac{12\delta}{L^3} \left(\frac{L^2}{4} - a^2 \right)$$

Using the above equations and strain in each CFRP plate ($\frac{2\theta_1 h}{L1}$); the force in each CFRP plate is computed.

$$\text{Elastic: } F = \frac{2AE}{L1} h \frac{12\delta}{L^3} \left(\frac{L^2}{4} - a^2 \right) \quad \text{Fully Plastic: } \frac{2AE}{L1} h \frac{2\delta}{L}$$

By substituting the values of a (1872 mm), L1 (8128 mm), L (10008 mm), A (4.76 x 101.6 mm = 483.9 mm²), the following relations between F (in kN) and δ (in mm) are obtained for Beam 4.

$$\text{Elastic: } F = 0.0016297\delta h$$

$$\text{Fully Plastic: } F = 0.001263\delta h.$$

Since the beam does not crack extensively at the anchor points, the value of h is taken as the distance from the bottom fiber to the neutral axis of the uncracked section. For simplicity, the influence of reinforcement is ignored here. For Beam 4, the value of h = 444mm. Therefore,

$$\text{Elastic: } F = 0.724\delta$$

$$\text{Fully Plastic: } F = 0.561\delta$$

As seen from Figure 5, the measured force in the CFRP plates is bracketed by the computed values. Since the beam is neither completely elastic nor fully plastic, the average value of the coefficients for the elastic case and fully plastic case may be used, i.e., $F = 0.642\delta$. The resulting computed force in the CFRP plates matches the measured force (Figure 5) remarkably well. The aforementioned model provides a simple, yet effective method, to compute the expected force in the CFRP plates as a function of the midspan deflection.

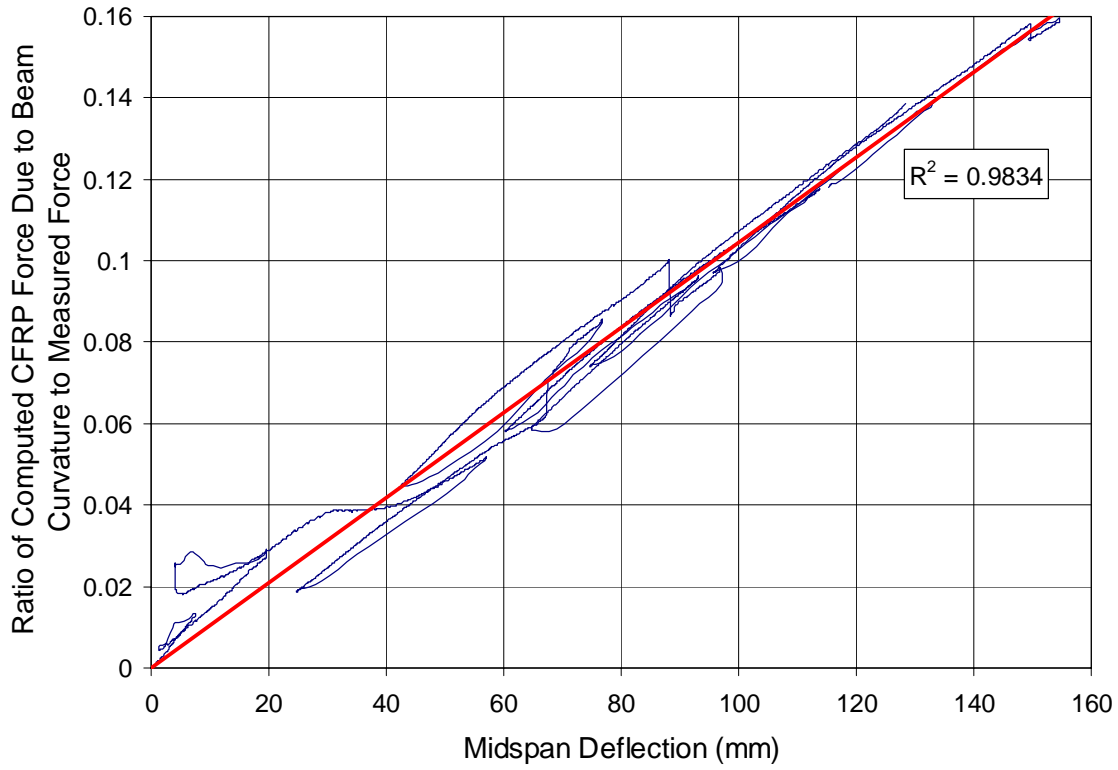


Figure 2 Contribution of Beam Curvature to Force in CFRP Plates

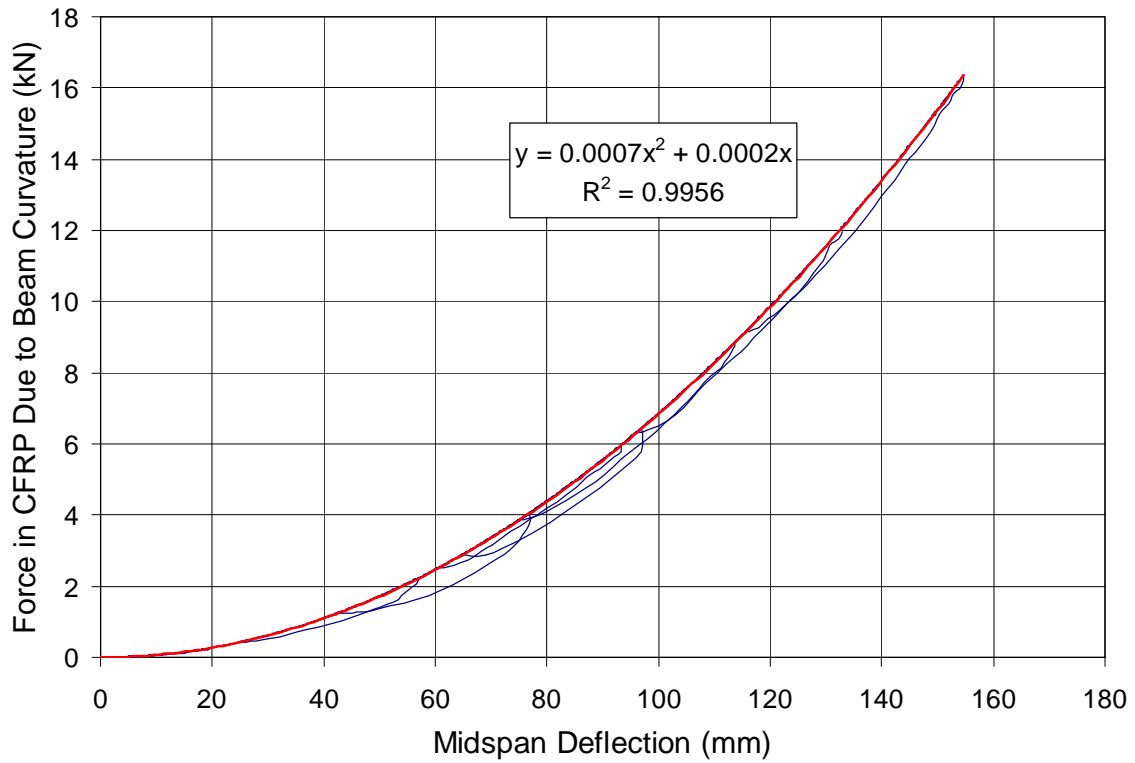


Figure 3 Simplification of Force in CFRP Plates due to Beam Curvature

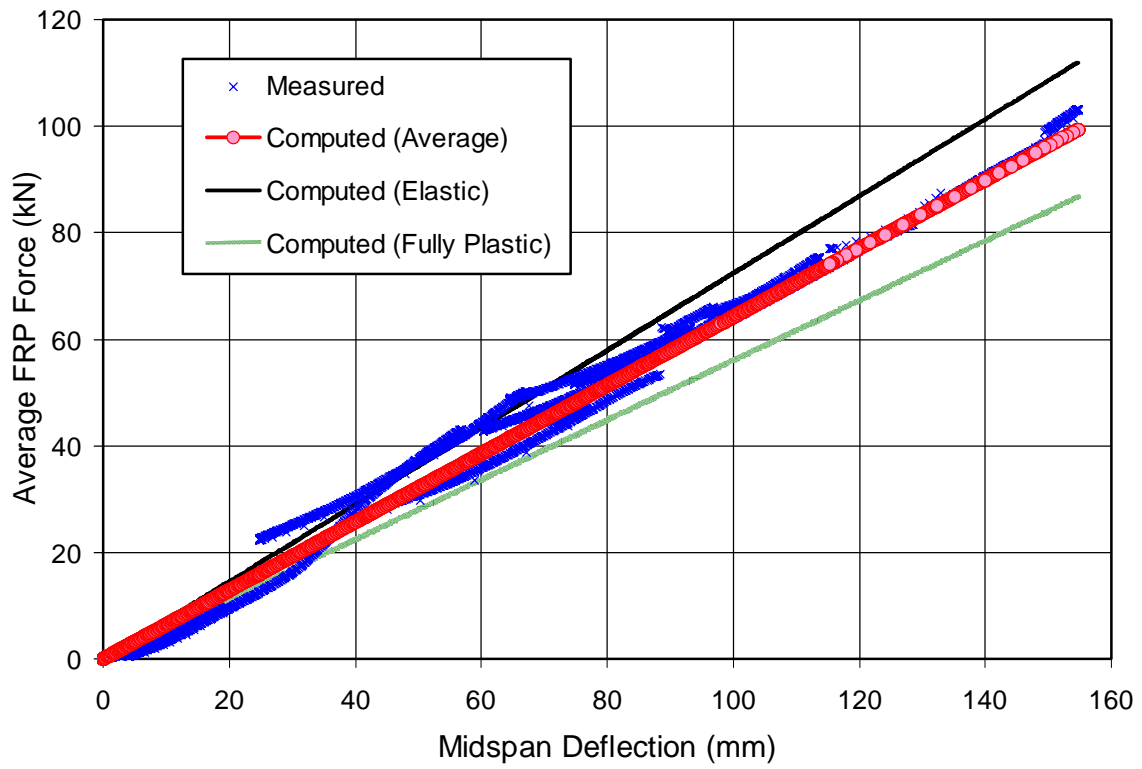


Figure 4 Verification of Analytical Model for Computing Force in CFRP Plates

APPENDIX B:
Supporting Documents and
Data for Part II

Table B.1 Measured Material Properties for Various FRP Systems

(a) Carbon Fiber Plates

Nominal Plate Width (mm)	Sample I.D.	F_u (MPa)	E (MPa)	Fracture Strain (%)
76.2	1	2245	----	
	2	2253	----	
	3	2199	----	
	4	2460	155052	
	Average	2289	155052	
127	1	1104	----	
	2	1109	----	
	3	1107	108602	
	4	1146	124425	
	Average	1117	116514	
102 (Bolted)	1	631	50938	
	2	633	54832	
	3	563	----	
	4	526	----	
	5	542	53515	
	6	607	----	
	7	611	----	
	8	567	----	
	Average	585	53095	

(b) One Layer of Carbon Fabric

Fabric Orientation	Sample I.D.	F_u (kN/mm)	E (kN/mm)	Fracture Strain (%)
Longitudinal	1	0.523	55.8	
	2	0.541	61.3	
	3	0.551	----	
	4	0.571	----	
	Average	0.547	58.5	
Transverse	1	0.0115	3.52	
	2	0.0127	3.51	
	3	0.0069	4.11	
	Average	0.0104	3.81	

Table B.2 Rating Factors and Load Limits (kN) Based on Moments Before Retrofitting

Load	Operating Level														
	AB 1		MS1		PR1		MS2		PR2		MS3		AB2		
	R.F.	Load	R.F.	Load	R.F.	Load	R.F.	Load	R.F.	Load	R.F.	Load	R.F.	Load	
HS20-44	83.8	13405	1.5	247	15.5	2474	1.4	232	14.4	2310	1.5	240	65	10360	Lane1
	64.8	10363	1.5	241	14.4	2312	1.4	232	15.5	2473	1.5	245	84	13401	Lane2
	64.8	10363	1.5	241	14.4	2312	1.4	232	14.4	2310	1.5	240	64.7	10360	Critical Value
2F1	121.5	8099	2.4	159	27.4	1830	2.2	150	27.1	1808	2.4	158	88	5888	Lane1
	88.3	5890	2.4	159	27.1	1809	2.2	150	27.4	1829	2.4	158	121	8097	Lane2
	88.3	5890	2.4	159	27.1	1809	2.2	150	27.1	1808	2.4	158	88.3	5888	Critical Value
3F1	83.9	8581	2.3	231	19.1	1957	2.1	213	19.2	1958	2.3	230	66	6717	Lane1
	65.7	6719	2.3	232	19.2	1960	2.1	213	19.1	1956	2.2	229	84	8578	Lane2
	65.7	6719	2.3	231	19.1	1957	2.1	213	19.1	1956	2.2	229	65.7	6717	Critical Value
4F1	78.6	9436	2.3	280	17.2	2063	2.1	257	17.5	2098	2.3	277	58	6981	Lane1
	58.2	6983	2.3	279	17.5	2099	2.1	257	17.2	2062	2.3	278	79	9433	Lane2
	58.2	6983	2.3	279	17.2	2063	2.1	257	17.2	2062	2.3	277	58.2	6981	Critical Value
5C1	86.0	15292	2.3	411	20.0	3563	2.2	383	19.8	3521	2.3	402	68	12125	Lane1
	68.2	12129	2.3	404	19.8	3523	2.2	383	20.0	3561	2.3	408	86	15287	Lane2
	68.2	12129	2.3	404	19.8	3523	2.2	383	19.8	3521	2.3	402	68.2	12125	Critical Value
Lane Load	140.7	20796	2.2	332	19.7	2889	2.1	318	18.7	2862	2.2	319	79	11615	Lane1
	78.6	11619	2.3	333	18.7	2742	2.1	318	19.7	3015	2.2	318	141	20790	Lane2
	78.6	11619	2.2	332	18.7	2742	2.1	318	18.7	2862	2.2	318	78.6	11615	Critical Value

See Figure B.21 for loads, number of axles, and distance between the axles.

AB1= Rear Abutment

AB2= Forward Abutment

MS1, MS2, and MS3 = Midspan of Span 1, Span 2, and Span 3, respectively.

See Figure B.22 for the locations of Lane 1 and Lane 2.

Table B.2 (Cont.) Rating Factors and Load Limits (kN) Based on Moments Before Retrofitting

Load	Inventory Level														
	AB 1		MS1		PR1		MS2		PR2		MS3		AB2		
	R.F.	Load	R.F.	Load	R.F.	Load	R.F.	Load	R.F.	Load	R.F.	Load	R.F.	Load	
HS20-44	50.2	8031	0.9	148	9.3	1482	0.9	139	8.6	1384	0.9	143	38.8	6206	Lane1
	38.8	6208	0.9	144	8.7	1385	0.9	139	9.3	1482	0.9	147	50.2	8028	Lane2
	38.8	6208	0.9	144	8.7	1385	0.9	139	8.6	1384	0.9	143	38.8	6206	Critical Value
2F1	72.8	4852	1.4	95	16.4	1096	1.3	90	16.2	1083	1.4	95	52.9	3527	Lane1
	52.9	3528	1.4	95	16.3	1084	1.3	90	16.4	1096	1.4	95	72.8	4851	Lane2
	52.9	3528	1.4	95	16.3	1084	1.3	90	16.2	1083	1.4	95	52.9	3527	Critical Value
3F1	50.3	5141	1.4	138	11.5	1172	1.3	128	11.5	1173	1.4	138	39.4	4024	Lane1
	39.4	4025	1.4	139	11.5	1174	1.3	128	11.5	1172	1.3	137	50.3	5139	Lane2
	39.4	4025	1.4	138	11.5	1172	1.3	128	11.5	1172	1.3	137	39.4	4024	Critical Value
4F1	47.1	5653	1.4	168	10.3	1236	1.3	154	10.5	1257	1.4	166	34.8	4182	Lane1
	34.9	4184	1.4	167	10.5	1257	1.3	154	10.3	1235	1.4	167	47.1	5651	Lane2
	34.9	4184	1.4	167	10.3	1236	1.3	154	10.3	1235	1.4	166	34.8	4182	Critical Value
5C1	51.5	9161	1.4	246	12.0	2134	1.3	229	11.9	2109	1.4	241	40.9	7264	Lane1
	40.9	7266	1.4	242	11.9	2110	1.3	229	12.0	2133	1.4	245	51.5	9158	Lane2
	40.9	7266	1.4	242	11.9	2110	1.3	229	11.9	2109	1.4	241	40.9	7264	Critical Value
Lane Load	84.3	12458	1.3	199	11.8	1731	1.3	191	11.2	1715	1.3	191	47.1	6958	Lane1
	47.1	6960	1.3	199	11.2	1643	1.3	191	11.8	1806	1.3	190	84.3	12455	Lane2
	47.1	6960	1.3	199	11.2	1643	1.3	191	11.2	1715	1.3	190	47.1	6958	Critical Value

Table B.2 Rating Factors and Load Limits (kN) Based on Shear Before Retrofitting

Load	Operating Level														
	AB 1		MS1		PR1		MS2		PR2		MS3		AB2		
	R.F.	Load	R.F.	Load	R.F.	Load	R.F.	Load	R.F.	Load	R.F.	Load	R.F.	Load	
HS20-44	19.8	3162	22.8	3641	29.8	4761	23.0	3675	30.2	4825	22.4	3577	20.2	3235	Lane1
	20.2	3235	22.4	3579	30.2	4830	23.0	3675	29.7	4756	22.7	3639	19.8	3162	Lane2
	19.8	3162	22.4	3579	29.8	4761	23.0	3675	29.7	4756	22.4	3577	19.8	3162	Critical Value
2F1	31.5	2098	37.7	2511	48.0	3198	35.9	2393	48.2	3215	35.7	2382	32.2	2149	Lane1
	32.2	2149	35.7	2383	48.3	3219	35.9	2393	47.9	3194	37.6	2510	31.5	2099	Lane2
	31.5	2098	35.7	2383	48.0	3198	35.9	2393	47.9	3194	35.7	2382	31.5	2099	Critical Value
3F1	32.8	3357	39.1	3997	49.7	5076	39.2	4009	50.3	5139	38.6	3946	31.3	3197	Lane1
	31.3	3196	38.6	3948	50.3	5144	39.2	4009	49.6	5071	39.1	3995	32.8	3357	Lane2
	31.3	3196	38.6	3948	49.7	5076	39.2	4009	49.6	5071	38.6	3946	31.3	3197	Critical Value
4F1	36.6	4397	51.1	6132	55.0	6602	45.6	5474	56.1	6737	45.2	5427	36.4	4362	Lane1
	36.4	4362	45.2	5430	56.2	6744	45.6	5474	55.0	6595	51.1	6129	36.6	4397	Lane2
	36.4	4362	45.2	5430	55.0	6602	45.6	5474	55.0	6595	45.2	5427	36.4	4362	Critical Value
5C1	31.3	5561	29.9	5324	34.8	6186	21.7	3866	28.5	5062	32.4	5756	32.6	5795	Lane1
	32.6	5795	32.4	5759	28.5	5068	21.7	3866	34.8	6179	29.9	5321	31.3	5561	Lane2
	31.3	5561	29.9	5324	28.5	5068	21.7	3866	28.5	5062	29.9	5321	31.3	5561	Critical Value
Lane Load	58.1	8587	27.3	4034	34.6	5074	27.2	4087	115.0	17602	26.4	3765	22.8	3374	Lane1
	22.8	3374	26.4	3905	115.2	16871	27.2	4087	34.6	5294	27.3	3889	58.1	8587	Lane2
	22.8	3374	26.4	3905	34.6	5074	27.2	4087	34.6	5294	26.4	3765	22.8	3374	Critical Value

Table B.2 Rating Factors and Load Limits (kN) Based on Shear Before Retrofitting

Load	Inventory Level														
	AB 1		MS1		PR1		MS2		PR2		MS3		AB2		
	R.F.	Load	R.F.	Load	R.F.	Load	R.F.	Load	R.F.	Load	R.F.	Load	R.F.	Load	
HS20-44	11.8	1894	13.6	2182	17.8	2852	13.8	2202	18.1	2891	13.4	2143	12.1	1938	Lane1
	12.1	1938	13.4	2144	18.1	2894	13.8	2202	17.8	2849	13.6	2180	11.8	1894	Lane2
	11.8	1894	13.4	2144	17.8	2852	13.8	2202	17.8	2849	13.4	2143	11.8	1894	Critical Value
2F1	18.9	1257	22.6	1504	28.7	1916	21.5	1433	28.9	1926	21.4	1427	19.3	1287	Lane1
	19.3	1287	21.4	1428	28.9	1928	21.5	1433	28.7	1914	22.5	1503	18.9	1257	Lane2
	18.9	1257	21.4	1428	28.7	1916	21.5	1433	28.7	1914	21.4	1427	18.9	1257	Critical Value
3F1	19.7	2011	23.4	2395	29.7	3041	23.5	2402	30.1	3079	23.1	2364	18.7	1915	Lane1
	18.7	1915	23.1	2365	30.1	3082	23.5	2402	29.7	3038	23.4	2393	19.7	2011	Lane2
	18.7	1915	23.1	2365	29.7	3041	23.5	2402	29.7	3038	23.1	2364	18.7	1915	Critical Value
4F1	22.0	2634	30.6	3674	33.0	3955	27.3	3279	33.6	4036	27.1	3251	21.8	2613	Lane1
	21.8	2613	27.1	3253	33.7	4040	27.3	3279	32.9	3951	30.6	3672	22.0	2634	Lane2
	21.8	2613	27.1	3253	33.0	3955	27.3	3279	32.9	3951	27.1	3251	21.8	2613	Critical Value
5C1	18.7	3331	17.9	3190	20.8	3706	13.0	2316	17.1	3033	19.4	3448	19.5	3472	Lane1
	19.5	3472	19.4	3450	17.1	3036	13.0	2316	20.8	3702	17.9	3188	18.7	3331	Lane2
	18.7	3331	17.9	3190	17.1	3036	13.0	2316	17.1	3033	17.9	3188	18.7	3331	Critical Value
Lane Load	34.8	5144	16.3	2417	20.7	3040	16.3	2448	68.9	10545	15.8	2256	13.7	2021	Lane1
	13.7	2021	15.8	2340	69.0	10107	16.3	2448	20.7	3171	16.3	2330	34.8	5144	Lane2
	13.7	2021	15.8	2340	20.7	3040	16.3	2448	20.7	3171	15.8	2256	13.7	2021	Critical Value

Table B.3 Rating Factors and Load Limits (kN) Based on Moments After Retrofitting

Load	Operating Level														
	AB 1		MS1		PR1		MS2		PR2		MS3		AB2		
	R.F.	Load	R.F.	Load	R.F.	Load	R.F.	Load	R.F.	Load	R.F.	Load	R.F.	Load	
HS20-44	83.8	13405	2.2	355	15.5	2474	1.8	283	14.4	2310	2.0	312	64.7	10360	Lane1
	64.8	10363	2.2	347	14.4	2312	2.1	335	15.5	2473	2.3	375	83.7	13401	Lane2
	64.8	10363	2.2	347	14.4	2312	1.8	283	14.4	2310	2.0	312	64.7	10360	Critical Value
2F1	121.5	8099	3.4	229	27.4	1830	2.7	183	27.1	1808	3.1	206	88.3	5888	Lane1
	88.3	5890	3.4	229	27.1	1809	3.2	216	27.4	1829	3.6	242	121.4	8097	Lane2
	88.3	5890	3.4	229	27.1	1809	2.7	183	27.1	1808	3.1	206	88.3	5888	Critical Value
3F1	83.9	8581	3.2	332	19.1	1957	2.5	260	19.2	1958	2.9	301	65.7	6717	Lane1
	65.7	6719	3.3	334	19.2	1960	3.0	309	19.1	1956	3.4	351	83.9	8578	Lane2
	65.7	6719	3.2	332	19.1	1957	2.5	260	19.1	1956	2.9	301	65.7	6717	Critical Value
4F1	78.6	9436	3.4	403	17.2	2063	2.6	313	17.5	2098	3.0	361	58.2	6981	Lane1
	58.2	6983	3.3	401	17.5	2099	3.1	371	17.2	2062	3.6	426	78.6	9433	Lane2
	58.2	6983	3.3	401	17.2	2063	2.6	313	17.2	2062	3.0	361	58.2	6981	Critical Value
5C1	86.0	15292	3.3	592	20.0	3563	2.6	467	19.8	3521	2.9	524	68.2	12125	Lane1
	68.2	12129	3.3	582	19.8	3523	3.1	554	20.0	3561	3.5	626	86.0	15287	Lane2
	68.2	12129	3.3	582	19.8	3523	2.6	467	19.8	3521	2.9	524	68.2	12125	Critical Value
Lane Load	140.7	20796	3.2	477	19.7	2889	2.6	388	18.7	2862	2.9	416	78.6	11615	Lane1
	78.6	11619	3.2	479	18.7	2742	3.1	460	19.7	3015	3.4	487	140.7	20790	Lane2
	78.6	11619	3.2	477	18.7	2742	2.6	388	18.7	2862	2.9	416	78.6	11615	Critical Value

See Figure B.21 for loads, number of axles, and distance between the axles.

AB1= Rear Abutment

AB2= Forward Abutment

MS1, MS2, and MS3 = Midspan of Span 1, Span 2, and Span 3, respectively.

See Figure B.22 for the locations of Lane 1 and Lane 2.

Table B.3 (Cont.) Rating Factors and Load Limits (kN) Based on Moments After Retrofitting

Load	Inventory Level														
	AB 1		MS1		PR1		MS2		PR2		MS3		AB2		
	R.F.	Load	R.F.	Load	R.F.	Load	R.F.	Load	R.F.	Load	R.F.	Load	R.F.	Load	
HS20-44	50.2	8031	1.3	213	9.3	1482	1.1	169	8.6	1384	1.2	187	38.8	6206	Lane1
	38.8	6208	1.3	208	8.7	1385	1.3	201	9.3	1482	1.4	225	50.2	8028	Lane2
	38.8	6208	1.3	208	8.7	1385	1.1	169	8.6	1384	1.2	187	38.8	6206	Critical Value
2F1	72.8	4852	2.1	137	16.4	1096	1.6	109	16.2	1083	1.9	123	52.9	3527	Lane1
	52.9	3528	2.1	137	16.3	1084	1.9	130	16.4	1096	2.2	145	72.8	4851	Lane2
	52.9	3528	2.1	137	16.3	1084	1.6	109	16.2	1083	1.9	123	52.9	3527	Critical Value
3F1	50.3	5141	1.9	199	11.5	1172	1.5	156	11.5	1173	1.8	180	39.4	4024	Lane1
	39.4	4025	2.0	200	11.5	1174	1.8	185	11.5	1172	2.1	210	50.3	5139	Lane2
	39.4	4025	1.9	199	11.5	1172	1.5	156	11.5	1172	1.8	180	39.4	4024	Critical Value
4F1	47.1	5653	2.0	242	10.3	1236	1.6	188	10.5	1257	1.8	216	34.8	4182	Lane1
	34.9	4184	2.0	240	10.5	1257	1.9	222	10.3	1235	2.1	255	47.1	5651	Lane2
	34.9	4184	2.0	240	10.3	1236	1.6	188	10.3	1235	1.8	216	34.8	4182	Critical Value
5C1	51.5	9161	2.0	355	12.0	2134	1.6	280	11.9	2109	1.8	314	40.9	7264	Lane1
	40.9	7266	2.0	349	11.9	2110	1.9	332	12.0	2133	2.1	375	51.5	9158	Lane2
	40.9	7266	2.0	349	11.9	2110	1.6	280	11.9	2109	1.8	314	40.9	7264	Critical Value
Lane Load	84.3	12458	1.9	286	11.8	1731	1.5	233	11.2	1715	1.7	249	47.1	6958	Lane1
	47.1	6960	1.9	287	11.2	1643	1.8	276	11.8	1806	2.0	292	84.3	12455	Lane2
	47.1	6960	1.9	286	11.2	1643	1.5	233	11.2	1715	1.7	249	47.1	6958	Critical Value

Table B.3 (Cont.) Rating Factors and Load Limits (kN) Based on Shears After Retrofitting

Load	Operating Level														
	AB 1		MS1		PR1		MS2		PR2		MS3		AB2		
	R.F.	Load	R.F.	Load	R.F.	Load	R.F.	Load	R.F.	Load	R.F.	Load	R.F.	Load	
HS20-44	19.8	3162	22.8	3641	29.8	4761	23.0	3675	30.2	4825	22.4	3577	20.2	3235	Lane1
	20.2	3235	22.4	3579	30.2	4830	23.0	3675	29.7	4756	22.7	3639	19.8	3162	Lane2
	19.8	3162	22.4	3579	29.8	4761	23.0	3675	29.7	4756	22.4	3577	19.8	3162	Critical Value
2F1	31.5	2098	37.7	2511	48.0	3198	35.9	2393	48.2	3215	35.7	2382	32.2	2149	Lane1
	32.2	2149	35.7	2383	48.3	3219	35.9	2393	47.9	3194	37.6	2510	31.5	2099	Lane2
	31.5	2098	35.7	2383	48.0	3198	35.9	2393	47.9	3194	35.7	2382	31.5	2099	Critical Value
3F1	32.8	3357	39.1	3997	49.7	5076	39.2	4009	50.3	5139	38.6	3946	31.3	3197	Lane1
	31.3	3196	38.6	3948	50.3	5144	39.2	4009	49.6	5071	39.1	3995	32.8	3357	Lane2
	31.3	3196	38.6	3948	49.7	5076	39.2	4009	49.6	5071	38.6	3946	31.3	3197	Critical Value
4F1	36.6	4397	51.1	6132	55.0	6602	45.6	5474	56.1	6737	45.2	5427	36.4	4362	Lane1
	36.4	4362	45.2	5430	56.2	6744	45.6	5474	55.0	6595	51.1	6129	36.6	4397	Lane2
	36.4	4362	45.2	5430	55.0	6602	45.6	5474	55.0	6595	45.2	5427	36.4	4362	Critical Value
5C1	31.3	5561	29.9	5324	34.8	6186	21.7	3866	28.5	5062	32.4	5756	32.6	5795	Lane1
	32.6	5795	32.4	5759	28.5	5068	21.7	3866	34.8	6179	29.9	5321	31.3	5561	Lane2
	31.3	5561	29.9	5324	28.5	5068	21.7	3866	28.5	5062	29.9	5321	31.3	5561	Critical Value
Lane Load	58.1	8587	27.3	4034	34.6	5074	27.2	4087	115.0	17602	26.4	3765	22.8	3374	Lane1
	22.8	3374	26.4	3905	115.2	16871	27.2	4087	34.6	5294	27.3	3889	58.1	8587	Lane2
	22.8	3374	26.4	3905	34.6	5074	27.2	4087	34.6	5294	26.4	3765	22.8	3374	Critical Value

Table B.3 (Cont.) Rating Factors and Load Limits (kN) Based on Shears After Retrofitting

Load	Inventory Level														
	AB 1		MS1		PR1		MS2		PR2		MS3		AB2		
	R.F.	Load	R.F.	Load	R.F.	Load	R.F.	Load	R.F.	Load	R.F.	Load	R.F.	Load	
HS20-44	11.8	1894	13.6	2182	17.8	2852	13.8	2202	18.1	2891	13.4	2143	12.1	1938	Lane1
	12.1	1938	13.4	2144	18.1	2894	13.8	2202	17.8	2849	13.6	2180	11.8	1894	Lane2
	11.8	1894	13.4	2144	17.8	2852	13.8	2202	17.8	2849	13.4	2143	11.8	1894	Critical Value
2F1	18.9	1257	22.6	1504	28.7	1916	21.5	1433	28.9	1926	21.4	1427	19.3	1287	Lane1
	19.3	1287	21.4	1428	28.9	1928	21.5	1433	28.7	1914	22.5	1503	18.9	1257	Lane2
	18.9	1257	21.4	1428	28.7	1916	21.5	1433	28.7	1914	21.4	1427	18.9	1257	Critical Value
3F1	19.7	2011	23.4	2395	29.7	3041	23.5	2402	30.1	3079	23.1	2364	18.7	1915	Lane1
	18.7	1915	23.1	2365	30.1	3082	23.5	2402	29.7	3038	23.4	2393	19.7	2011	Lane2
	18.7	1915	23.1	2365	29.7	3041	23.5	2402	29.7	3038	23.1	2364	18.7	1915	Critical Value
4F1	22.0	2634	30.6	3674	33.0	3955	27.3	3279	33.6	4036	27.1	3251	21.8	2613	Lane1
	21.8	2613	27.1	3253	33.7	4040	27.3	3279	32.9	3951	30.6	3672	22.0	2634	Lane2
	21.8	2613	27.1	3253	33.0	3955	27.3	3279	32.9	3951	27.1	3251	21.8	2613	Critical Value
5C1	18.7	3331	17.9	3190	20.8	3706	13.0	2316	17.1	3033	19.4	3448	19.5	3472	Lane1
	19.5	3472	19.4	3450	17.1	3036	13.0	2316	20.8	3702	17.9	3188	18.7	3331	Lane2
	18.7	3331	17.9	3190	17.1	3036	13.0	2316	17.1	3033	17.9	3188	18.7	3331	Critical Value
Lane Load	34.8	5144	16.3	2417	20.7	3040	16.3	2448	68.9	10545	15.8	2256	13.7	2021	Lane1
	13.7	2021	15.8	2340	69.0	10107	16.3	2448	20.7	3171	16.3	2330	34.8	5144	Lane2
	13.7	2021	15.8	2340	20.7	3040	16.3	2448	20.7	3171	15.8	2256	13.7	2021	Critical Value



Figure B.1 Photographs of Test Bridge Before Repair

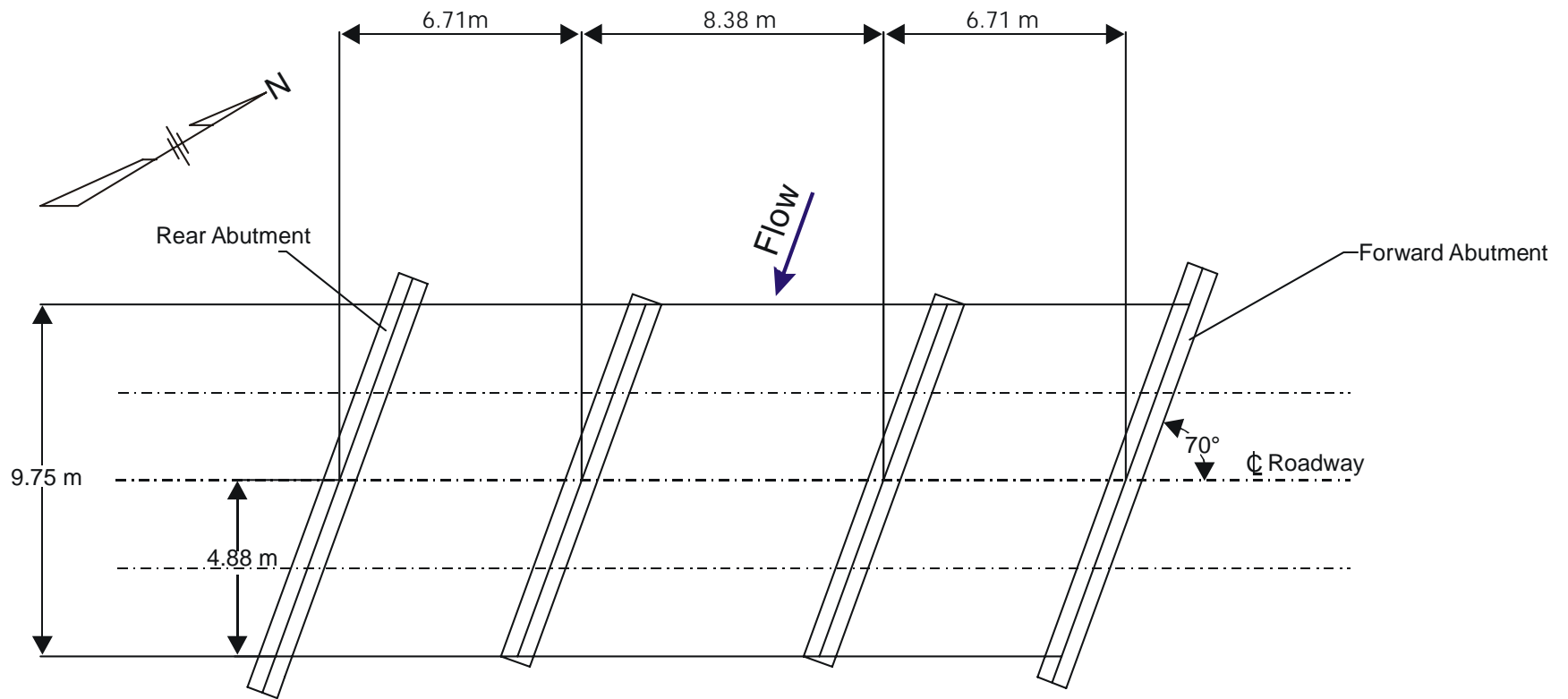
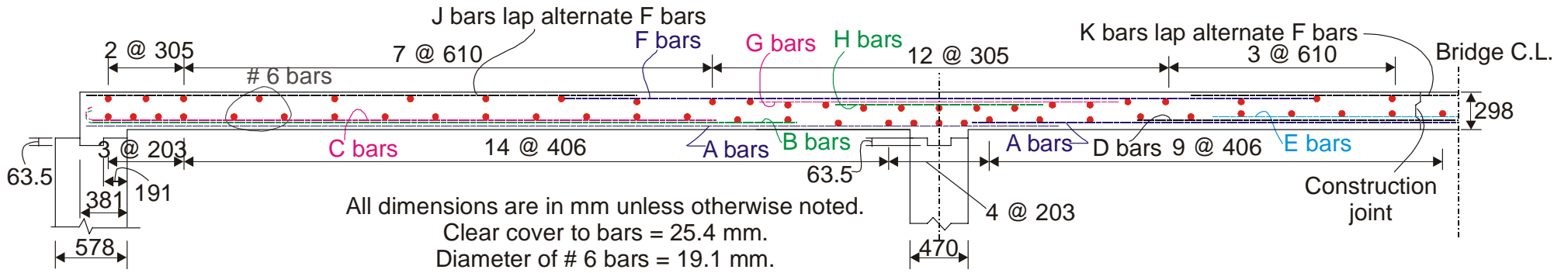


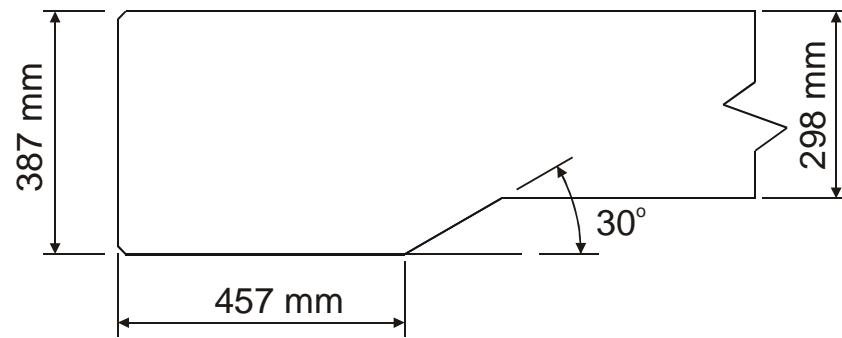
Figure B.2 Plan View of Test Bridge



(a) Reinforcement Details

Bar	Diameter (mm)	Spacing (mm)	Length (m)
A	22.2	318	7.85
B	22.2	635	5.74
C	22.2	635	5.08
D	22.2	635	5.44
E	22.2	635	4.42
F	25.4	318	5.64
G	25.4	635	2.72
H	25.4	635	1.68
J	19.1	635	4.45
K	19.1	635	4.32

(b) Bar Data



(c) Edge "Beam"

Figure B.3 Details of Bridge Deck

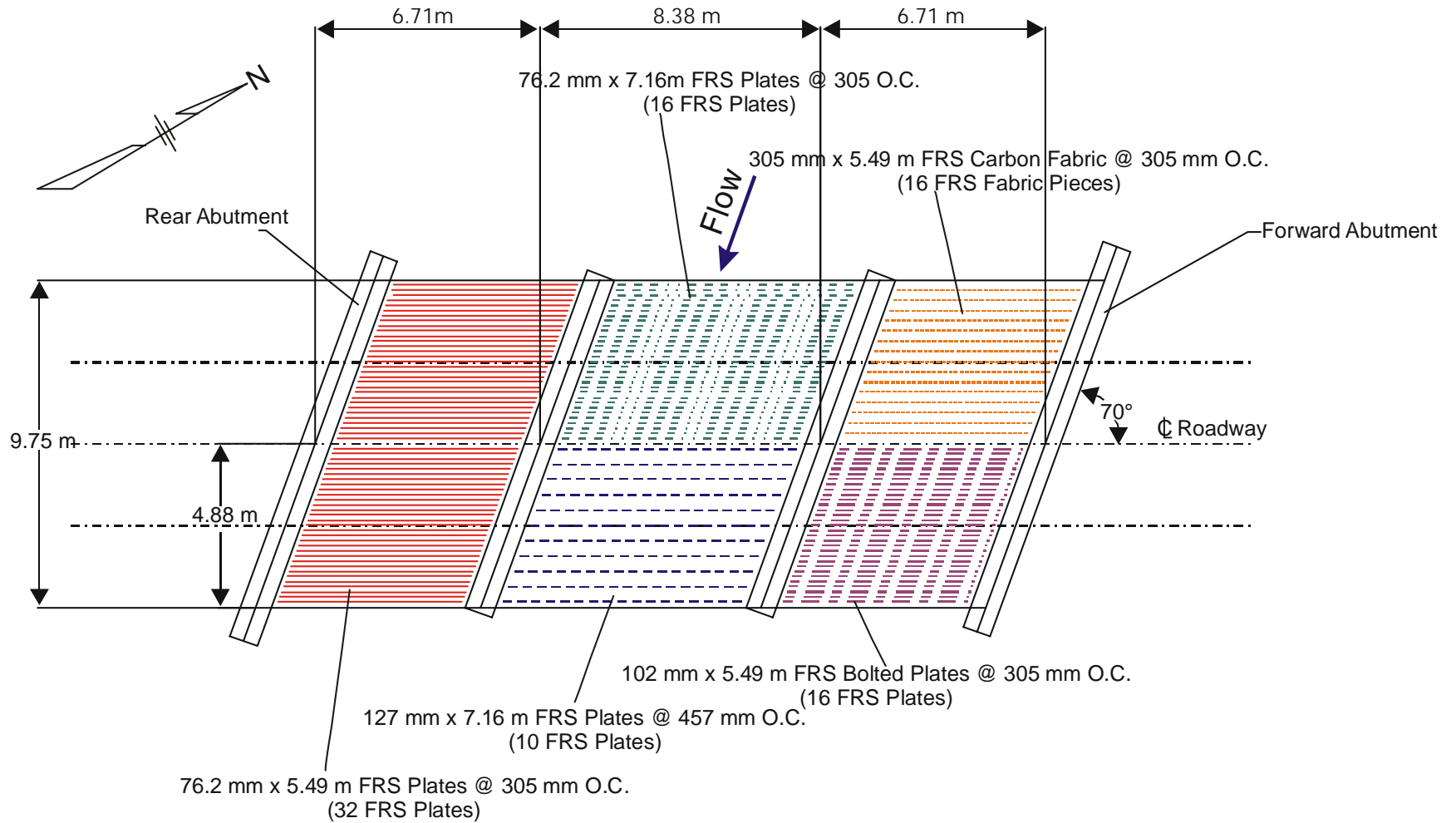


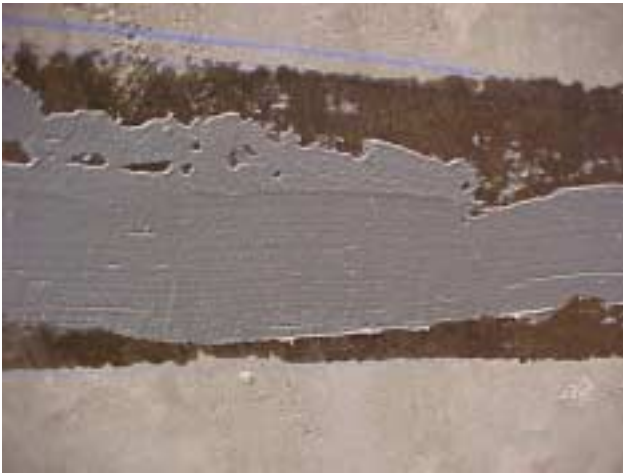
Figure B.4 Locations of Various FRP Systems



(a) Application of structural epoxy on primed surface



(d) Installation of FRP plates



(b) Close-up view of layer of structural epoxy on primed surface



(e) Close-up view of FRP shortly after installation



(c) Application of structural epoxy on cleaned FRP plates



(f) Drilled 102-mm FRP plate

Figure B.5 Installation of FRP Systems



(g) Installation of anchors



(h) Driving anchors into slab



(i) Tightening of anchors

Figure B.5 (Cont.) Installation of FRP Systems



(a) Bonded CFRP Plates



(b) Bolted CFRP Plates



(c) CFRP Fabric

Figure B.6 Photographs of Various FRP Systems

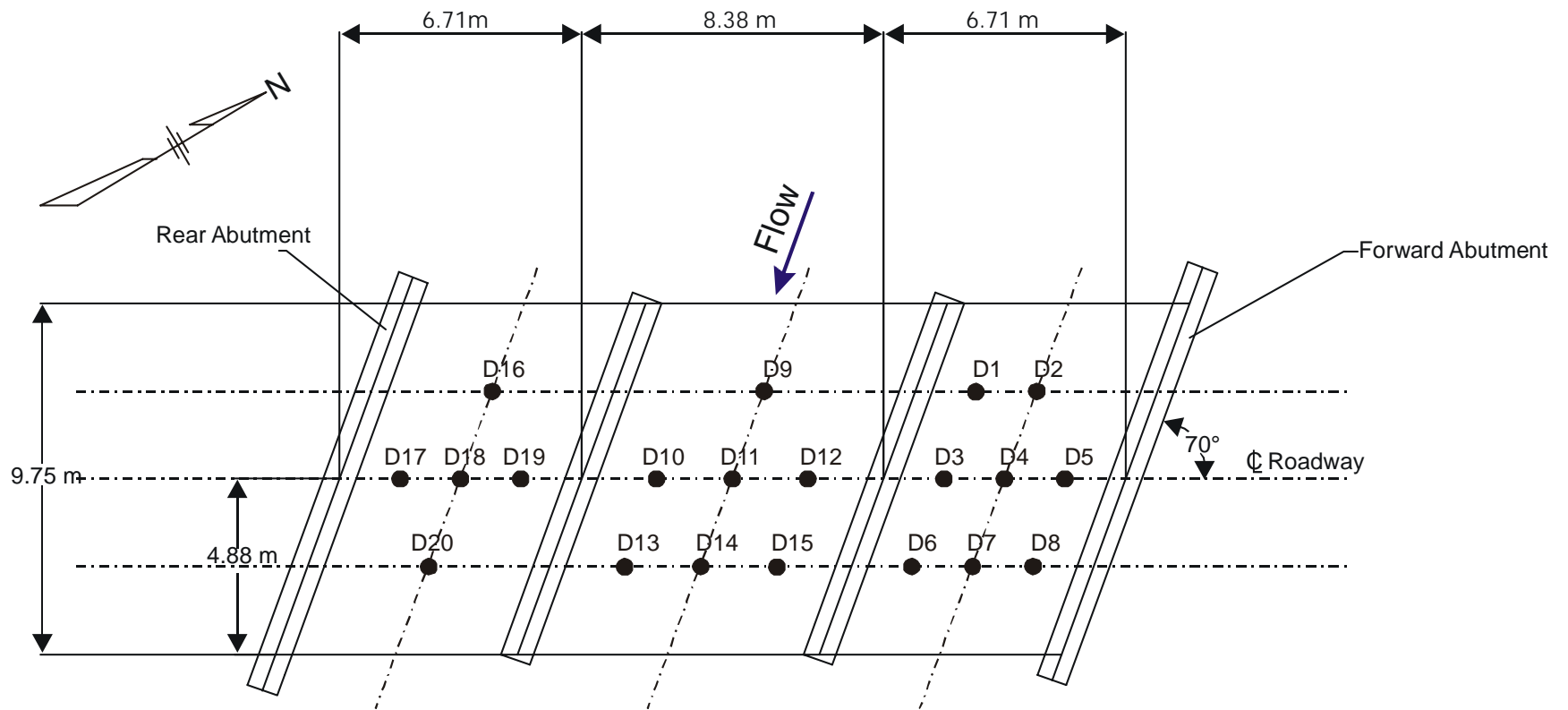


Figure B.7 Location of Displacement Transducers to Measured Slab Vertical Deflections

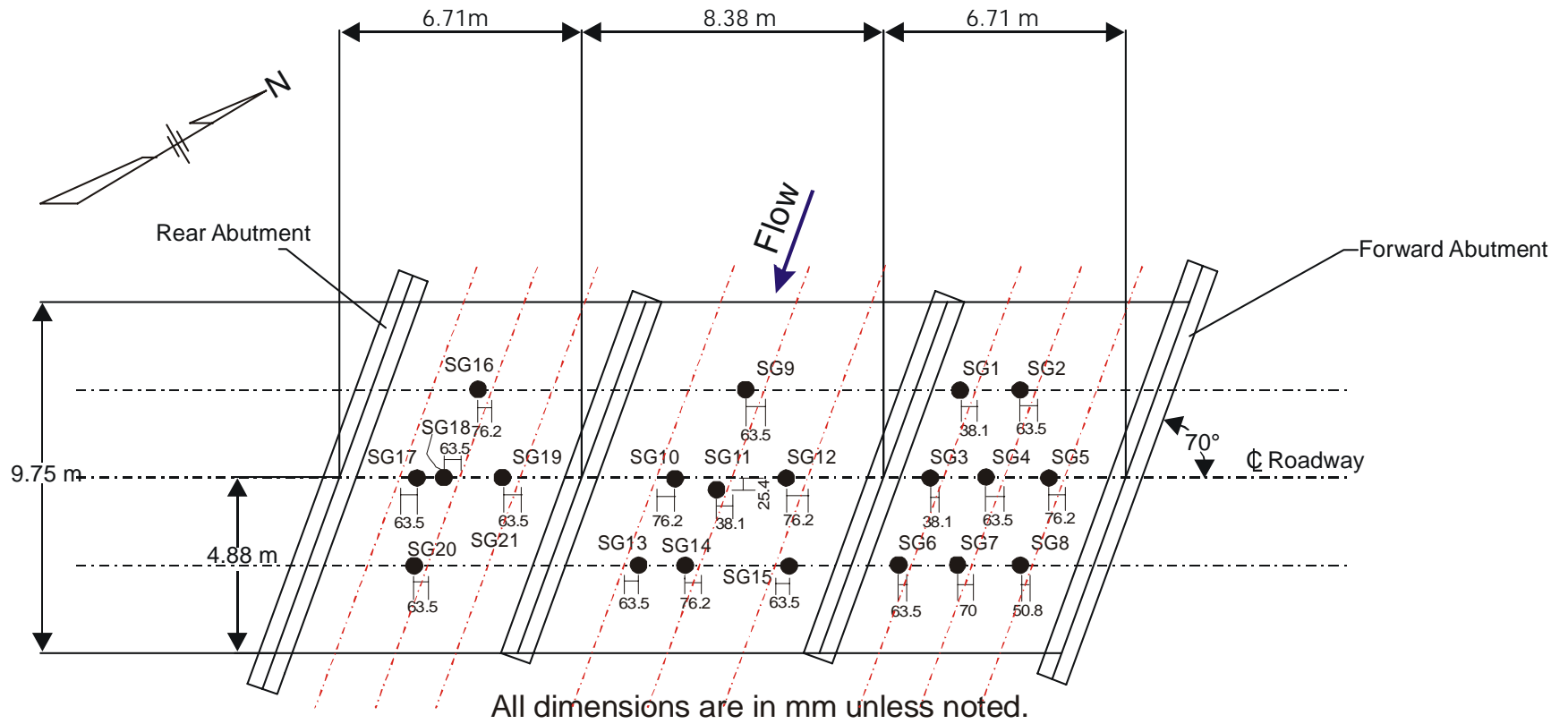


Figure B.8 Locations of Strain Gages Mounted on Bottom Surface of Slab – Before Retrofit

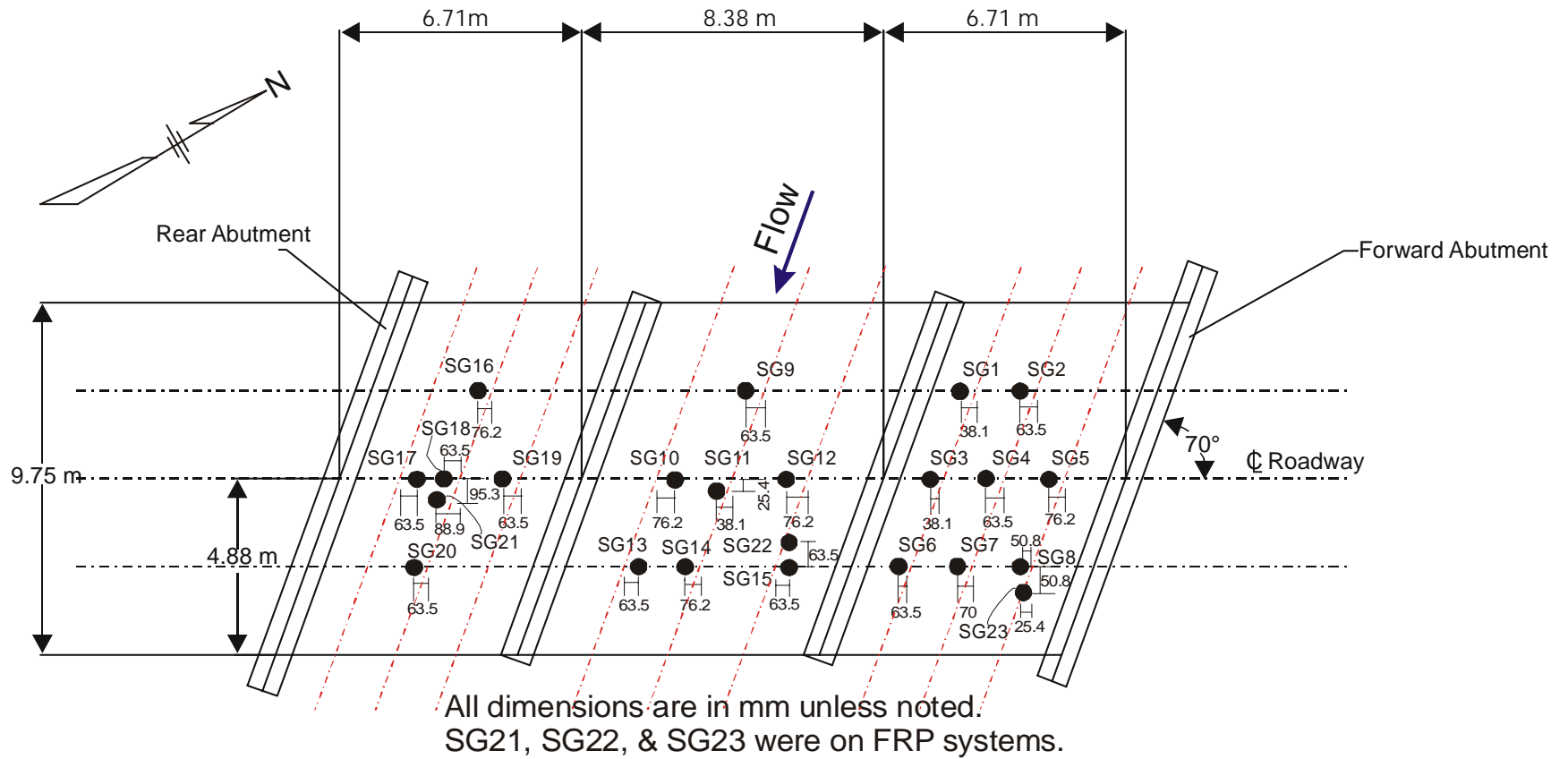


Figure B.9 Locations of Strain Gages on Bottom Surface of Slab –After Retrofit

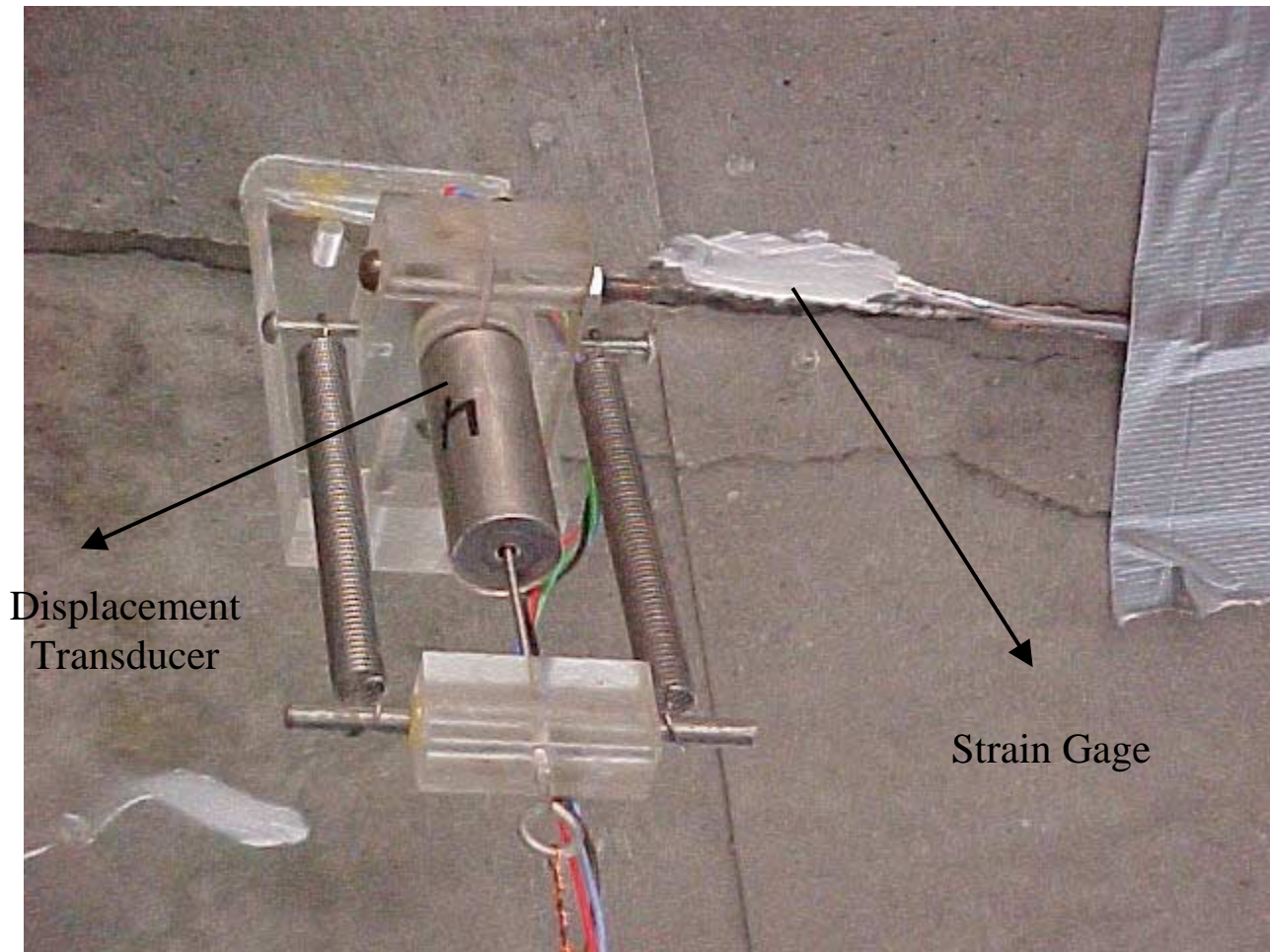
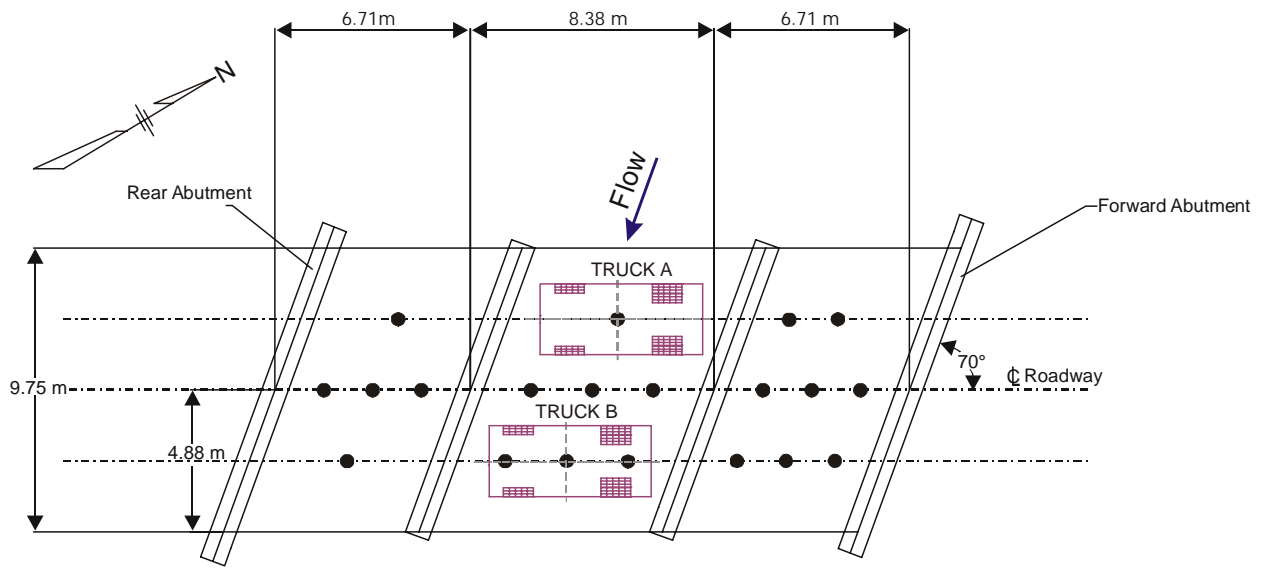
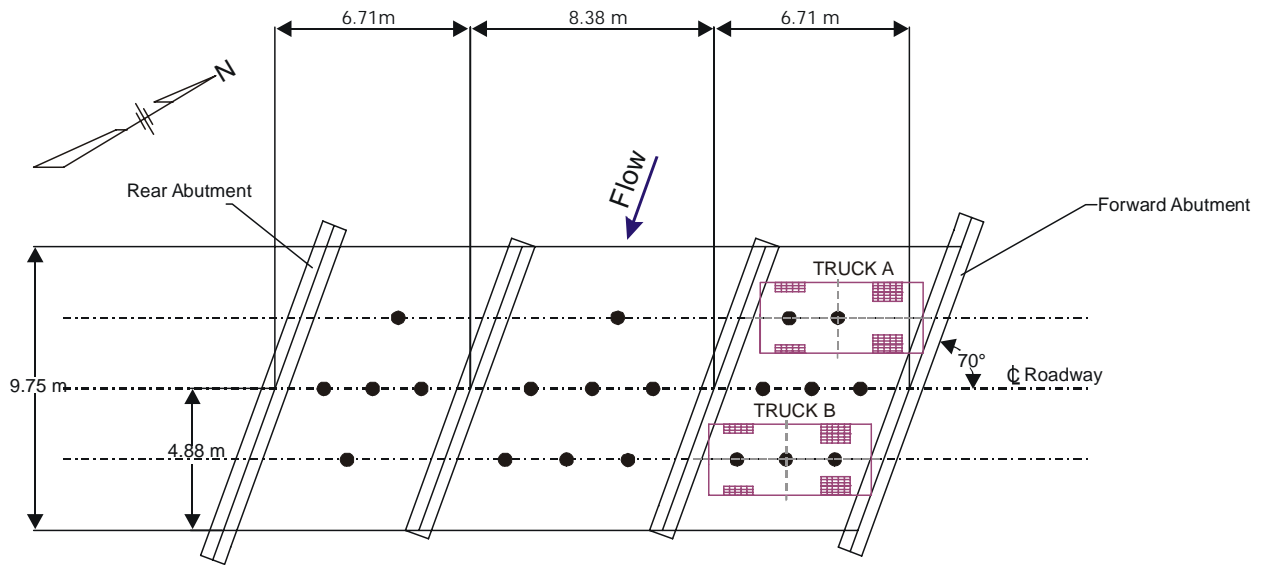


Figure B.10 Photographs of Representative Displacement Transducer and Strain Gage

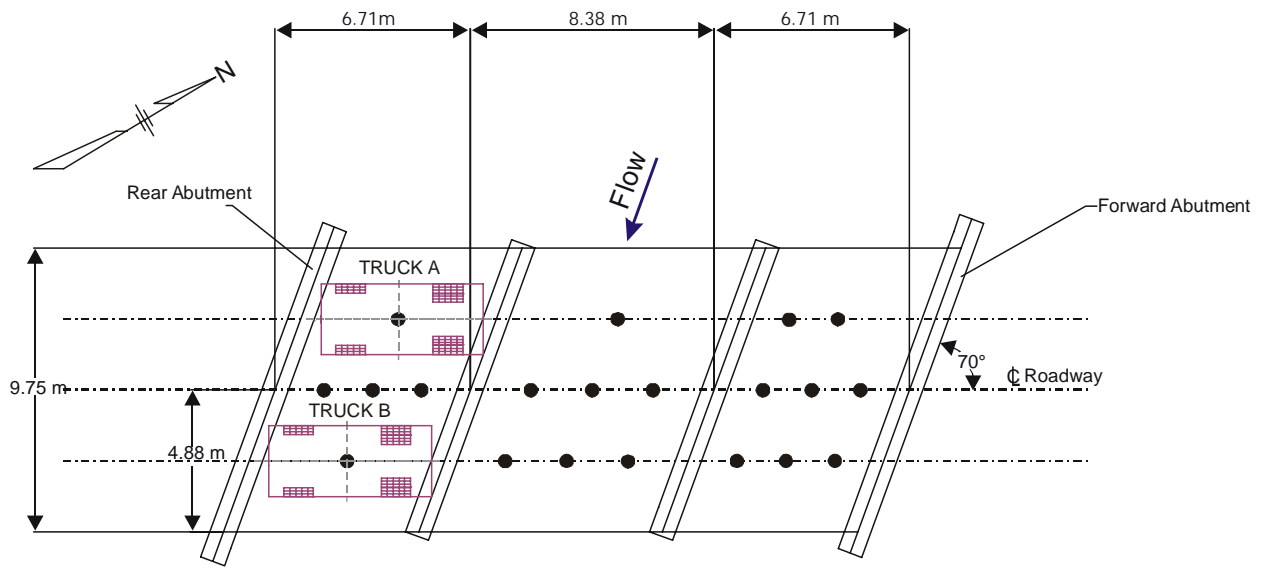


Truck Test No. 1 – Maximum Positive Moment in Midspan

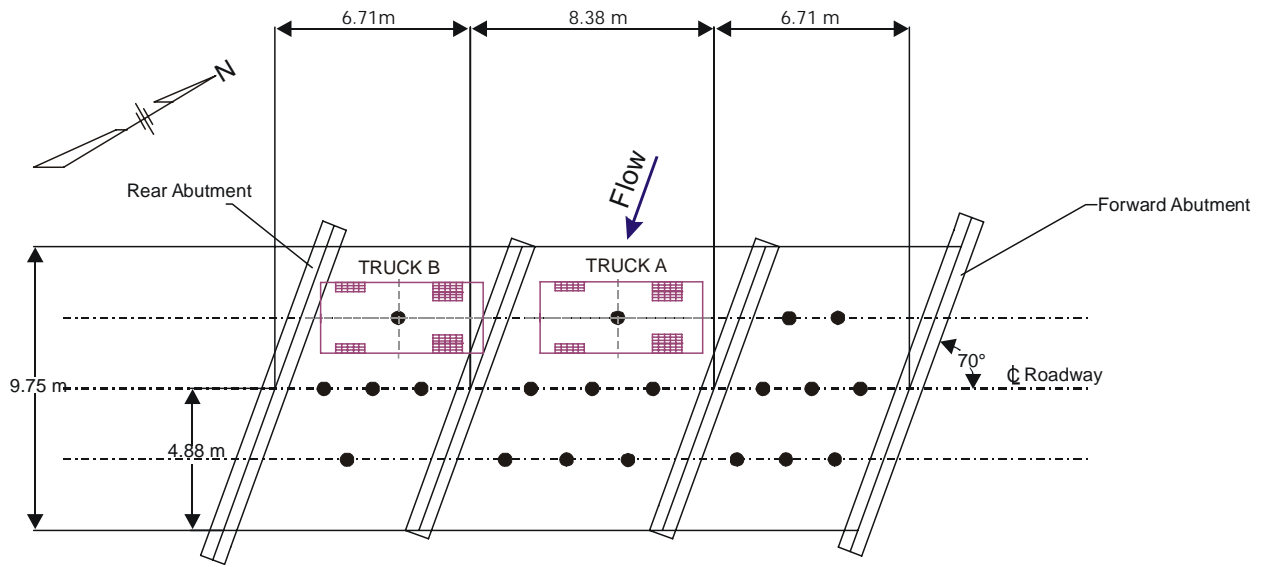


Truck Test No. 2 – Maximum Positive Moment in Span 3

Figure B.11 Locations of Trucks During Various Tests



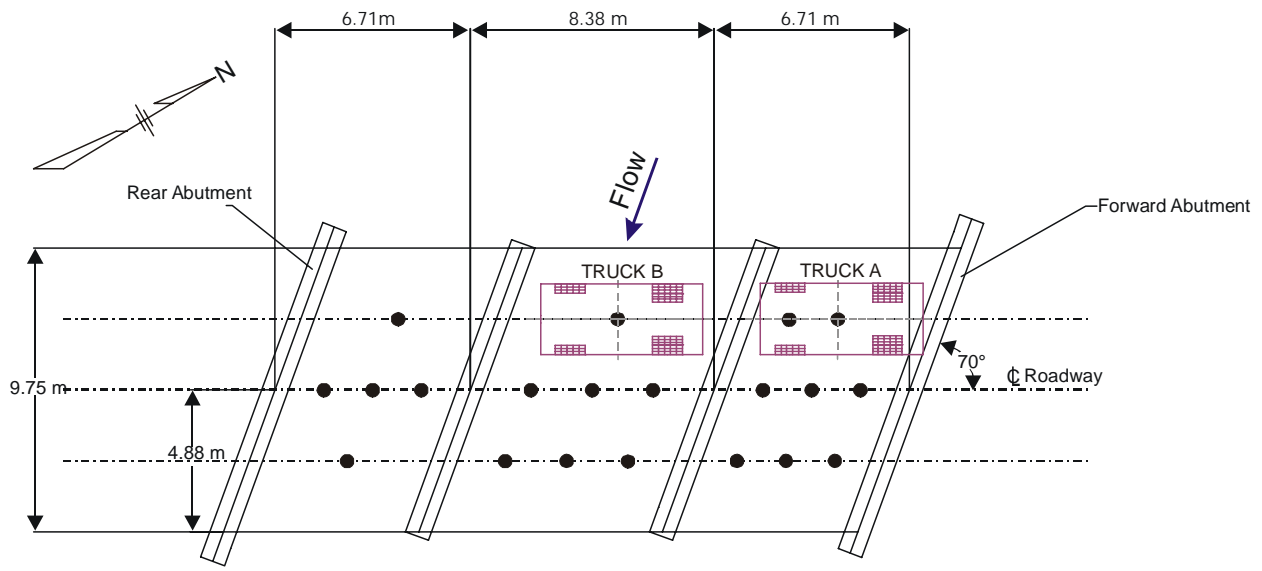
Truck Test No. 3 – Maximum Positive Moment in Span 1



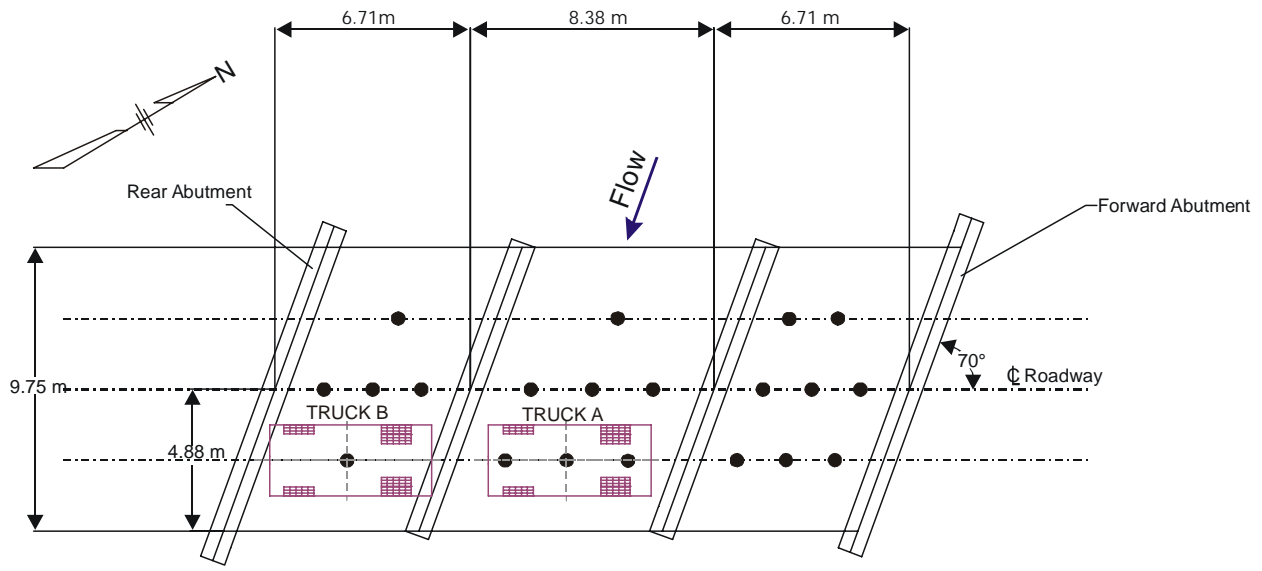
Truck Test No. 4 – Maximum Negative Moment over Pier 1 (Part a)

(Note: During Before-Retrofit Tests, the locations of trucks A&B were opposite to those shown.)

Figure B.11 (Cont.) Locations of Trucks During Various Tests

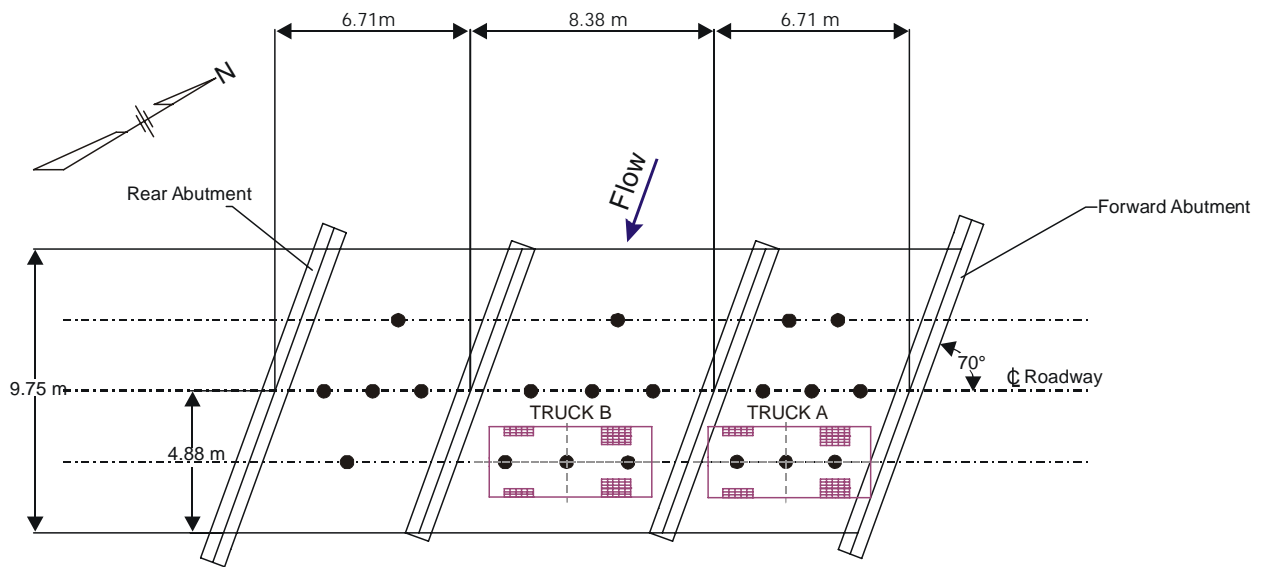


Truck Test No. 5 – Maximum Negative Moment over Pier 2 (Part a)
 (Note: During Before-Retrofit Tests, the locations of trucks A&B were opposite to those shown.)



Truck Test No. 6 – Maximum Negative Moment over Pier 1 (Part b)
 (Note: During Before-Retrofit Tests, the locations of trucks A&B were opposite to those shown.)

Figure B.11 (Cont.) Locations of Trucks During Various Tests

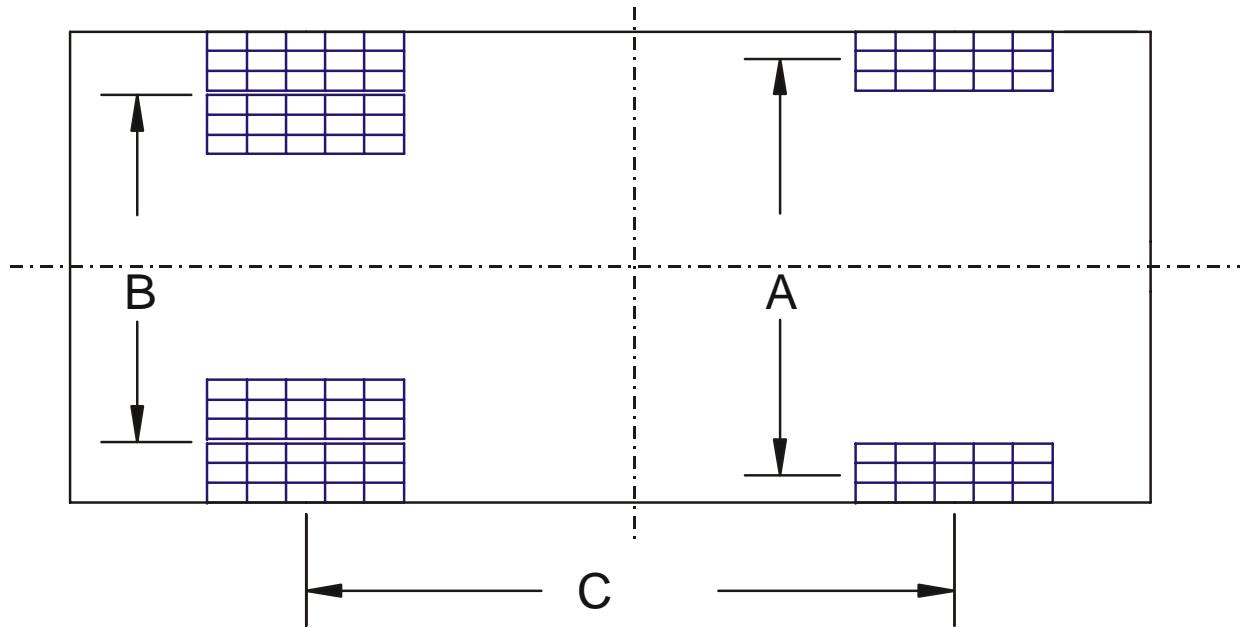


Truck Test No. 7 – Maximum Negative Moment over Pier 2 (Part b)
 (Note: During Before-Retrofit Tests, the locations of trucks A&B were opposite to those shown.)

Figure B.11 (Cont.) Locations of Trucks During Various Tests

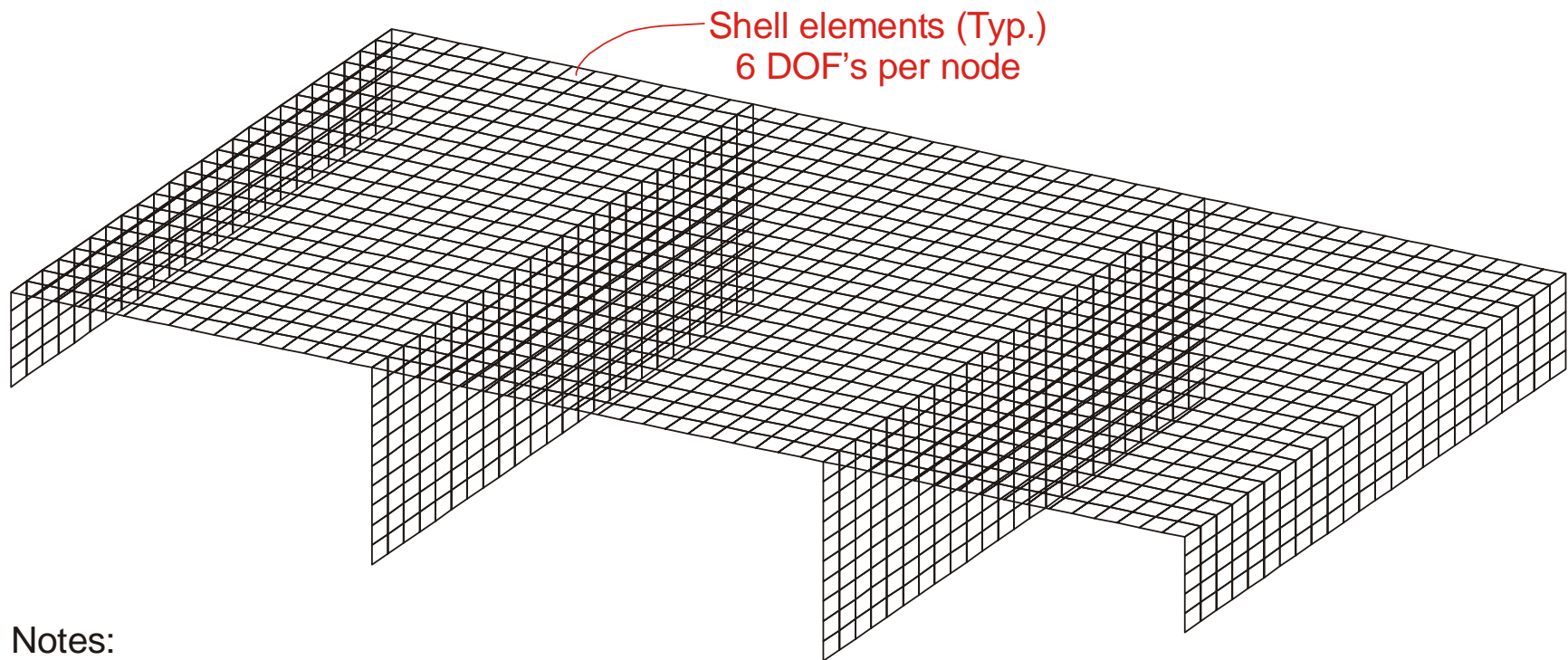


Figure B.12 Photograph of Trucks During Truck Load Tests



Test	TRUCK A			TRUCK B			TRUCK A			TRUCK B		
	Dimensions (mm)			Weight (kN)			Dimensions (mm)			Weight (kN)		
	A	B	C	Front Axle	Back Axle	Total	A	B	C	Front Axle	Back Axle	Total
Before Retrofit	80	80	140	38	77	115	80	80	140	42	84	125
After Retrofit (2000)	80	80	140	46	93	139	80	80	140	49	99	148
After Retrofit (2001)	78	74	140	42	85	127	78	74	140	45	91	136

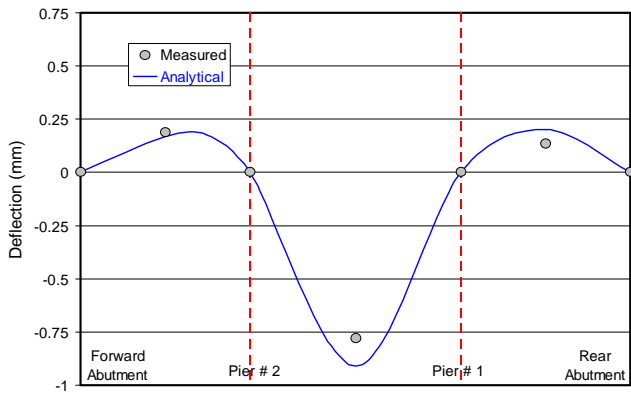
Figure B.13 Dimensions and Weights of Trucks Used for Various Tests



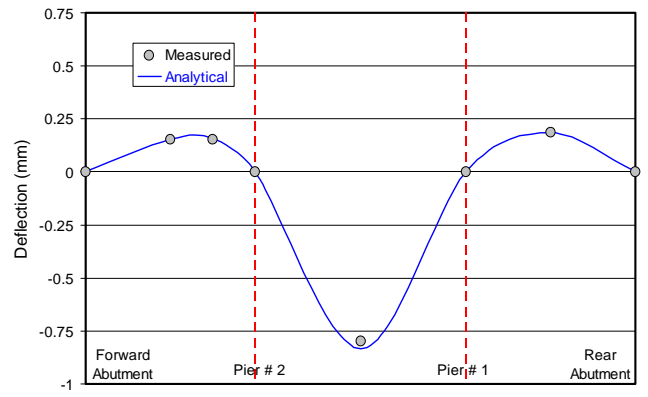
Notes:

1. All DOF's are fixed at the base of abutment and pier elements.
2. Rotational springs in x, y, and z with $K_{\theta} = 16,948 \text{ kN-m/rad}$. were used at all adjacent nodes in the slab shell elements and in the abutment/pier shell elements.
3. Translations in x, y, and z directions are the same at all adjacent nodes in the slab shell elements and in the abutment/pier shell elements.

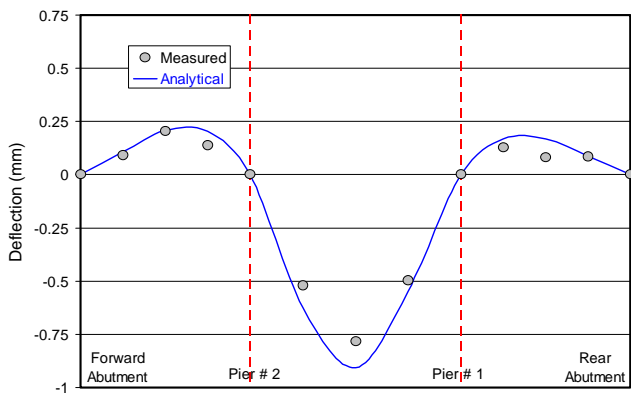
Figure B.14 Three-Dimensional Finite Element Model of Bridge



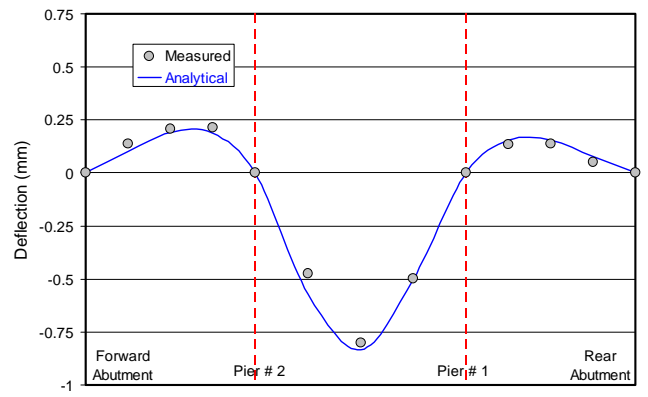
(a) Strip 1



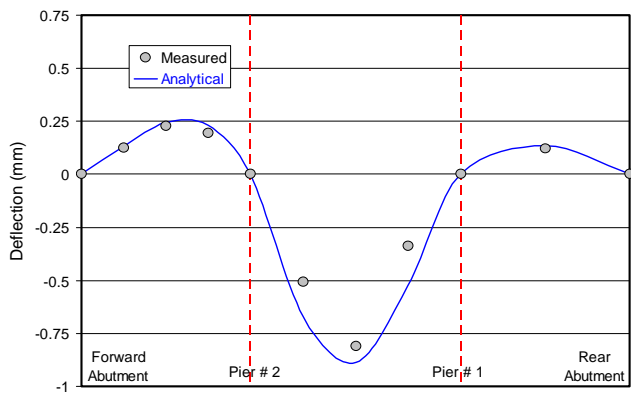
(a) Strip 1



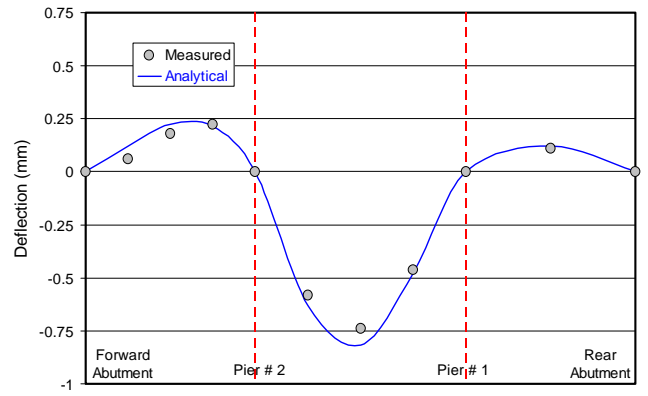
(b) Strip 2



(b) Strip 2



(c) Strip 3

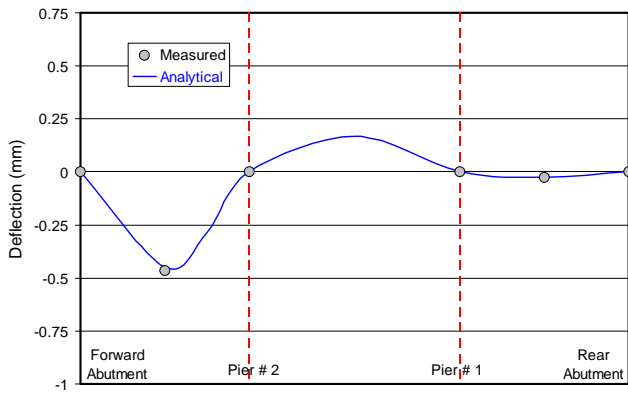


(c) Strip 3

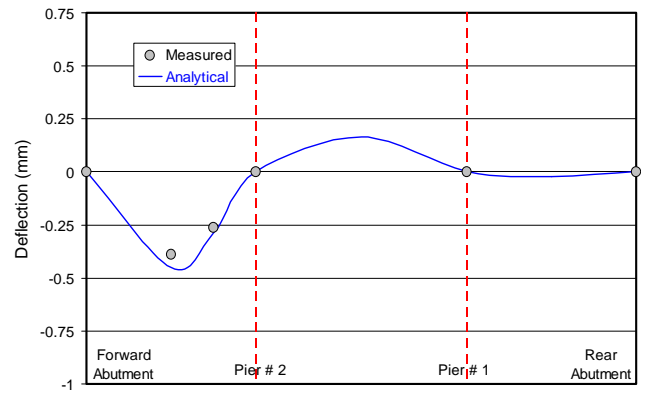
(I) After Retrofit 1999

(II) After Retrofit 2000

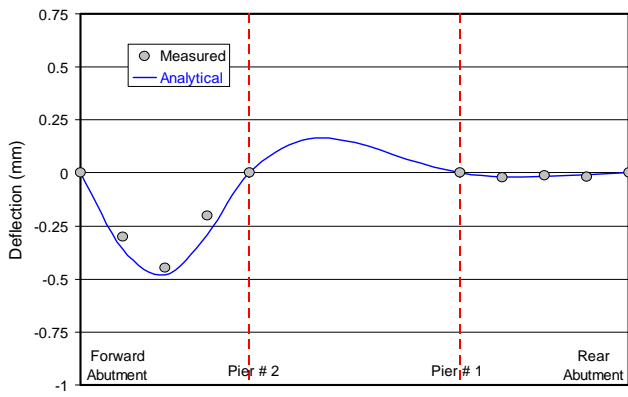
Figure B.15 Analytical v.s. Measured Deflection Profiles – Truck Load Test No. 1



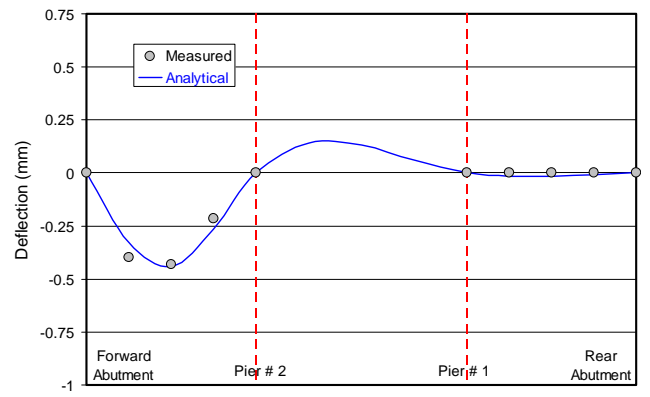
(a) Strip 1



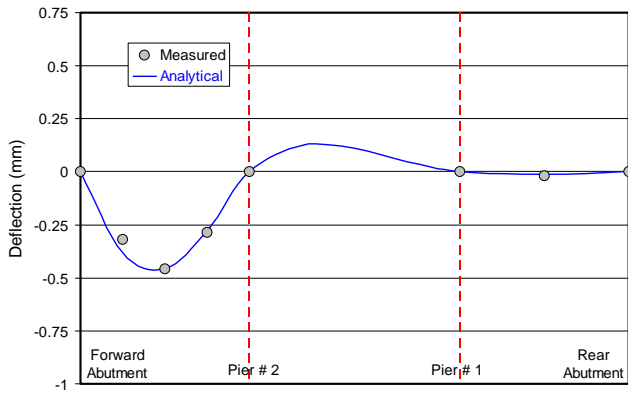
(a) Strip 1



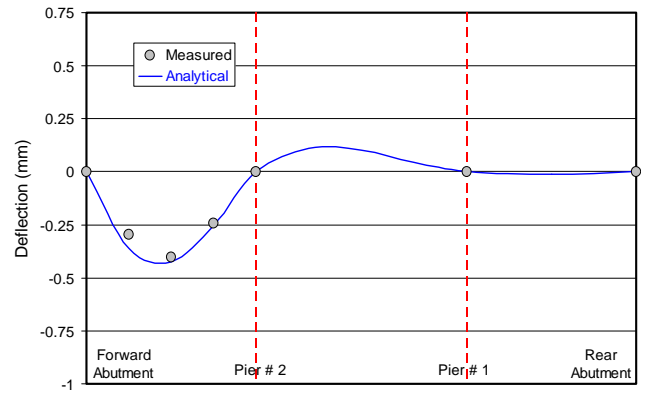
(b) Strip 2



(b) Strip 2



(c) Strip 3

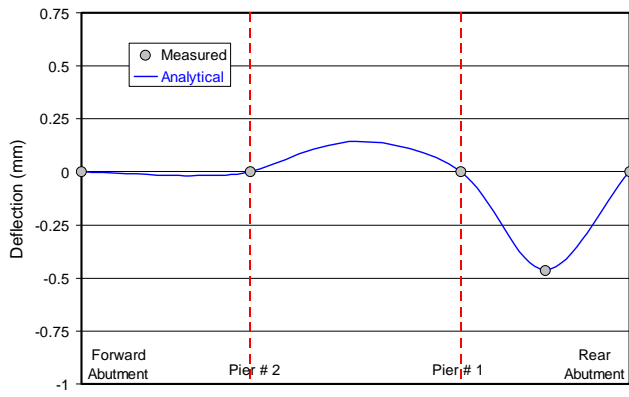


(c) Strip 3

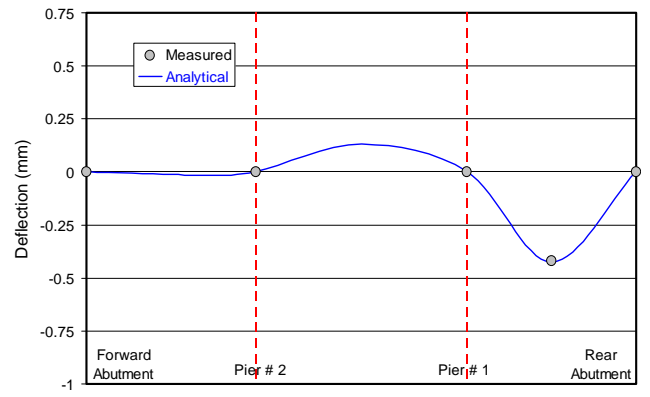
(I) After Retrofit 1999

(II) After Retrofit 2000

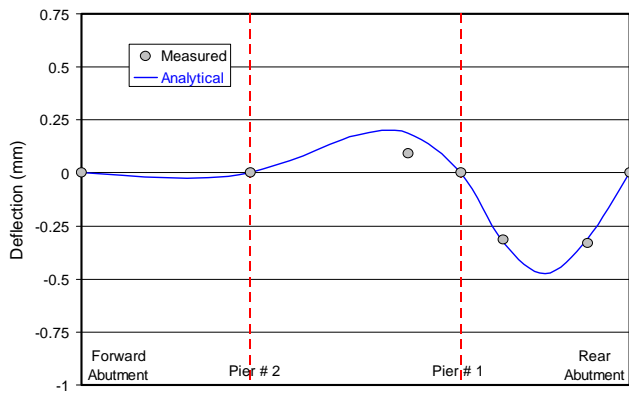
Figure B.15 (Cont.) Analytical v.s. Measured Deflection Profiles – Truck Load Test No. 2



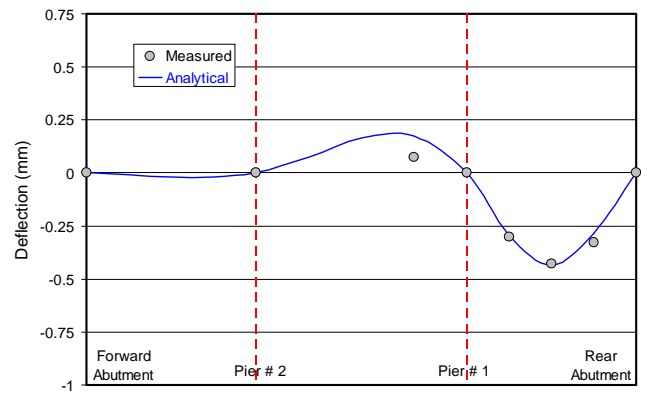
(a) Strip 1



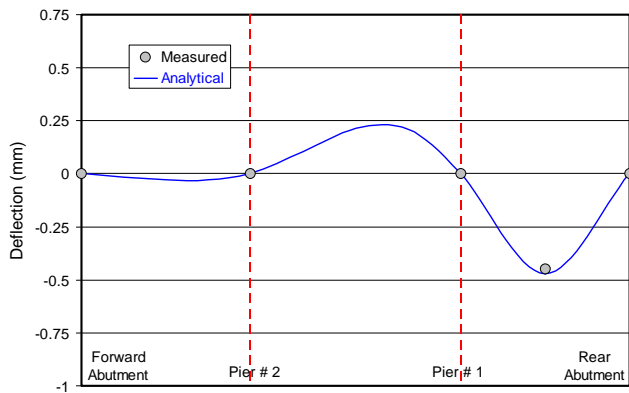
(a) Strip 1



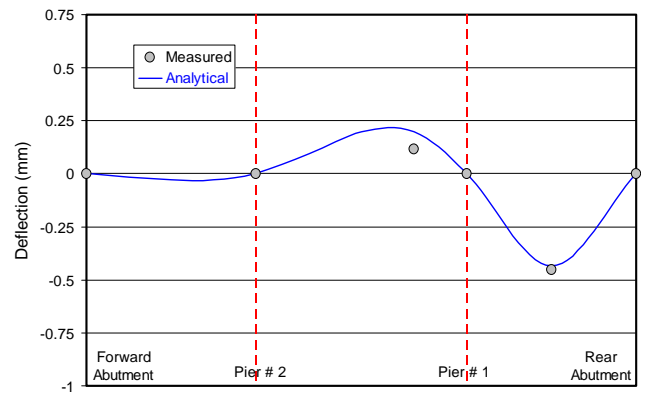
(b) Strip 2



(b) Strip 2



(c) Strip 3

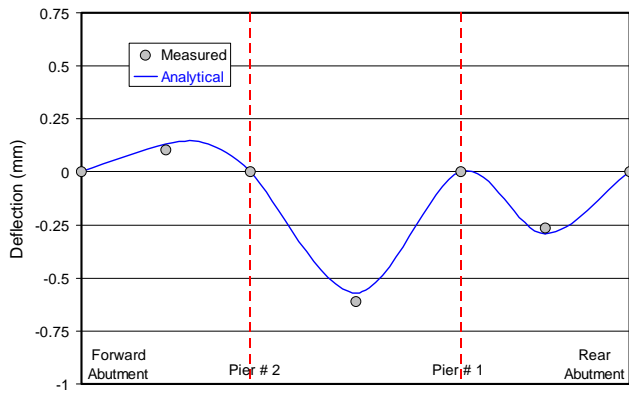


(c) Strip 3

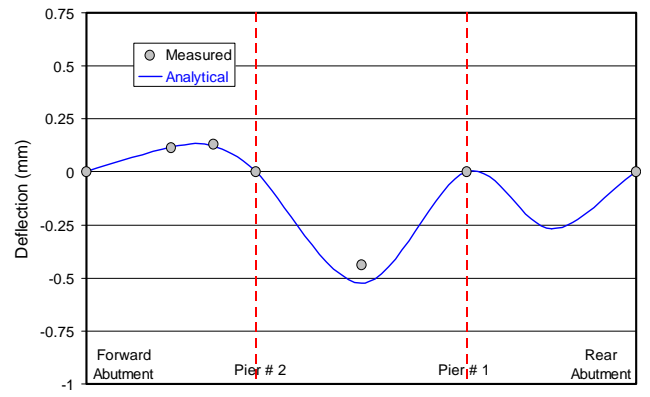
(I) After Retrofit 1999

(II) After Retrofit 2000

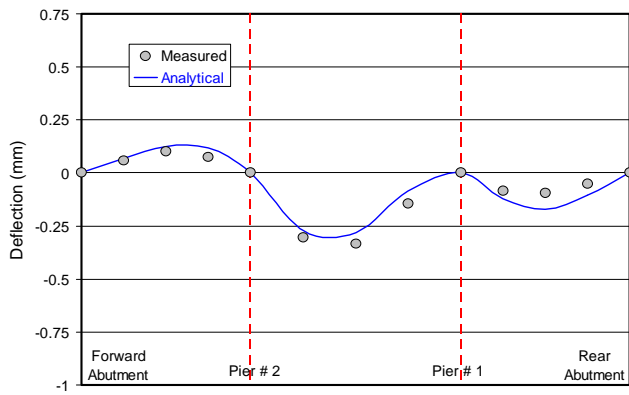
Figure B.15 (Cont.) Analytical v.s. Measured Deflection Profiles – Truck Load Test No. 3



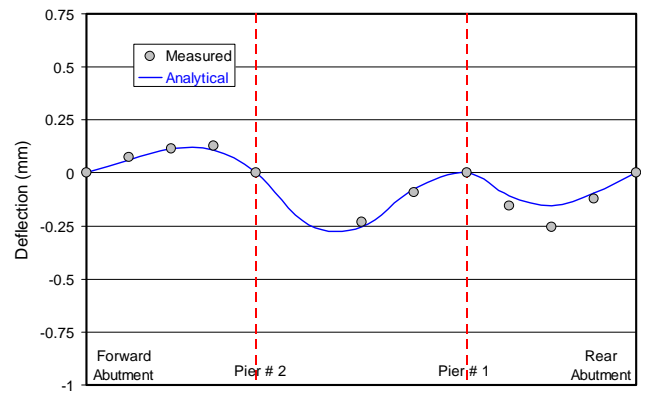
(a) Strip 1



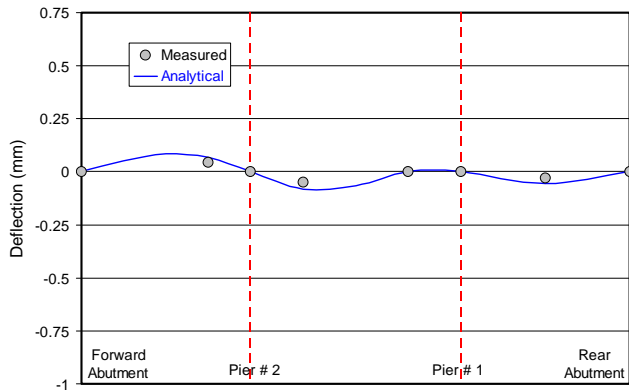
(a) Strip 1



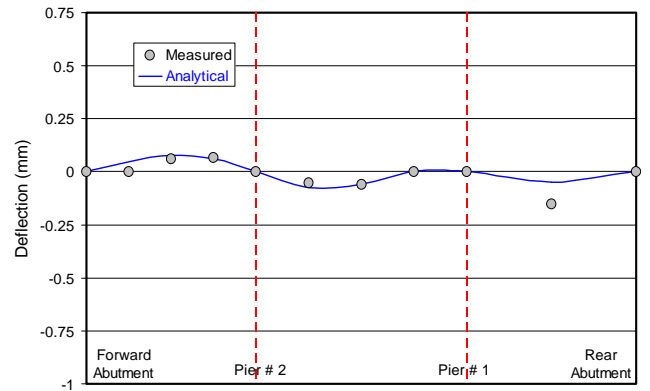
(b) Strip 2



(b) Strip 2



(c) Strip 3

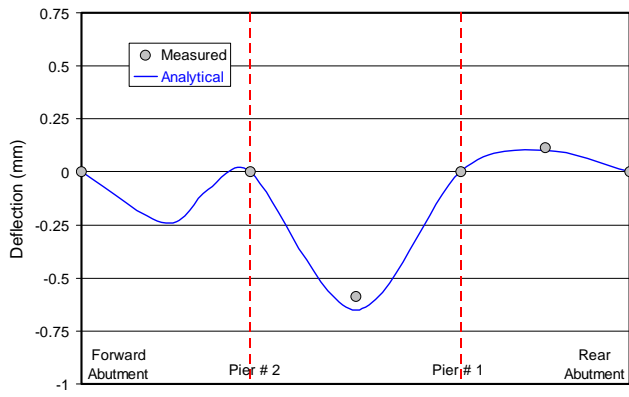


(c) Strip 3

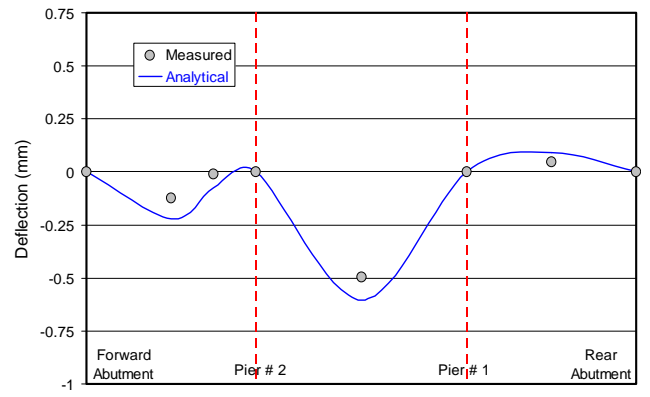
(I) After Retrofit 1999

(II) After Retrofit 2000

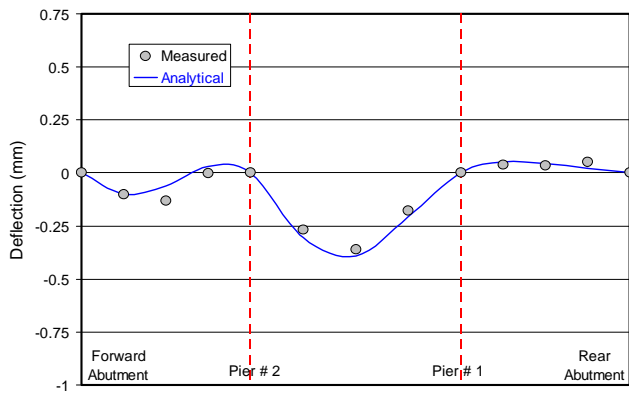
Figure B.15 (Cont.) Analytical v.s. Measured Deflection Profiles – Truck Load Test No. 4



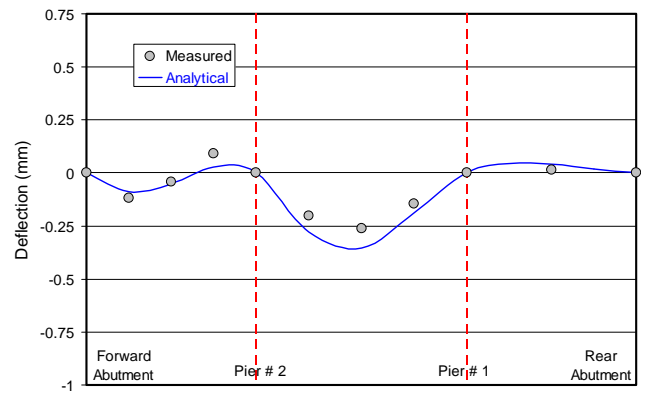
(a) Strip 1



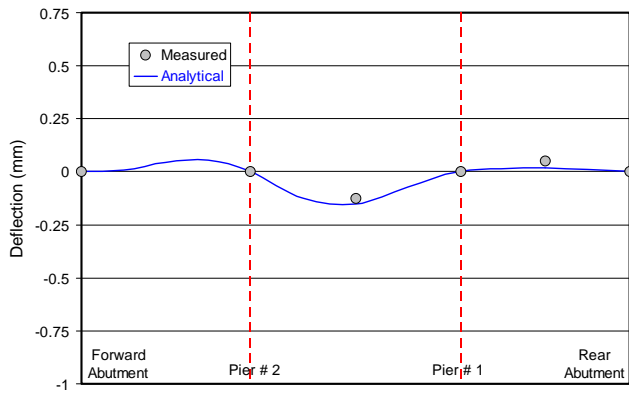
(a) Strip 1



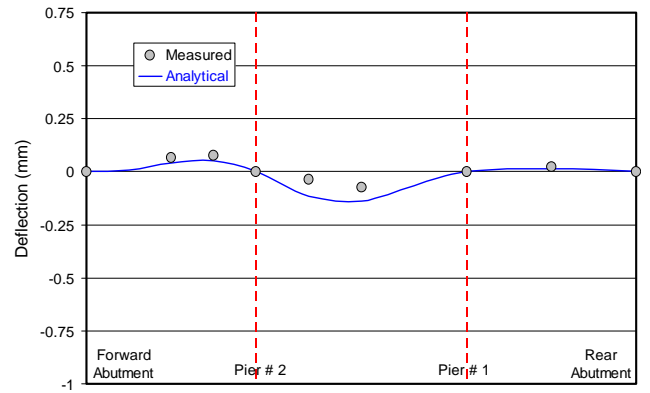
(b) Strip 2



(b) Strip 2



(c) Strip 3

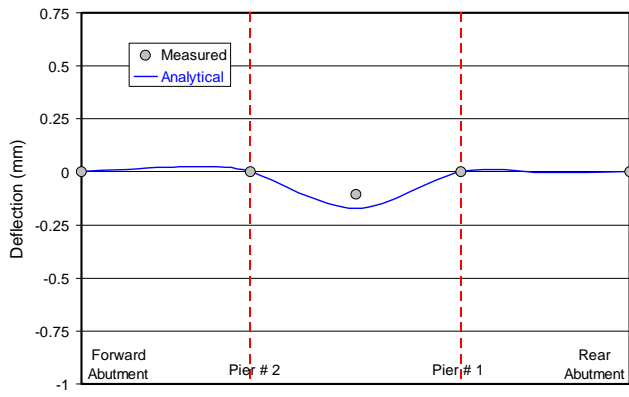


(c) Strip 3

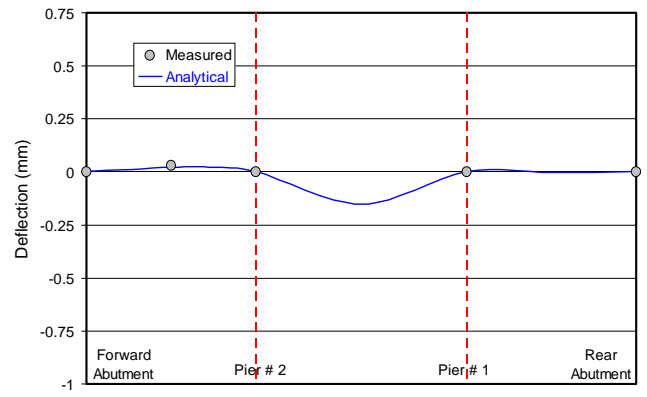
(I) After Retrofit 1999

(II) After Retrofit 2000

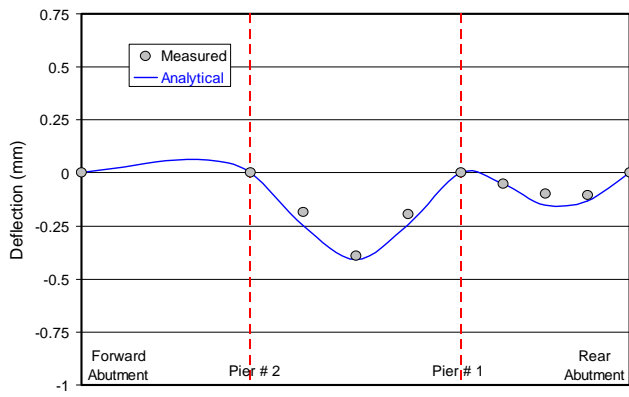
Figure B.15 (Cont.) Analytical v.s. Measured Deflection Profiles – Truck Load Test No. 5



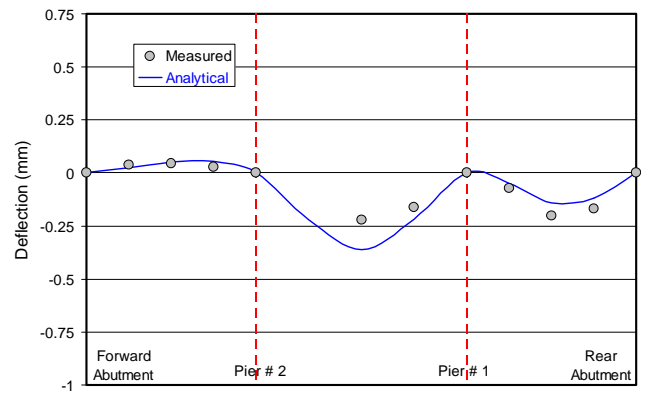
(a) Strip 1



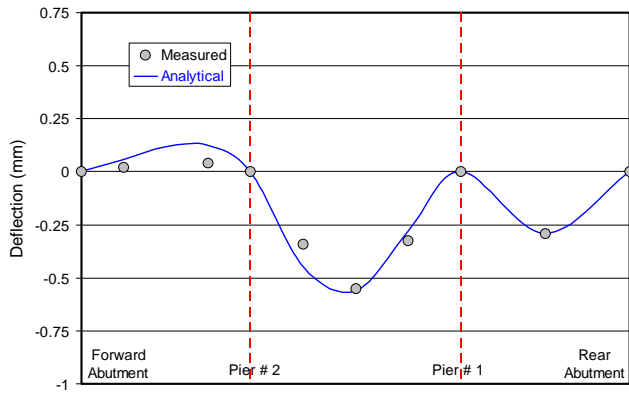
(a) Strip 1



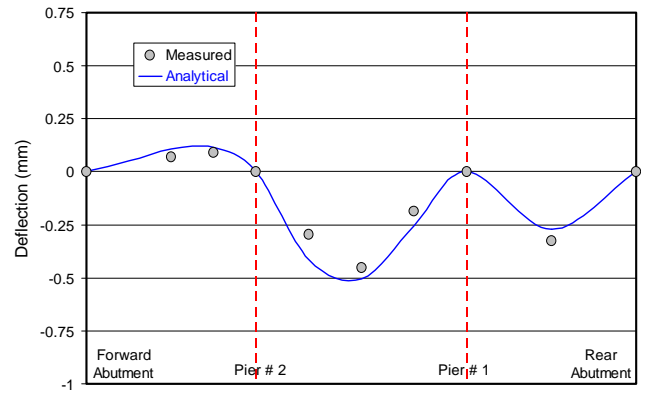
(b) Strip 2



(b) Strip 2



(c) Strip 3

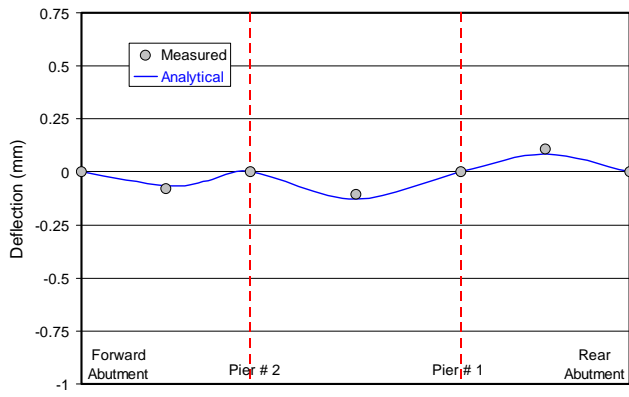


(c) Strip 3

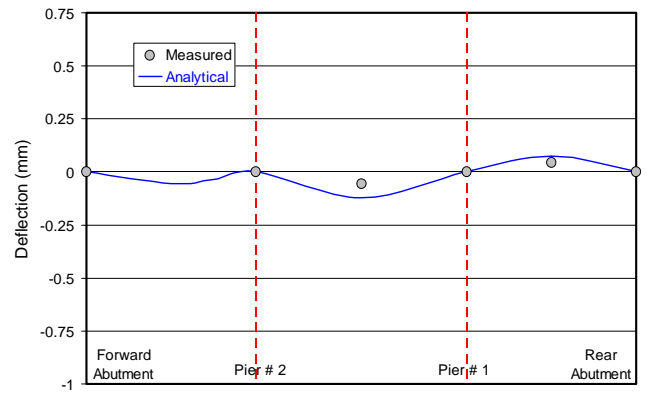
(I) After Retrofit 1999

(II) After Retrofit 2000

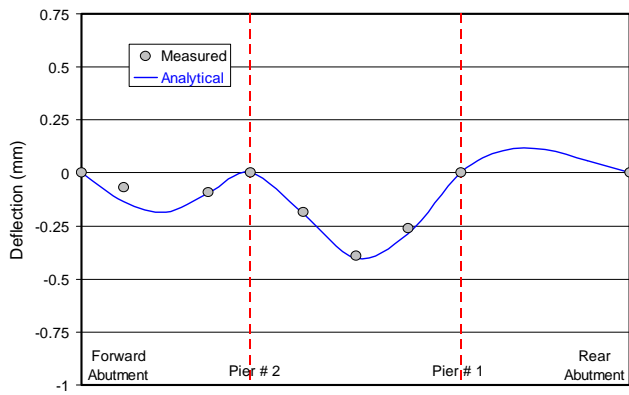
Figure B.15 (Cont.) Analytical v.s. Measured Deflection Profiles – Truck Load Test No. 6



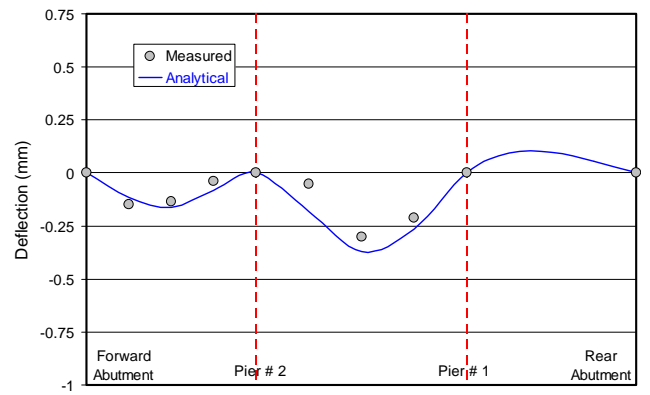
(a) Strip 1



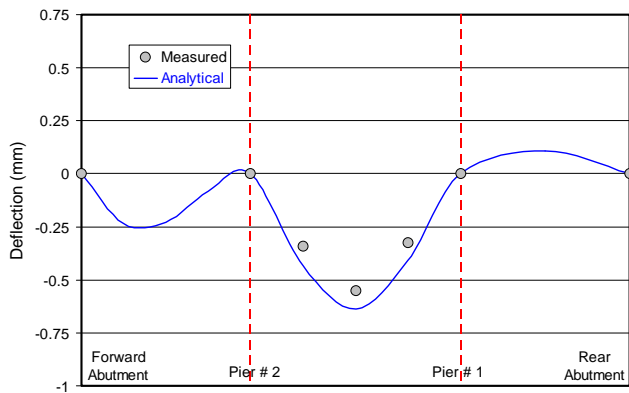
(a) Strip 1



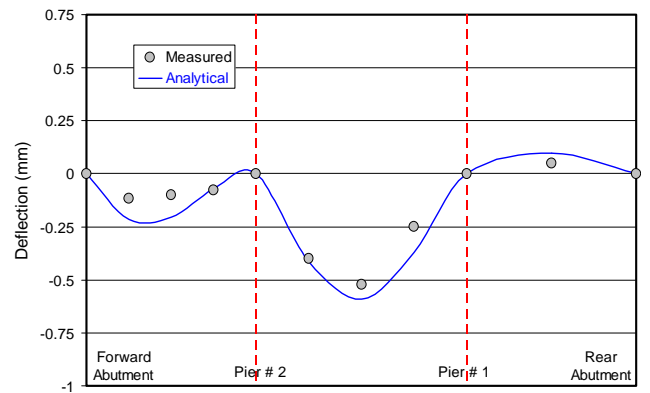
(b) Strip 2



(b) Strip 2



(c) Strip 3

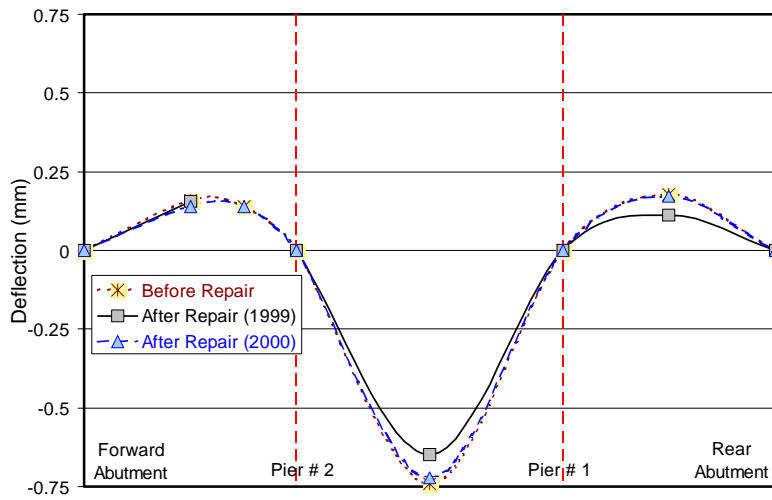


(c) Strip 3

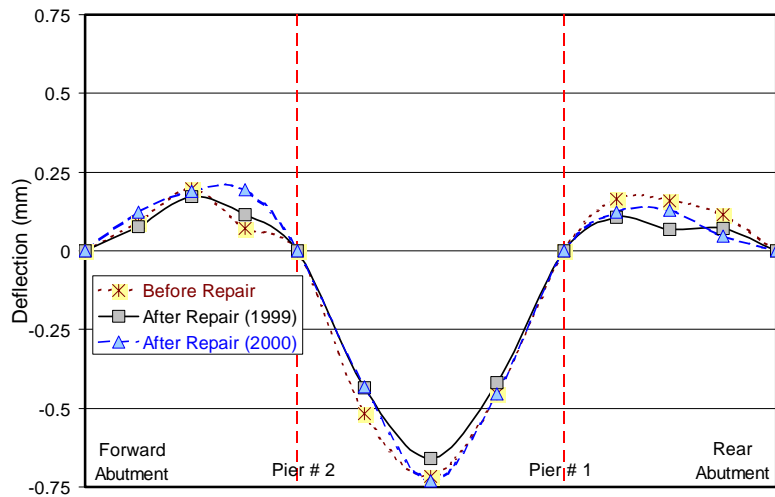
(I) After Retrofit 1999

(II) After Retrofit 2000

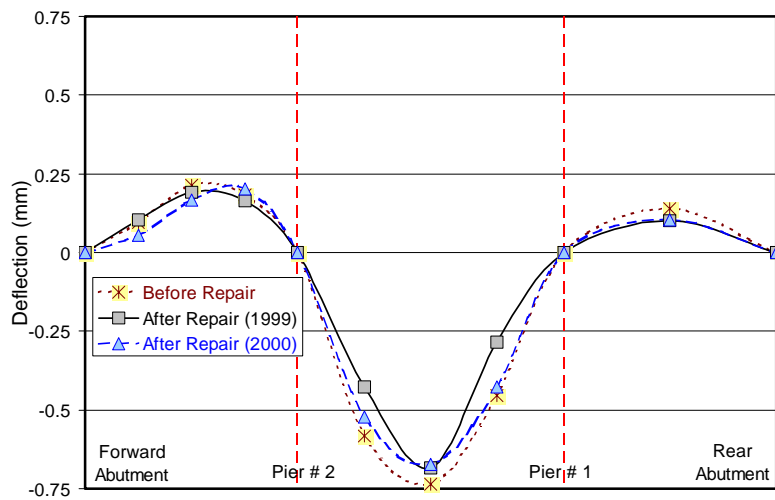
Figure B.15 (Cont.) Analytical v.s. Measured Deflection Profiles – Truck Load Test No. 7



(a) Strip 1

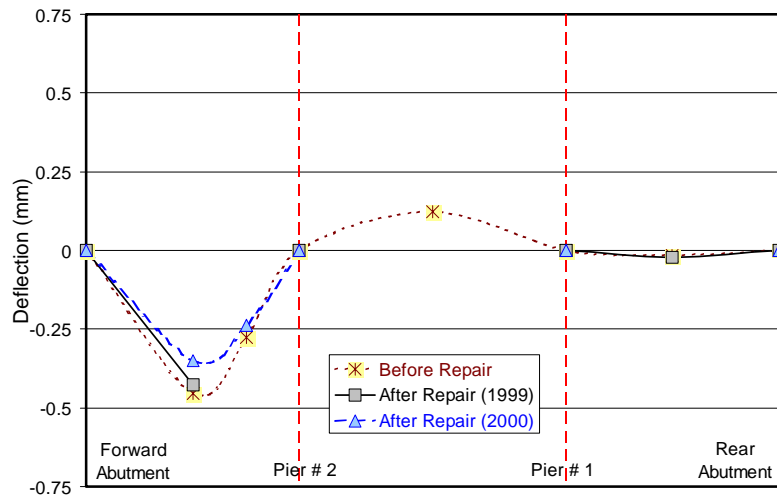


(b) Strip 2

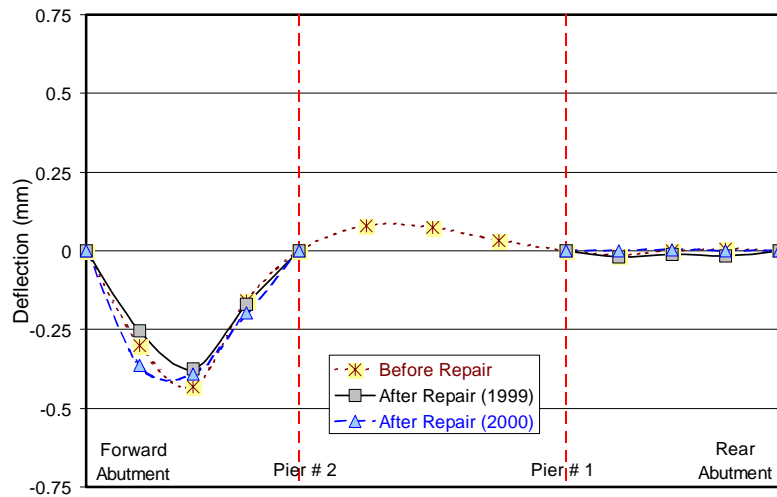


(c) Strip 3

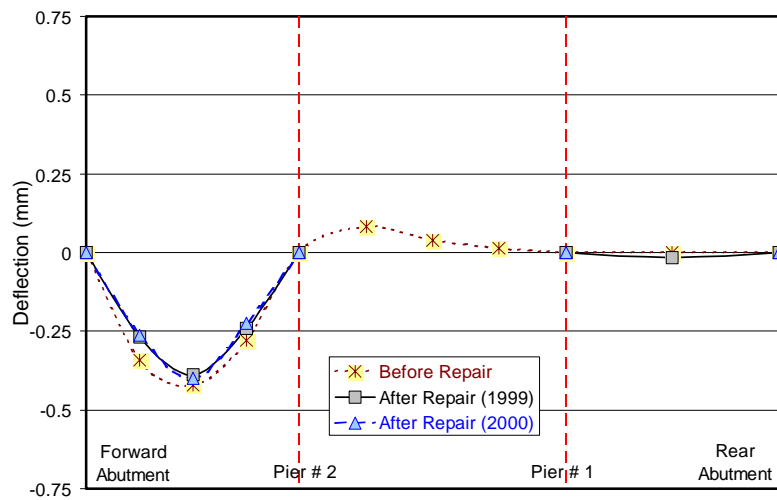
Figure B.16 Deflection Profiles – Truck Load Test No. 1



(a) Strip 1

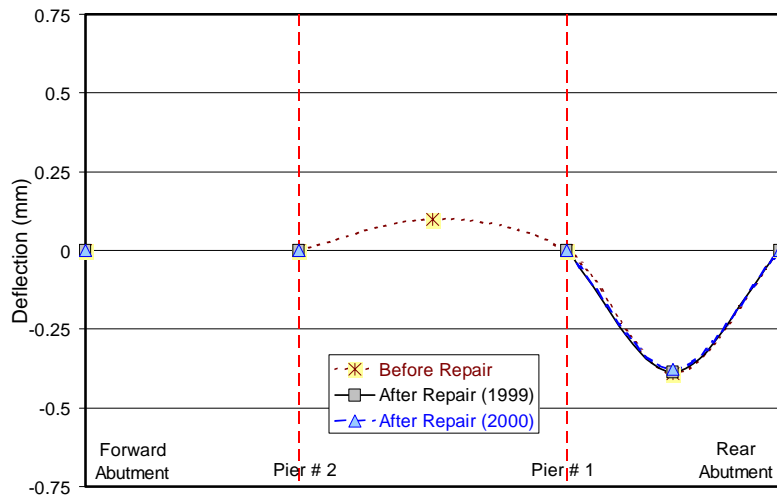


(b) Strip 2

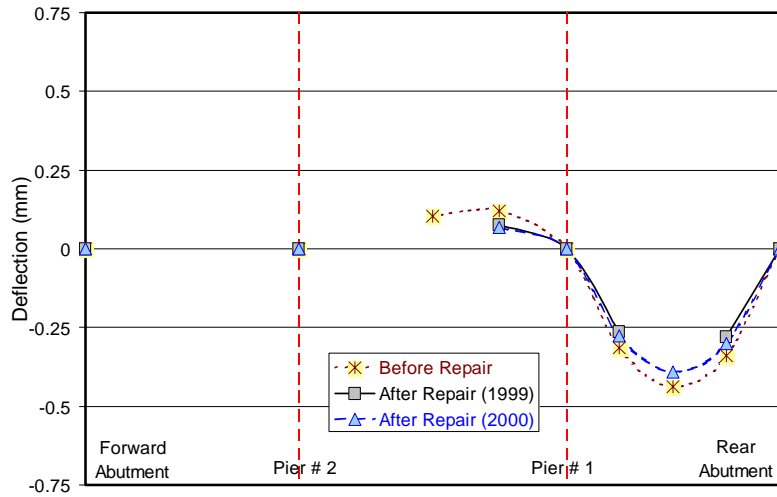


(c) Strip 3

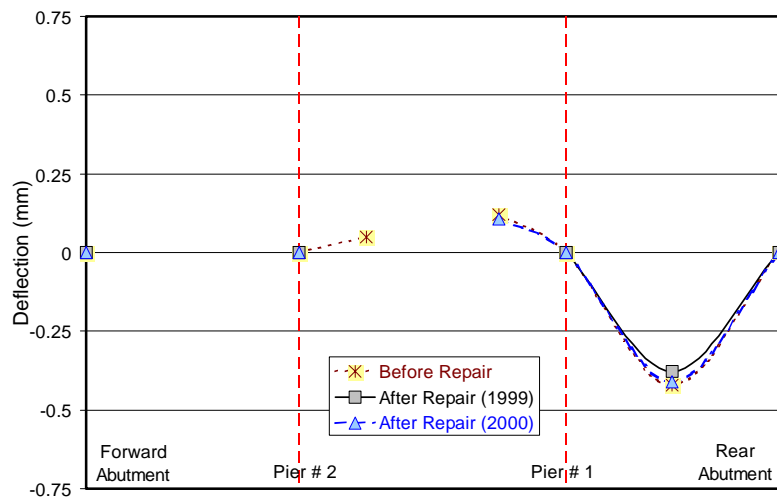
Figure B.16 (Cont.) Deflection Profiles – Truck Load Test No. 2



(a) Strip 1

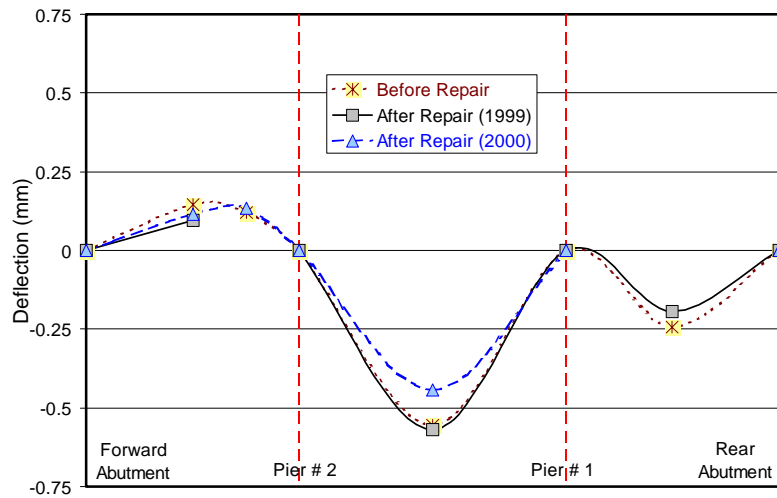


(b) Strip 2

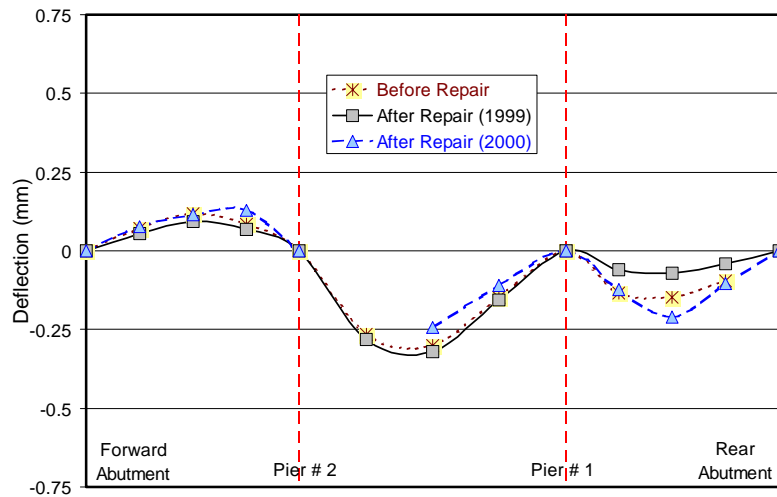


(c) Strip 3

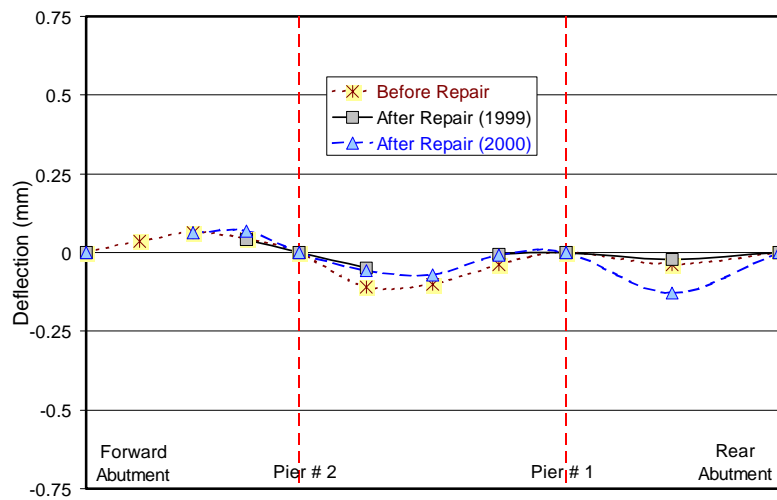
Figure B.16 (Cont.) Deflection Profiles – Truck Load Test No. 3



(a) Strip 1

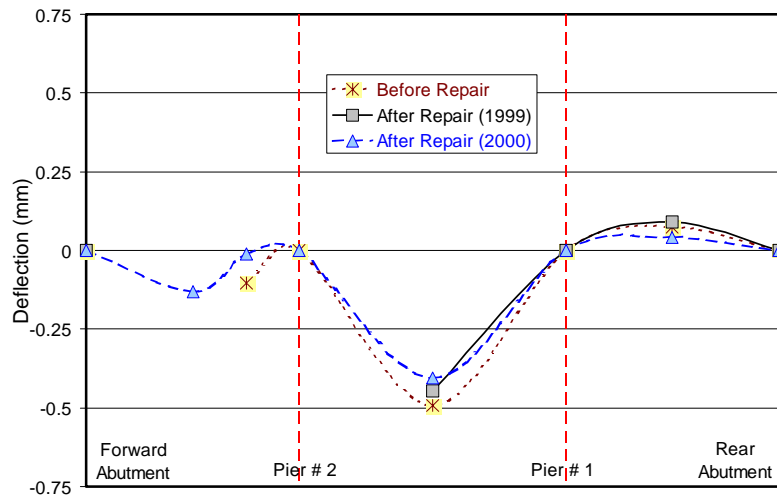


(b) Strip 2

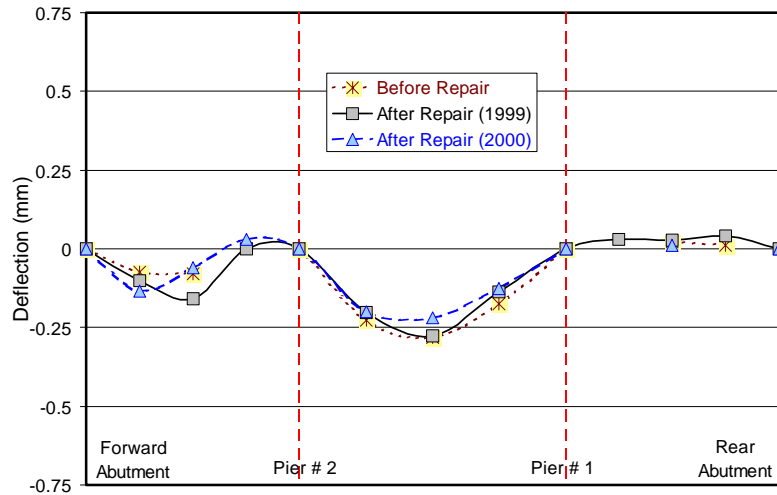


(c) Strip 3

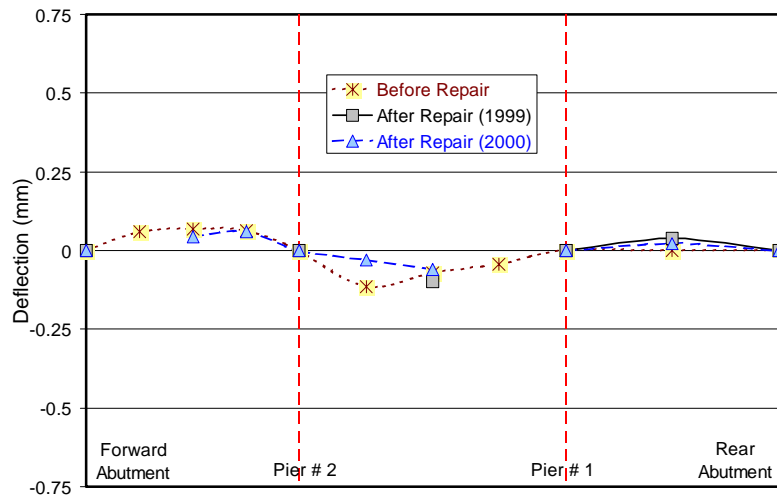
Figure B.16 (Cont.) Deflection Profiles – Truck Load Test No. 4



(a) Strip 1

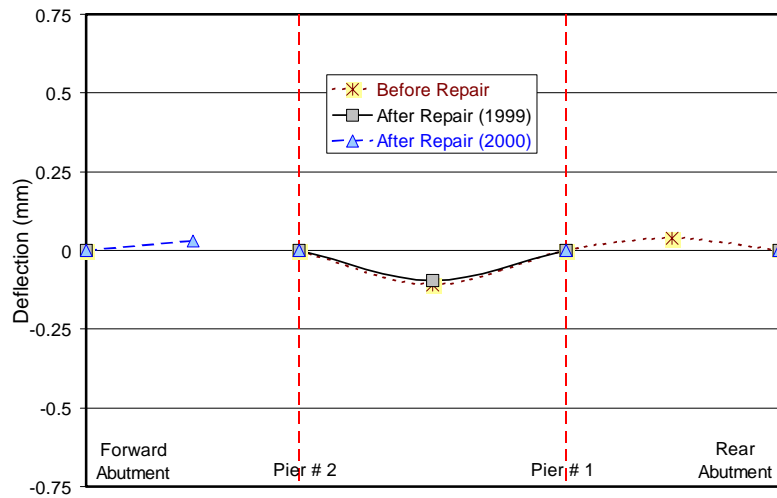


(b) Strip 2

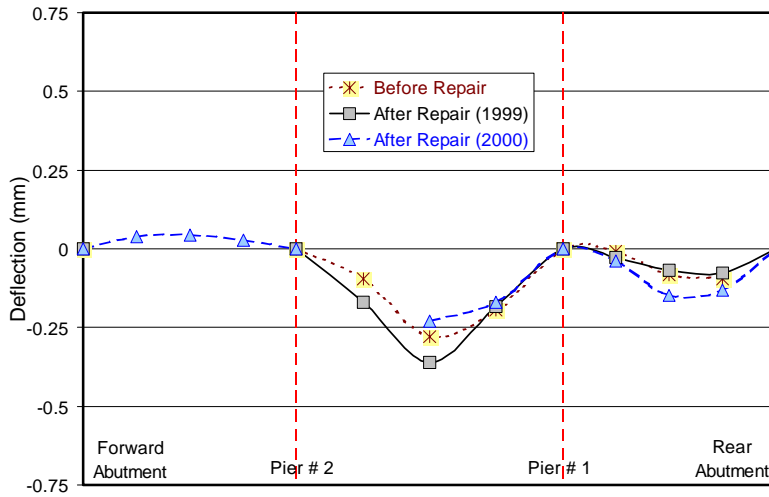


(c) Strip 3

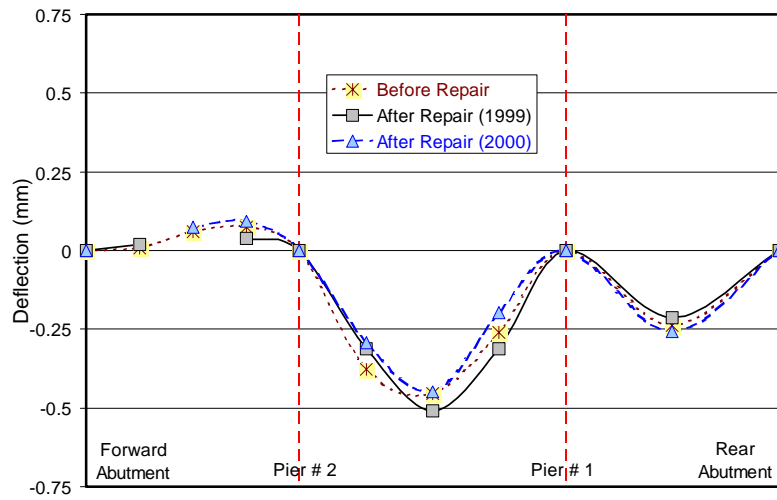
Figure B.16 (Cont.) Deflection Profiles – Truck Load Test No. 5



(a) Strip 1

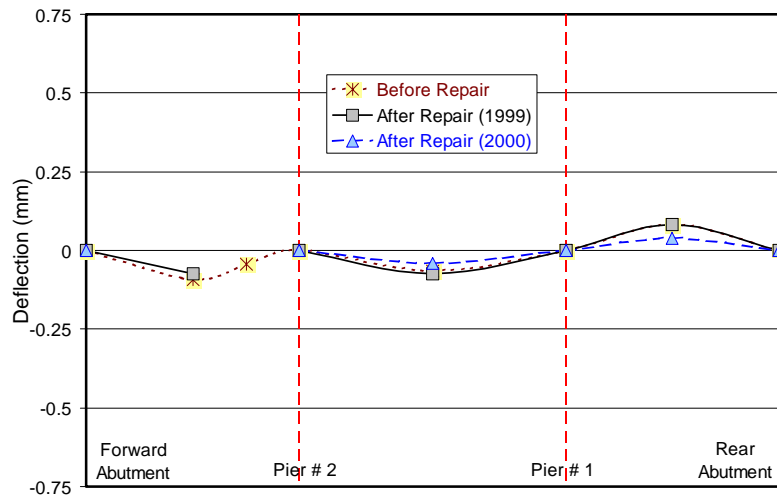


(b) Strip 2

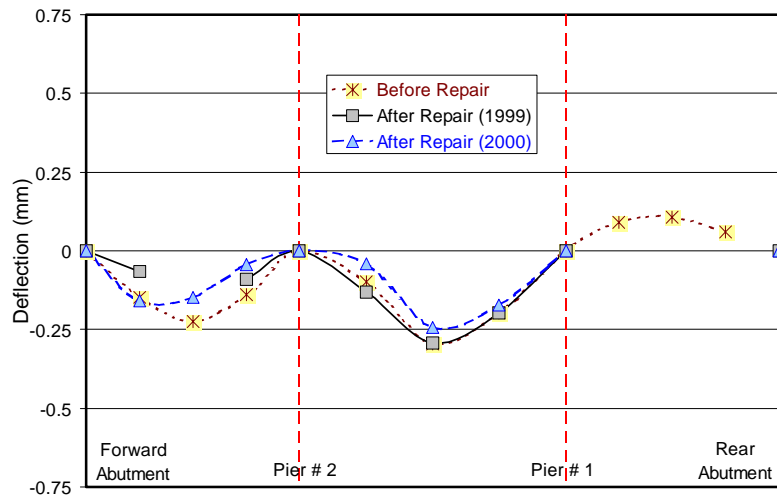


(c) Strip 3

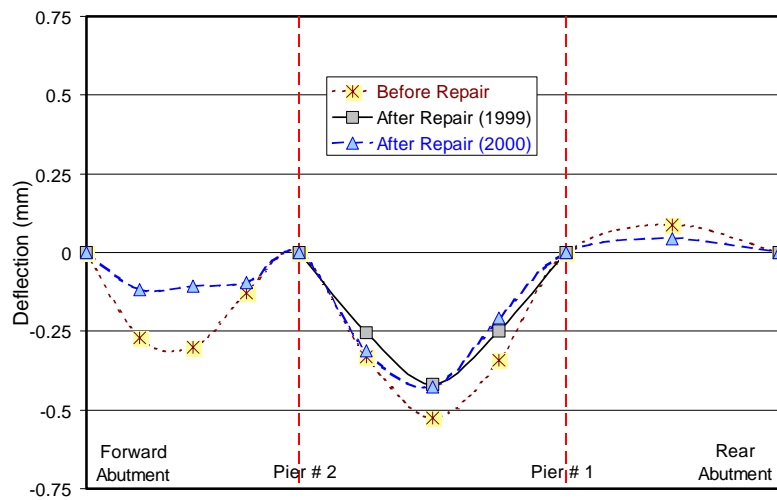
Figure B.16 (Cont.) Deflection Profiles – Truck Load Test No. 6



(a) Strip 1

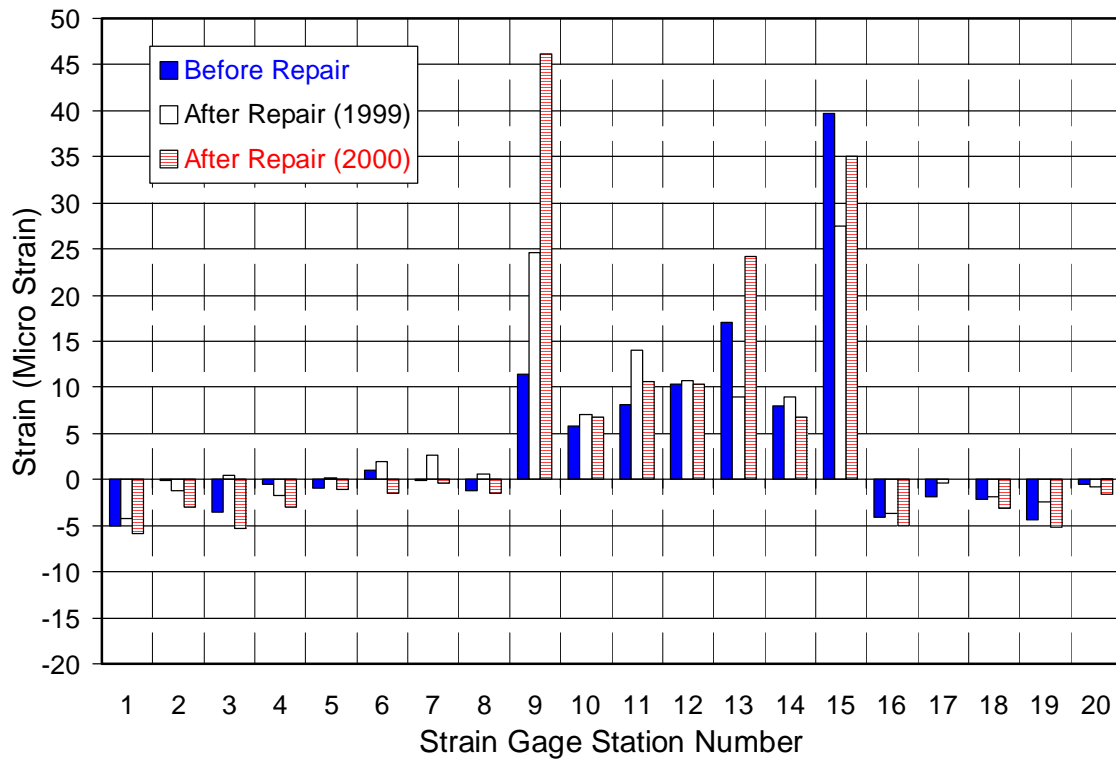


(b) Strip 2

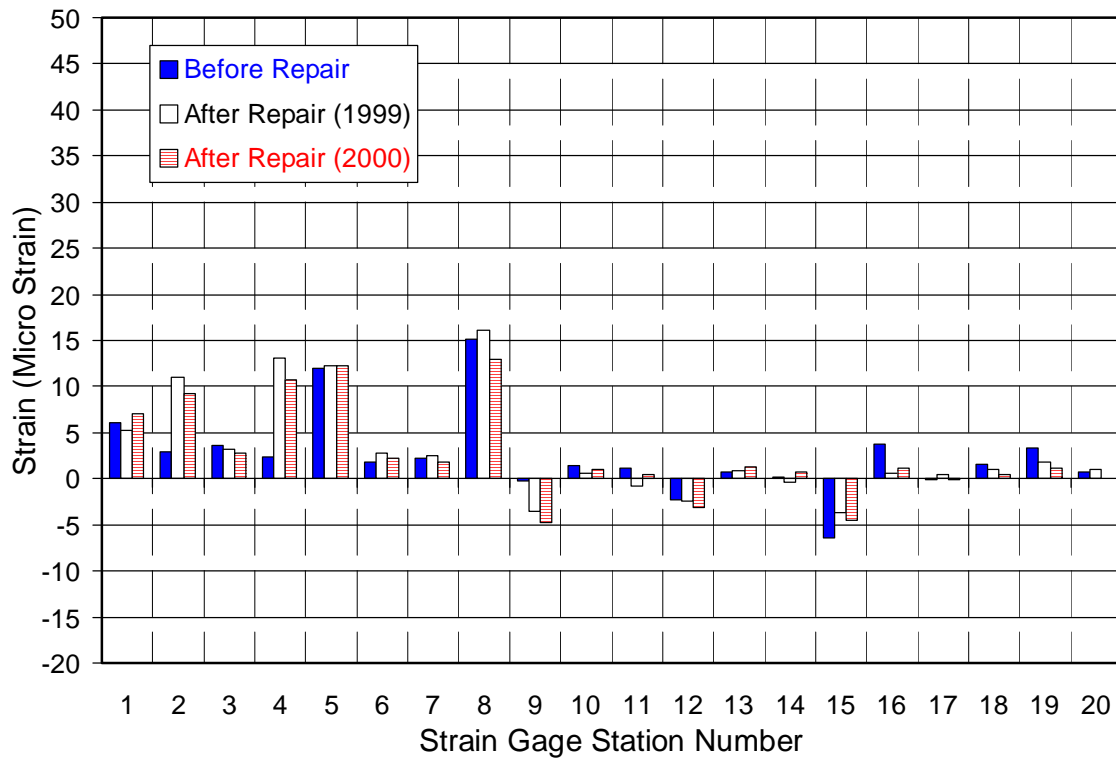


(c) Strip 3

Figure B.16 (Cont.) Deflection Profiles – Truck Load Test No. 7

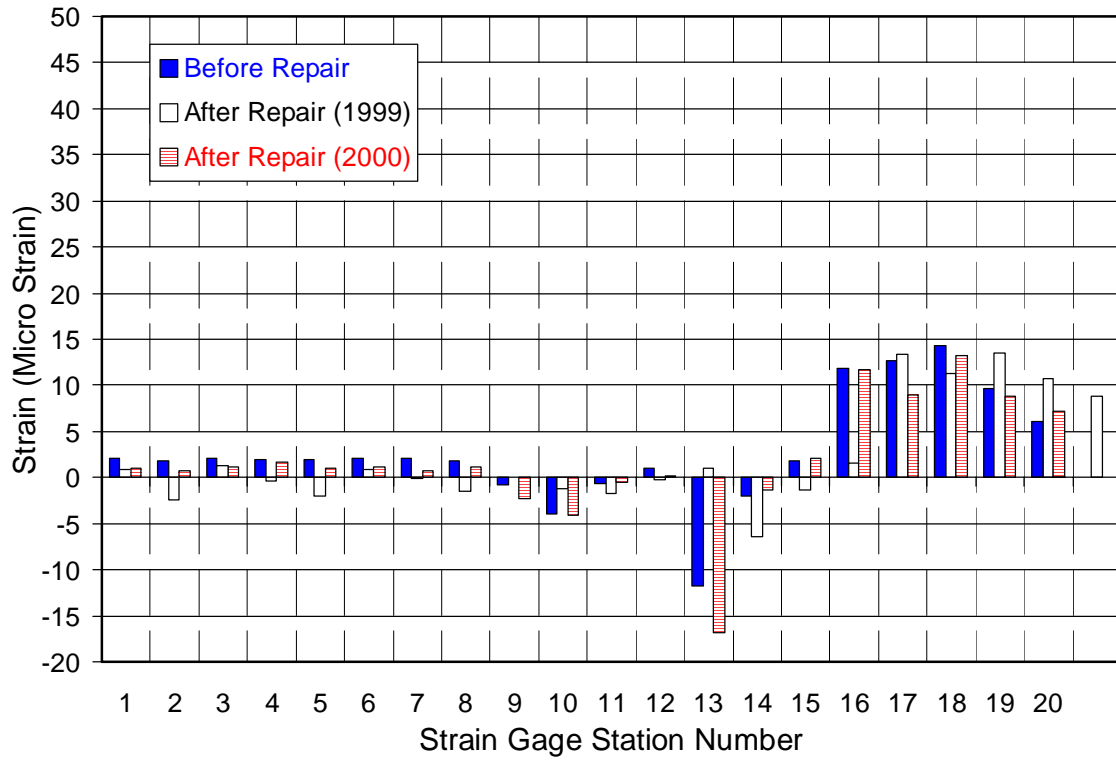


(a) Truck Load Test No. 1

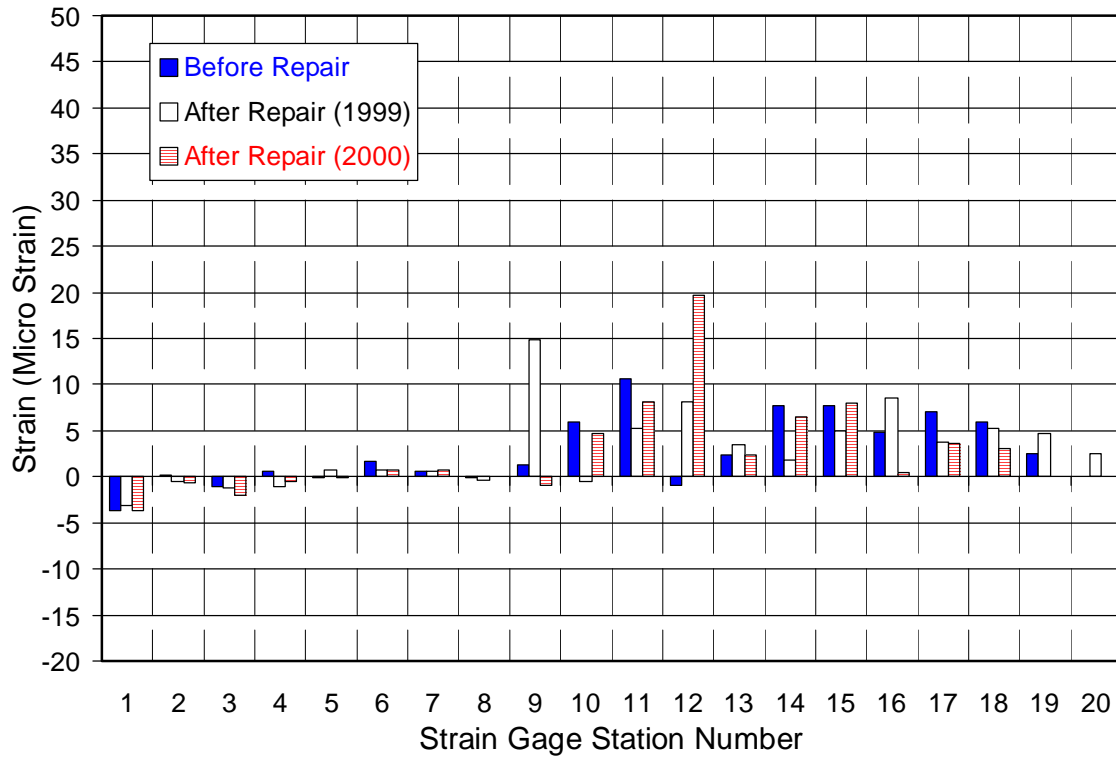


(b) Truck Load Test No. 2

Figure B.17 Concrete Surface Strains at Various Locations

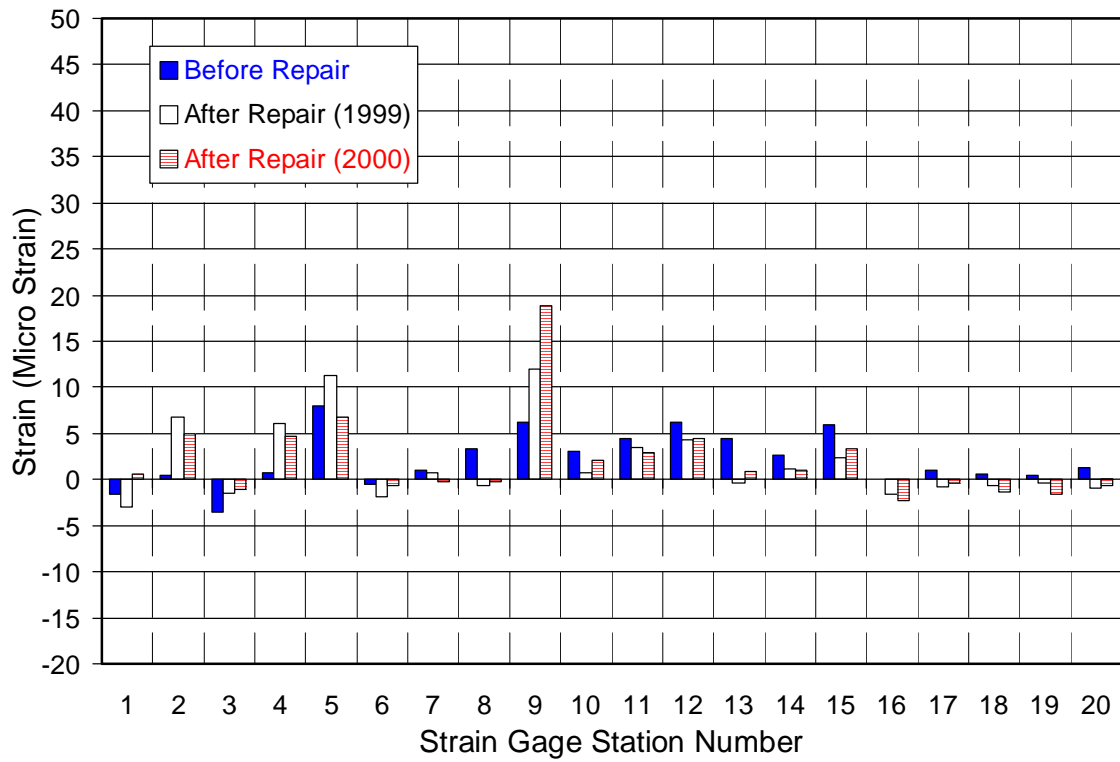


(c) Truck Load Test No. 3

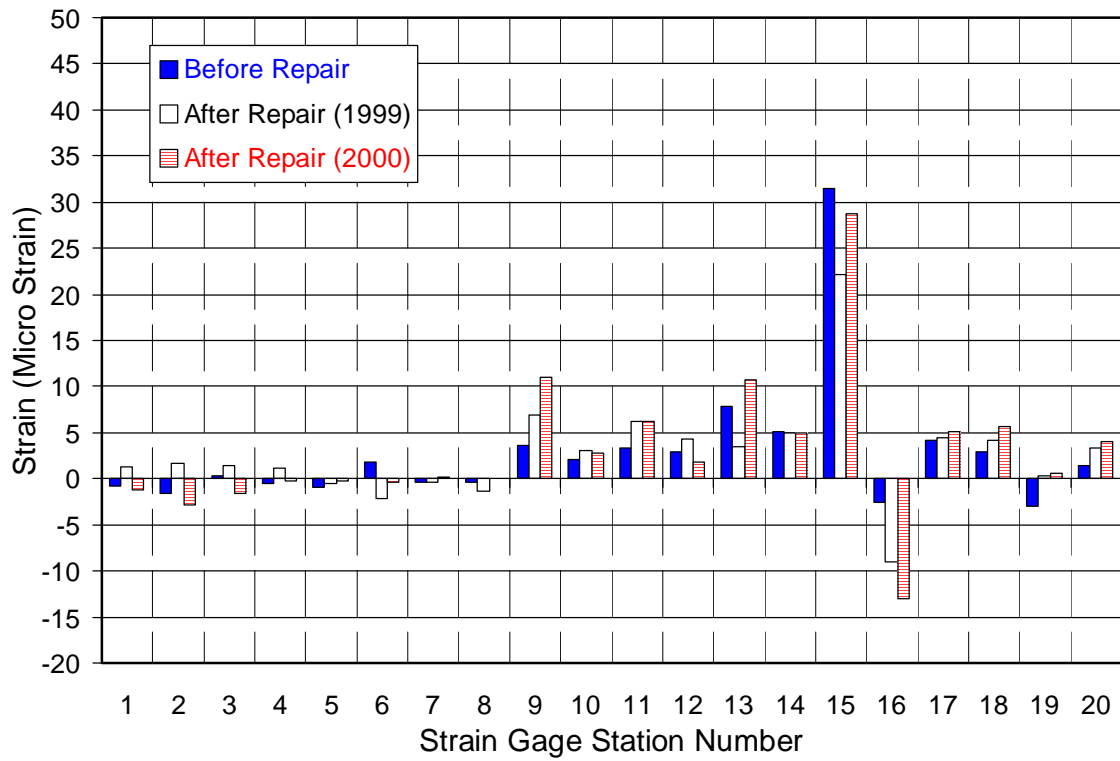


(d) Truck Load Test No. 4

Figure B.17 (Cont.) Concrete Surface Strains at Various Locations

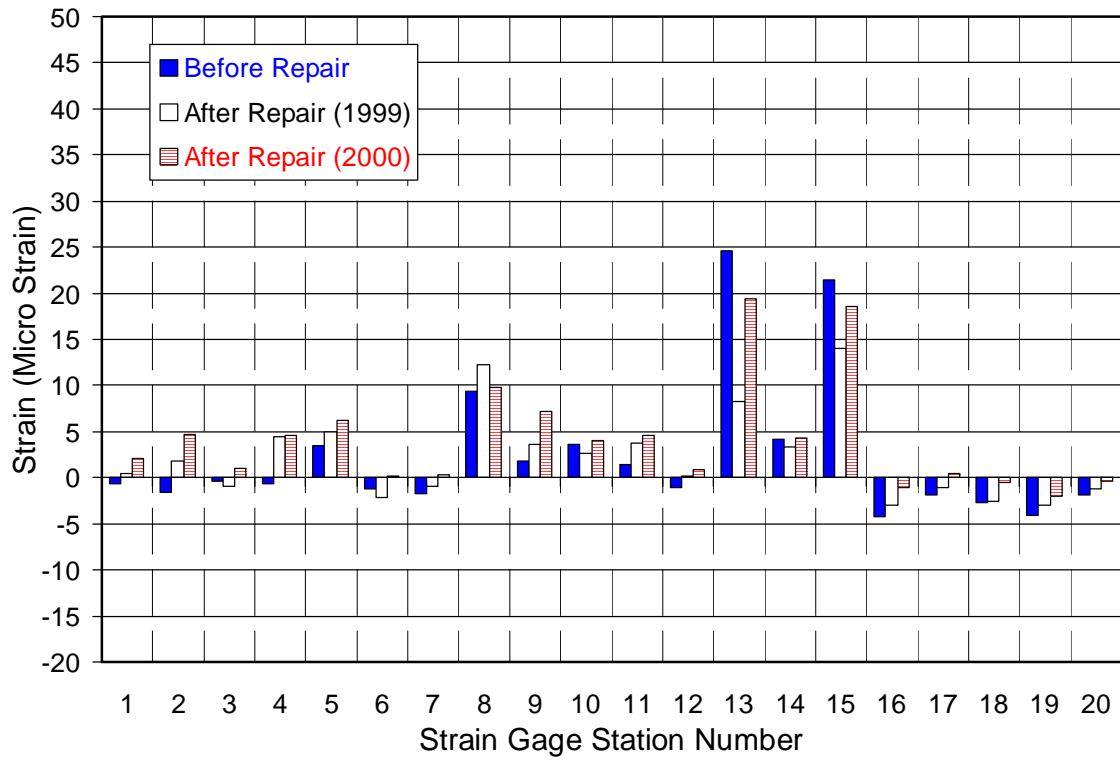


(e) Truck Load Test No. 5



(f) Truck Load Test No. 6

Figure B.17 (Cont.) Concrete Surface Strains at Various Locations



(g) Truck Load Test No. 6

Figure B.17 (Cont.) Concrete Surface Strains at Various Locations

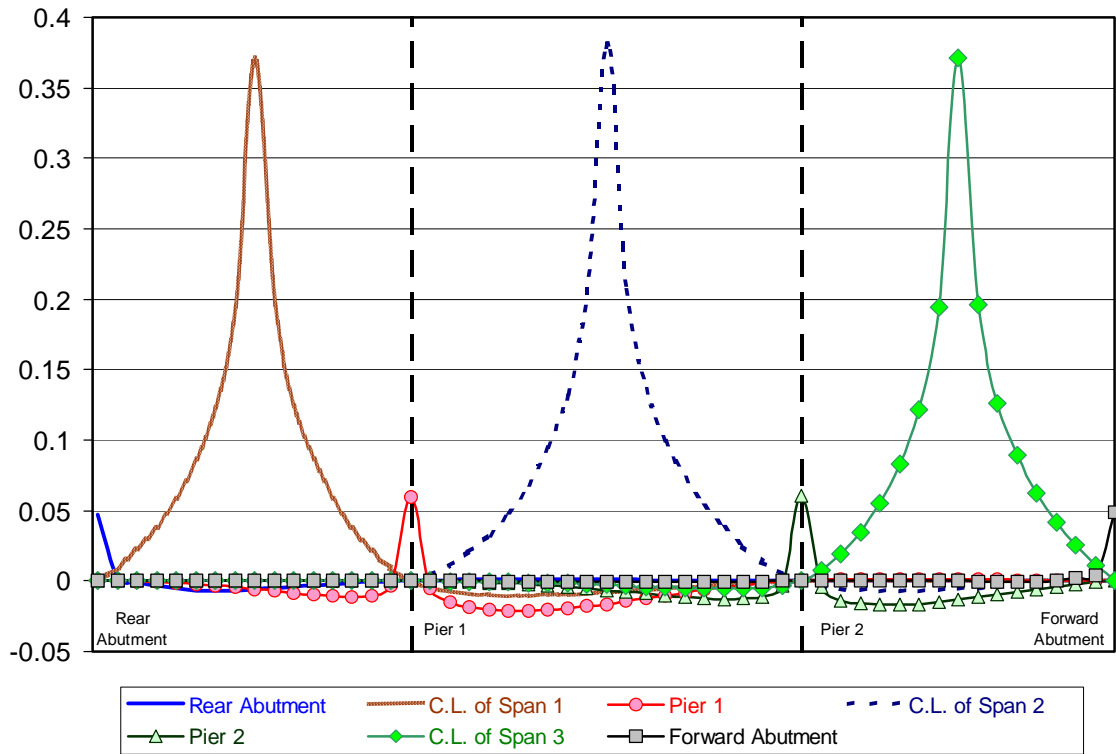


Figure B.18 Moment Influence Line Diagram – Unit Load in Lane 1

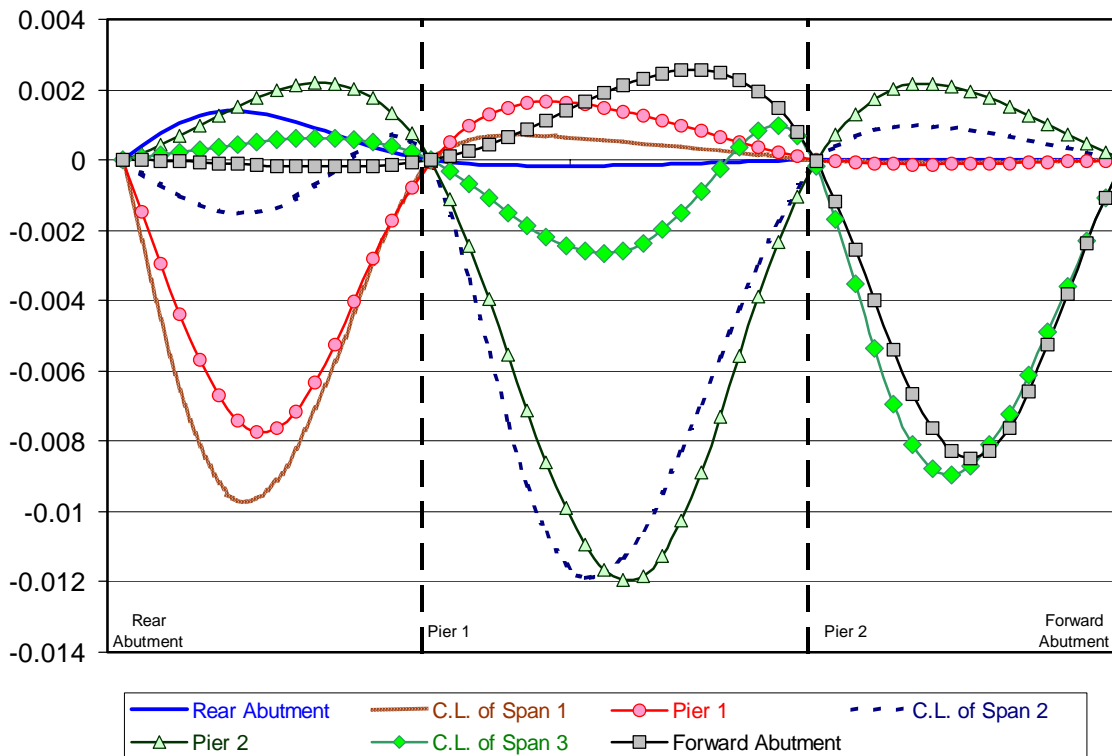


Figure B.19 Moment Influence Line Diagram – Unit Load in Lane 1

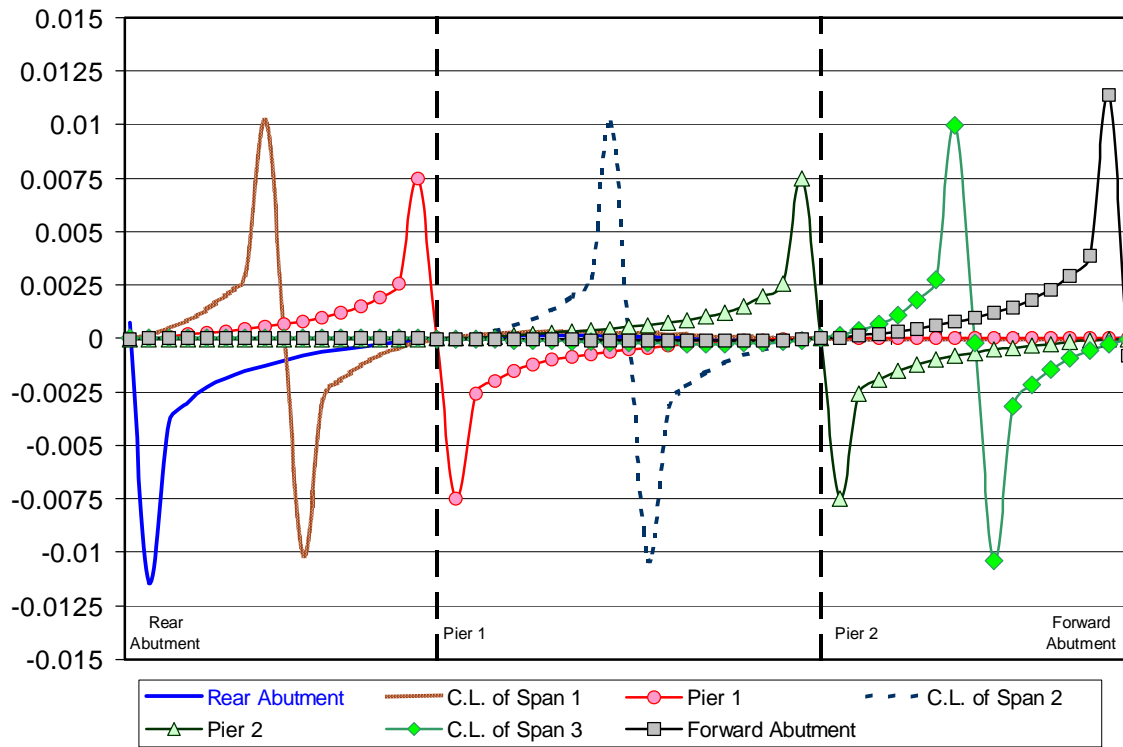


Figure B.20 Shear Influence Line Diagram – Unit Load in Lane 1

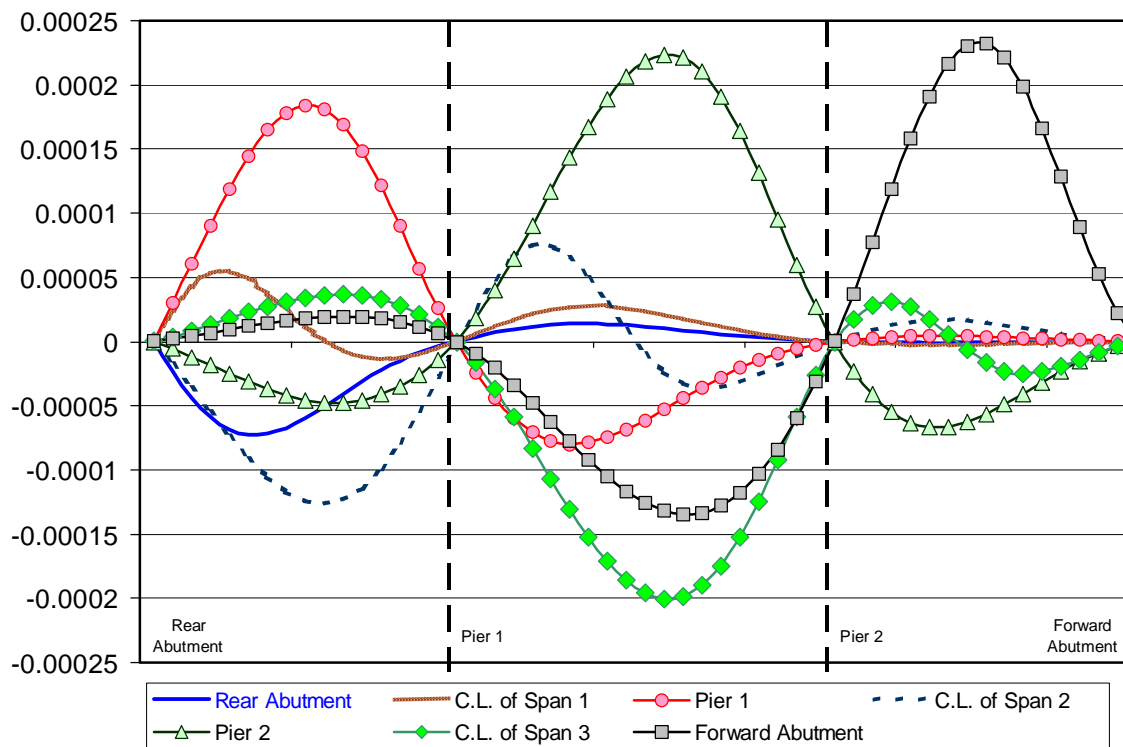
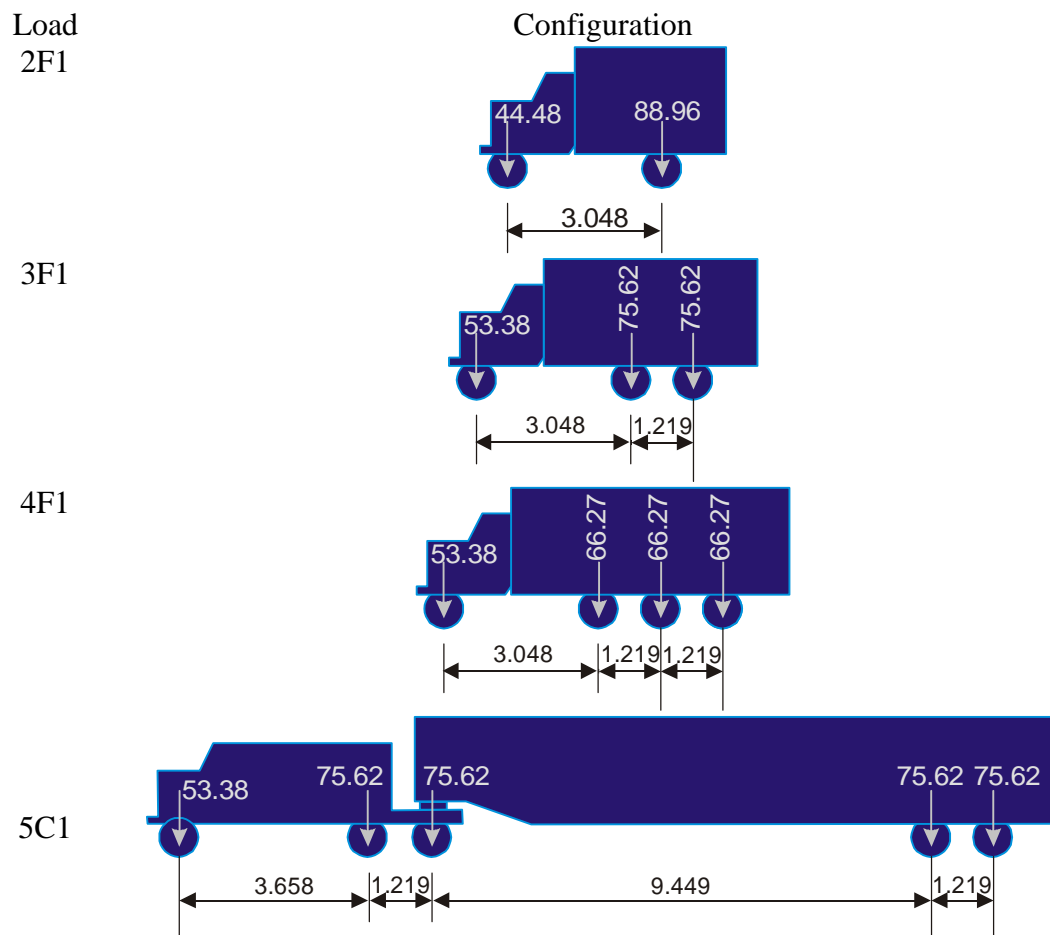


Figure B.21 Shear Influence Line Diagram – Unit Load in Lane 2



All dimensions are in m and loads are in kN.

Figure B.22 Configuration of Various Ohio Legal Loads

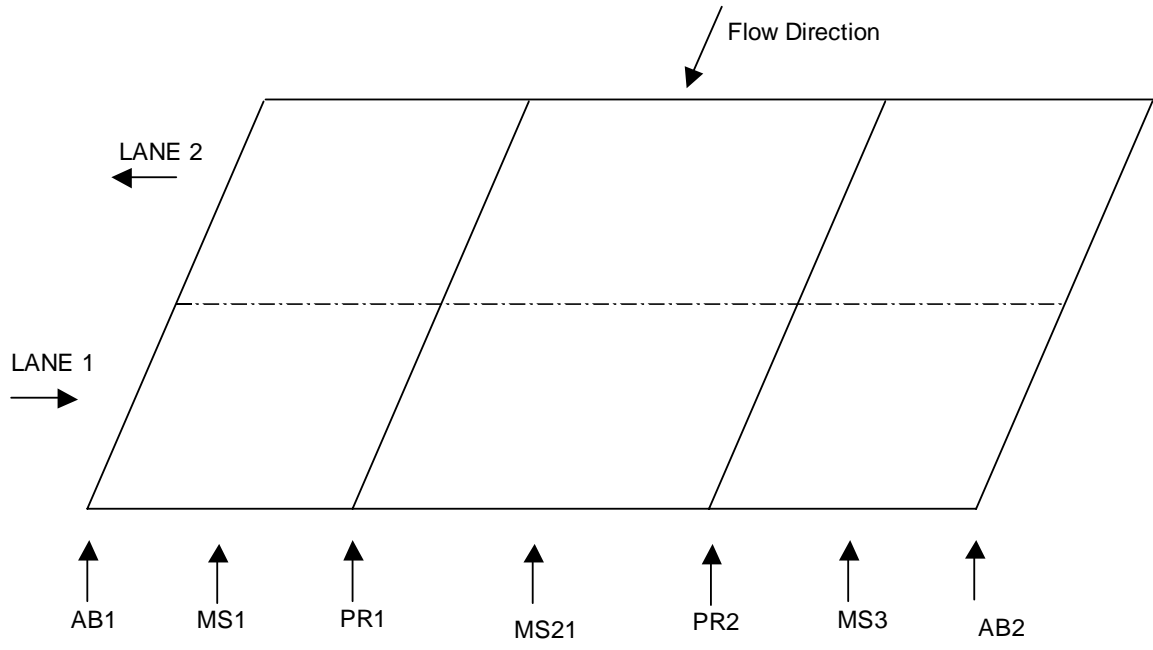


Figure B. 23 Locations of Lane 1 and Lane 2